Artem Alikhanyan National Laboratory
(Yerevan Physics Institute)

Karen V. Arakelyan

New Electronics for Space Environmental Viewing and Analysis Network (SEVAN) and Aragats Space Environment Center

Thesis

to take a Ph.D. in Engineering Sciences A.04.16
“Nuclear, elementary particle and cosmic ray physics”

Scientific adviser:
Doctor of Science, professor
Ashot A. Chilingarian

Yerevan - 2012

Table of Contents

INTRODUCTION

Enlarging human Space activities through scientific research in space and through developing space-based technologies is acknowledged as strategic to the scientific and industrial development. Space plays a leading role in Earth, Universe, Environmental, Physical and Life sciences as a privileged observation tool for our planet and objects of the universe in synergy with ground observations, data analysis and modeling tools and research in laboratories. However, the infrastructure and the activities of our modern, technologically based society can be harmfully affected by the rapid variations of our nearest star, the Sun, controlling the so-called Space Weather nearby our planet. Space weather is defined as “the conditions on the sun and in the solar wind, magnetosphere, ionosphere, and thermosphere that can influence the performance and reliability of space-borne and ground-based technological systems and endanger human life or health” [57]. Violent Space Weather can cause major failures onboard spacecraft, disrupting satellite communication, satellite navigation and space based observing systems. Space Storms are also dangerous for surface technological system like electrical power grids and pipelines. The sun influences Earth in different ways by emissions of electromagnetic radiation, interplanetary plasma structures and high-energy particles. The sun is a tremendously variable object, capable of changing radiation and fluxes of the Solar Cosmic Rays (SCR) by 3–4 orders of magnitude in the span of a few minutes. These transient events are called Solar Energetic Proton events (SEPs). Because of the sun’s closeness, the effects of the changing fluxes have major influence on Earth, including climate, safety and other issues. The influence of sun on the near-Earth radiation environments can be described as modulation of the stable galactic cosmic ray (GCR) “background” by the sun activity. The sun “modulates” the low energy GCR in several ways. The most energetic flaring process in the solar system releases up to 10^{33} erg of energy during few minutes. Along with broadband electromagnetic radiation, the explosive flaring process usually results in the Coronal Mass Ejection (CME) and in acceleration of the copious electrons and ions. These particles are effectively registered by the particle spectrometers on board of space stations (SOHO, ACE) and satellites (GOES, SDO). However, the direct measurement of highest energy SCR (above 1 GeV/nucleon) by space-born facilities is not feasible yet due to payload and time-of-flight limitations. Highest energy SCRs generates particle showers in interactions with atmosphere nuclei that can reach the Earth and generate additional (to ones initiated by GCR) signals in surface particle detectors. Therefore, surface particle detectors measure energetic SEP events also. This phenomenon is called Ground level enhancement (GLE). The latitudinal dependence of the geomagnetic field provides the possibility to use the dispersed worldwide network of Neutron Monitors [3] as a spectrometer registering GCR in the energy range from 0.5 to 10 GeV. The spectra of GCR and SCR can be approximated by the power law $dJ/dE \sim E^{\gamma}$, for the GCR $\gamma \sim -2.7$. SCR flux at GeV energies usually is very weak ($\gamma > 6$), only at some events, such as at 23 February 1956 or 20 January 2005, the spectra of SCR are considerably ‘‘hard’’: $\gamma \sim -4$ - -5 at highest energies. Thus, for energies greater than 10 GeV the intensity of the GCR becomes increasingly higher than the intensity of the largest known SEP events and we confront a very complicated problem of detecting a small signal of the SCR against the huge ‘‘background’’ of the GCR. Existing networks of particle detectors are unable to reliably detect very low fluxes of the SCR above 10 GeV; low statistics experiments often demonstrate fake peaks with high significances. Therefore, the maximal energy E_{max} of solar accelerators is still not determined. Recent measurements at Aragats Space-Environmental Center [1,2] based on the huge SEP of January 2005 put the maximal energy of solar accelerators up to 20 GeV [19,58]. Preceding from measured enhanced secondary fluxes of the different charged and neutral particles at earth surface it is possible to estimate the energy spectra power law index of the SEP event. The estimated index of $\gamma = -4$ - -5 at GeV energies is a very good indicator for the severe radiation storm (abundant SCR protons and ions with energies 50 - 100 MeV, see [16], extremely dangerous for the astronauts and high over-polar flights, as well as for satellite electronics. Each of the measured secondary fluxes has a different most probable energy of primary “parent” proton/nuclei. As was demonstrated in [33], for the Aragats facilities these energies vary from 7 (most probable energy of primary protons generated neutrons) to 20-40 GeV (dependent on the spectra; index of SCR, most probable energy of primary protons generating muons with energies greater than 5 GeV). Thus, for predicting upcoming radiation storm it is necessary to monitor changing fluxes of the different species of secondary cosmic rays with various energy thresholds. To cover wide range of SCR energies we need networks of particle detector at different latitudes longitudes and altitudes. Other solar modulation effects also influence the intensity of the cosmic rays in the vicinity of Earth. Huge magnetized plasma structures usually headed by shock waves travel in the interplanetary space with velocities up to 3000 km/s (so-called interplanetary coronal mass ejection - ICME) and disturb the interplanetary IMF and magnetosphere. These disturbances lead to major geomagnetic storms harming multibillion assets in space; in the same time these disturbances introduce anisotropy in the GCR flux making depletion and enhancement regions manifested themselves as anisotropic distribution of GCR. Thus, time series of intensities of high-energy particles can provide highly cost-effective information also for the forecasting of the geomagnetic storm [18]. With data from networks of particle detectors we can estimate the GCR energy range affected by ICME and reveal the energy-dependent pattern of the ICME modulation effects, namely Forbush decreases [19], are the attenuations of the GCR flux in the course of a few hours with following recovering during several days. Measurements of the FD magnitude in the fluxes of different secondary CR species reveal important correlations with the speed, size of the ICME and the "frozen" in ICME magnetic field strength [58]. Measurements of all the secondary fluxes at one and the same location are preferable due to effects of the longitudinal dependence of the FD magnitudes [20]. The research of the diurnal variations of GCR in fluxes of charged and neutral secondary CR also opens possibilities to correlate the changes of parameters of daily wave (amplitude, phase, maximal limiting rigidity) with energy of GCRs [21]. Established in 2000 Aragats Space Environmental Center (ASEC) [1,2] in Armenia is world largest center for monitoring of the secondary particle fluxes. ASEC facilities measure and estimate intensities and important parameters of the following particle fluxes:

- neutral and charged fluxes at 1000, 2000 and 3200 m from different directions at geographical coordinates 40.25N Latitude and 44.15E Longitude.
- highest energy solar primaries incident on earth atmosphere;
- correlations of changing fluxes;
- histograms of energy releases in particle detectors;
- special physical events, selected by programmable software triggers.

The complex of ASEC facilities is a unique combination of particle detectors providing real-time data from many energetic channels, from different asymptotic directions with good temporal resolution and, thank to high altitude, also with high statistical accuracy. ASEC already returned results on relation of the changing intensities of the cosmic ray fluxes with Space Weather effects. One of the first ASEC launched test service of alerting on violent radiation storms by abrupt enhancements of count rates of ASEC monitors [59]. Several scientific centers are now operating Space Weather portals based on surface particle detector data [25,29,30], some of them include the ASEC data in their surveys. However, due to large anisotropy of violent solar events for research of solar-terrestrial connections and Space weather, establishing services of alerting and forecasting of dangerous consequences of space storm the networks of particle detectors located at different geographical coordinates and measuring various species of secondary cosmic rays are of vital importance.A network of particle detectors located at middle to low latitudes known as SEVAN (Space Environment Viewing and Analysis Network, was developed in the framework of the International Heliophysical Year (IHY-2007) and now operates and continue growth within International Space Weather Initiative (ISWI). SEVAN detectors measure time series of charged and neutral secondary particles born in cascades originating in the atmosphere by nuclear interactions of protons and nuclei accelerated in the Galaxy and nearby the sun. The SEVAN network is compatible with the currently operating high-latitude neutron monitor networks ‘‘Spaceship Earth’’ [25], coordinated by the Bartol Research Center, the Solar Neutron Telescopes (SNT) network coordinated by Nagoya University [26], the Global Muon Detector Network (GMDN) [27,28], the Eurasian Neutron Monitor Data Base [29, 30] and a new muon–neutron telescope constructed at Yangbajing, Tibet, China [31]. SEVAN modules are operating in Armenia (4 one m^2 standard modules and 2 super modules of 12 identical SEVAN units each arranged above and below 2 standard sections of Nor Amberd neutron monitor 6NM-64; both super modules are capable of muon direction estimation), in Croatia (Zagreb observatory), Bulgaria (Mt. Moussala, India (New-Delhi JNU Univ.) and are under construction in Slovakia (Mt. Lomnicky Stit).The potential recipients of SEVAN modules are Israel, Germany and Costa Rica. The analogical detector is in operation in Tibet [31]. The particle fluxes measured by the new network at medium to low latitudes, combined with information from satellites and particle detector networks at high latitudes, will provide experimental evidence on the most energetic processes in the solar system and will constitute an important element of the global space weather monitoring and forecasting service. In the dissertation we present the description of electronics of SEVAN and ASEC networks and several examples of network operations. Electronics was developed having in mind the distributed nature of particle detector networks worldwide. Therefore, the system is designed for autonomous operation, error recovery and remote management capabilities. In contrast to existing worldwide networks measuring only single component of secondary cosmic rays (muons or neutrons) ASEC intended to measure low energy charged component (mostly electrons and muons), neutrons and high-energy muons. Correlations between changing fluxes of elementary particle measured at same location gives additional valuable information on transient solar events. Therefore, the Data Acquisition (DAQ) electronics should be designed to issue control signals and provide information readout and store from multiple remote detectors. Secondary cosmic rays are products of interactions of the primary high-energy particle with terrestrial atmosphere; therefore fluxes of charged and neutral particles are correlated. Registration of the correlated time series, gives possibility not only detect peaks, deeps and other features connected with solar modulation effects, but also correlation matrices containing new interesting information on the nature of primary solar cosmic rays. Data acquisition and storage tasks assigned to electronics are realized using integrated systems of Complex Programmable Logic Devices (CPLDs), microcontrollers and Field Programmable Gate Arrays (FPGA). Incorporation of the "intellectual" elements allows fulfilling rather complicated tasks of particle detection and, also, performing remote control and tuning of most crucial parameters of the detector.

In the first chapter of dissertation we present detailed descriptions of the developed electronics system. The results are published in [64, 65]; in second chapter – the implementation of electronics to the SEVAN network, published in [67, 71, 72, 73] and in the third – to the ASEC network, published in [62, 66, 68, 70].

The main results of the work were presented and discussed at the following international forums:

- The First International Symposium on Space Education, Moscow, Russia, June 26-30, 2006 UNIVERSAT-2006

- 13th Young Scientists Conference on Astronomy and Space Physics, Kiev, Ukraine, April 25-29, 2006
- 36th COSPAR Scientific Assembly, Beijing, China, July 16-23, 2006
- Solar Extreme Events 2007: Fundamental Science and Applied Aspects, Athens, Greece, 24-27, September 2007
- JENAM 2007: Armenian Astronomical Society Joint European and National Astronomy Meeting,Yerevan, Armenia, August 20-25, 2007
- UN/ESA/NASA/JAXA Workshop on the International Heliophysical Year 2007 and Basic Space Science "First Results from the International Heliophysical Year 2007"hosted by the Solar-Terrestrial Influences Laboratory of the Bulgarian Academy of Sciences,on behalf of the Government of Bulgaria, Sozopol, Bulgaria, June 2-6, 2008
- 21st European Cosmic Ray Symposium, Kosice, Slovakia, September 9-12, 2008
- Forecasting of the Radiation and Geomagnetic Storms by Networks of Particle Detectors (FORGES-2008), Nor Amberd, Armenia, September 29- October 3, 2008
- International conference on the Heliophysical Phenomena and Earth Environment, September 4-18, Shibenik, Croatia, 2009
- UN/NASA/ESA/JAXA Workshop on Basic Space Science and the International Heliophysical Year 2007, Daejeon, Republic of Korea, 21-25 September 2009
- Seminar on Commercialisation of Sensor and Detector Technologies, Sevastopol, Ukraine, October 7-8, 2009
- Thunderstorms and Elementary Particle Acceleration (TEPA-2010), Nor Amberd, Armenia, 2010.
- 23rd European Cosmic Ray Symposium (and 32nd Russian Cosmic Ray Conference) Moscow, Russia, July, 9 – 11, 2012
- Thunderstorms and Elementary Particle Acceleration (TEPA-2010), Moscow, Russia, July, 3 – 7, 2012

Dissertation materials were printed in 12 publications (see [62-73], including articles in peer-reviewed journals and theses of international conferences. The dissertation consists of 111 pages, including 67 figures and 28 tables.

CHAPTER 1

NEW ELECTRONICS FOR THE DETECTORS OF SPACE WEATHER MONITORING WORLDWIDE NETWORK (SEVAN) AND ARAGATS SPACE ENVIRONMENTAL CENTER (ASEC)

INTRODUCTION

The standard requirements for the Data Acquisition Electronics (DAQ) system consist in reliable and consistent registration of the all-electronic signals from particle detectors. During multiyear measurements the parameters of DAQ system should be continuously monitored to keep them stable. Electronics should not introduce loss of particle detection efficiency due to “dead times” and miscounts. Additional options to DAQ design consist in physical requirement to measure as much as possible parameters of secondary Cosmic Rays (CRs) accepted by the Aragats Space Environmental Center [1, 2]. Following requirements were introduced to the new electronics to be fulfilled at the start of new 24^{th} solar activity cycle (2008):

1. Measured energy deposit in body of plastic scintillators provides valuable information on the particle type and energy. DAQ electronics should be able to measure and store not only count the number of registered particle in the definite time span (usually 1 minute), i.e., time series of count rates, but also histograms of energy deposits, i.e. amplitudes of the Photomultiplier (PM) signals. This amplitude is proportional to the amount of light reaching PM cathode. This light in turn is proportional to the energy release of particle in body of scintillator (you have to take into account also light attenuation, see [16]). For charged particles energy release (when properly calibrated) is proportional to the number of particles hitting the detector. And energy release is also good proxy of neutral particle energy when neutral particle generates nuclear cascades in the thick scintillator.. Information on the number of particles hitting array of plastic scintillators, along with relative timing can be used also for the reconstruction of the energy and angles of incidence of the very high energy Galactic Cosmic Rays (GCR).

2. Particle identification by registering of all logical combination of the signal occurrence in the multilayered particle detector systems; particle detectors of operating worldwide networks have very limited possibility of particle identification and energy estimation. New electronics combined with multilayered detectors interleaved by the lead filters allows to ASEC and SEVAN networks much wider options for the particle identification:

- to identify charged and neutral particles hitting detector;
- to identify primary solar particle hitting terrestrial atmosphere;
- to measure direction of the incident muons, which is good proxy of the incidence of the primary particle on the terrestrial atmosphere;
- to investigate very rare events of muon capture by lead nuclei;
- to measure burst spectra of cosmic rays;
- to measure spectra of horizontal muons, and many others…

3. In contrast to existing world-wide networks measuring only single component of secondary cosmic rays (muons or neutrons) SEVAN intended to measure low energy charged component (mostly electrons and muons), neutrons and high energy muons. Correlations between changing fluxes of elementary particle measured at same location gives additional valuable information on transient solar events [48]. DAQ electronics should be designed to issue control signals and provide information readout and store from multiple remote detectors. Secondary cosmic rays are products of interactions of the primary high-energy particle with terrestrial atmosphere; therefore fluxes of charged and neutral particles are correlated. Registration of the correlated time series, gives possibility not only detect peaks, deeps and other features connected with solar modulation effects, but also correlation matrices containing new interesting information on the nature of primary solar cosmic rays. Correlation matrices also are very useful for the continuous monitoring of trustworthiness of the detector channels and estimation of important parameters of detector, as, for instance, multiplication of neutrons in the sections of neutron monitor.

Mentioned tasks assigned to DAQ electronics are realized using integrated systems of Complex Programmable Logic Devices (CPLDs), microcontrollers and Field Programmable Gate Arrays (FPGA). Incorporation of the “intellectual” elements allows fulfilling rather complicated tasks mentioned in points 1-3 and, also, performing remote control and tuning of most crucial parameters of the detector. ASEC DAQ system is much more complicated comparing with ones often used in particle detectors of world-wide networks monitoring fluxes of cosmic ray. They usually use industrial 32 or less input cards, implementing simple pulse counting functions only. DAQ of Apatiti Neutron Monitor (NM) [47] consists of 500 kHz frequencies ADLINK PCI- 7233H card with 32 inputs. Dead time of card is 16 μsec. To feed NM signals to the card a shaper-discriminators are needed, as well as an on-line desktop computer. ASEC DAQ systems are fed by analog signals and output is read out from Ethernet port. Fast comparators and CPLDs reduce dead time down to 0.4 μsec. Total energy consumptions including DAQ electronics for 18 channels and build-in micro-PC did not exceed 100 wt. Therefore, accu-battery system powered by solar energy can be also used for feeding the detector, as usually is required for the CR experiments.

The chapter is organized in the following way: Electronics of the Aragats Neutron Telescope (ASNT) and Nor Amberd multidirectional Muon Monitor (NAMM); Electronics of Neutron Monitors; Electronics of Aragats Multichannel Muon Monitor (AMMM); Electronics of SEVAN detector; Description of the pressure sensor, it's electronics, and operation in Yerevan, Nor-Amberd and at Aragats.

1.1 Electronics of ASNT and NAMMM (scintillator detectors)

Functionally, the electronics of Aragats Solar Neutron Telescope (ASNT, see Figure 1) and Nor Amberd Multidirectional Muon Monitor (NAMMM, see Figure 2) consists of two parts: Data Acquisition (DAQ) and Detector Control System (DCS).

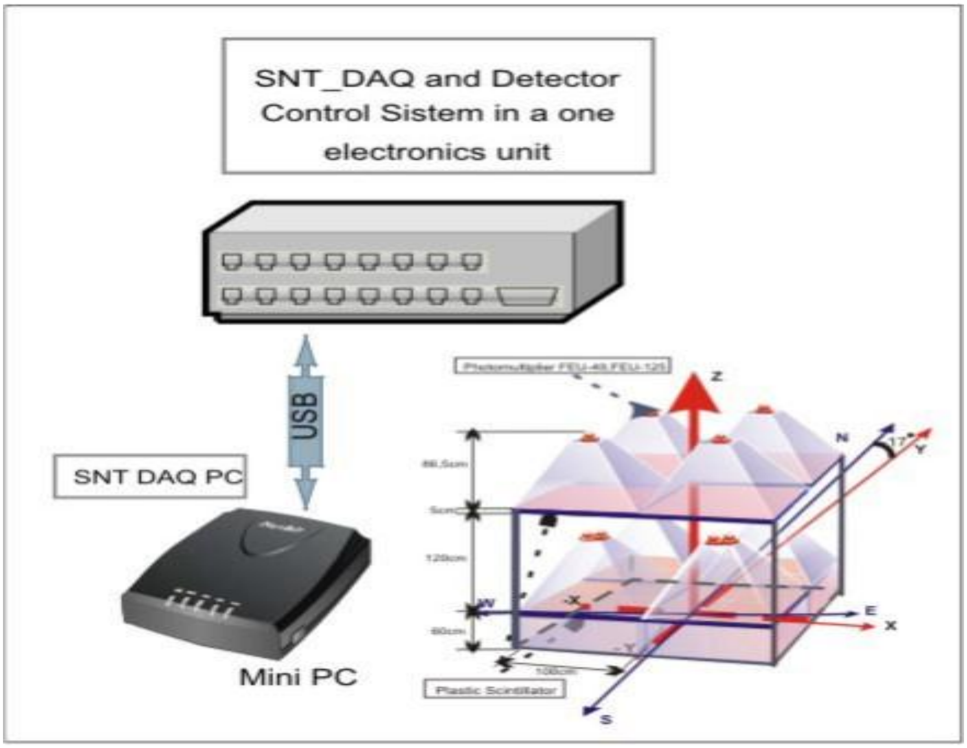

Figure 1 Layout of DAQ electronics of ASNT

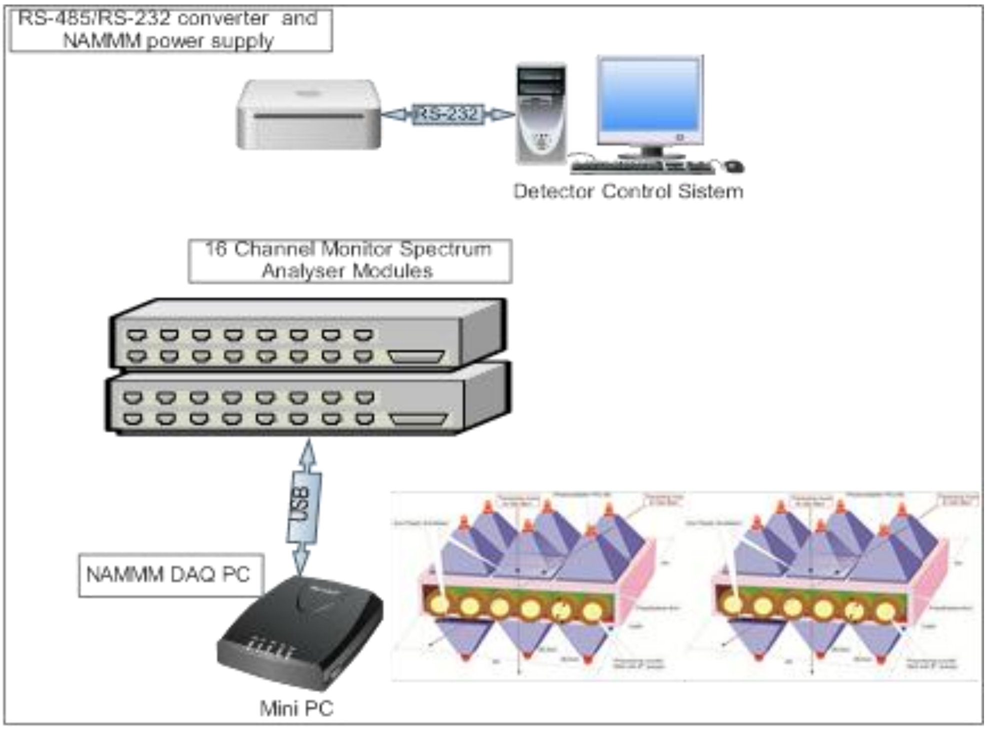

Figure 2 Layout of DAQ electronics of NAMMM

The DAQ chain comprises of Photomultipliers (PMT) FEU49 type, Buffer Preamplifier, Coaxial Cable, Logarithmic Analog-to-Digital Converter (LADC), 32-bit ARM Microcontroller board, USB/COM interfaces and the mini-PC. For the ASNT, all DAQ electronics, except of preamplifier is integrated into one 8-channel input unit, for the NAMMM in two 16-channel units, see Figure 3.

Figure 3 16-channel electronics unit of NAMMM detector

The DAQ of both detectors are similar, except for the channel numbers, while the DCS is slightly different. The ASNT is a single setup that is why one electronics unit is used for its both subsystems. The NAMMM is only a part of a large experimental setup, consisting of two identical NAMMM detectors and 3 neutron monitors sections. That is why, for the NAMMM, the DCS for all mentioned detectors are integrated into a separate (from DAQ) DCS net as shown in Figure 4.

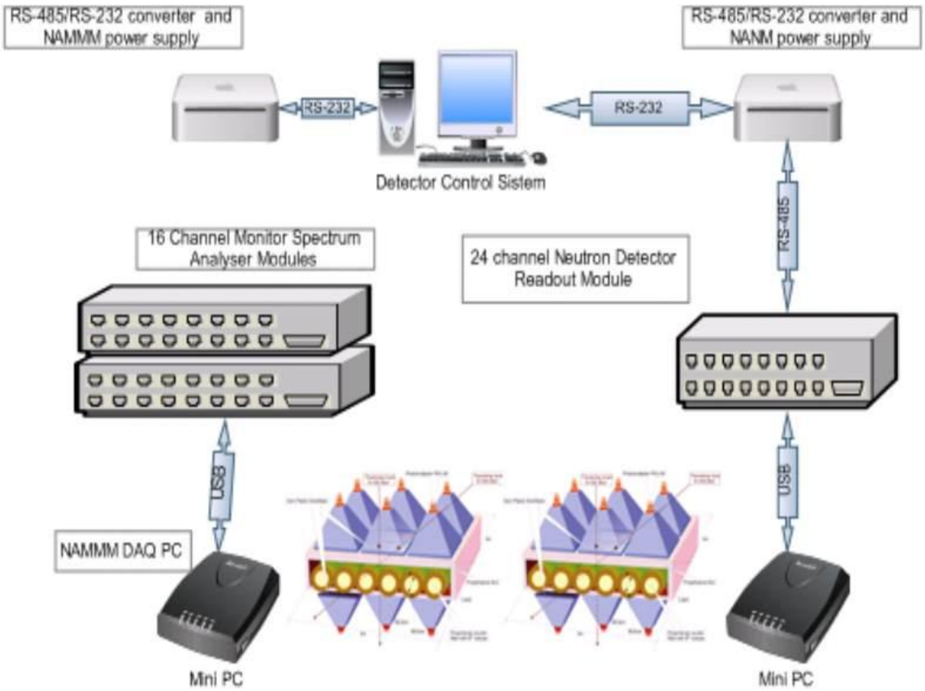

Figure 4 DAQ and DCS networks in Nor Amberd

The DCS of ASNT consists of: Programmable Local High Voltage Power Supply for PMT, RS-485 Local Net, Microcontroller and mini-PC. The same Microcontroller is shared by DAQ and DCS.

The DCS of the Nor Amberd setup includes all Programmable Local High Voltage Power Supplies for Muon scintillator detectors PMTs and Neuton Monitor proportional chambers as well as discriminators thresholds of the Neutron Detector Readout Module (see description of the 24 Channel Neutron Detector Readout Module below). As far as the frontend hardware is concerned, both DCS and DAQ subsystems are tightly integrated. The PMT, Preamplifier and HV Supply are placed inside the metal screen case on the top of the scintillation detector. There are two connectors on the case: standard BNC for the main signal connecting cable and round multiple connector for RS-485 interface and unregulated +15V for powering the Preamplifier and HV Source. The interface/power connections of the ASNT detector are divided into two daisy/chain lines, one line for the upper four detectors and the second one for the lower four. All electrical connections from the detectors come to the ASNT Electronics unit; see Figure 5, containing both DAQ and DCS circuits.

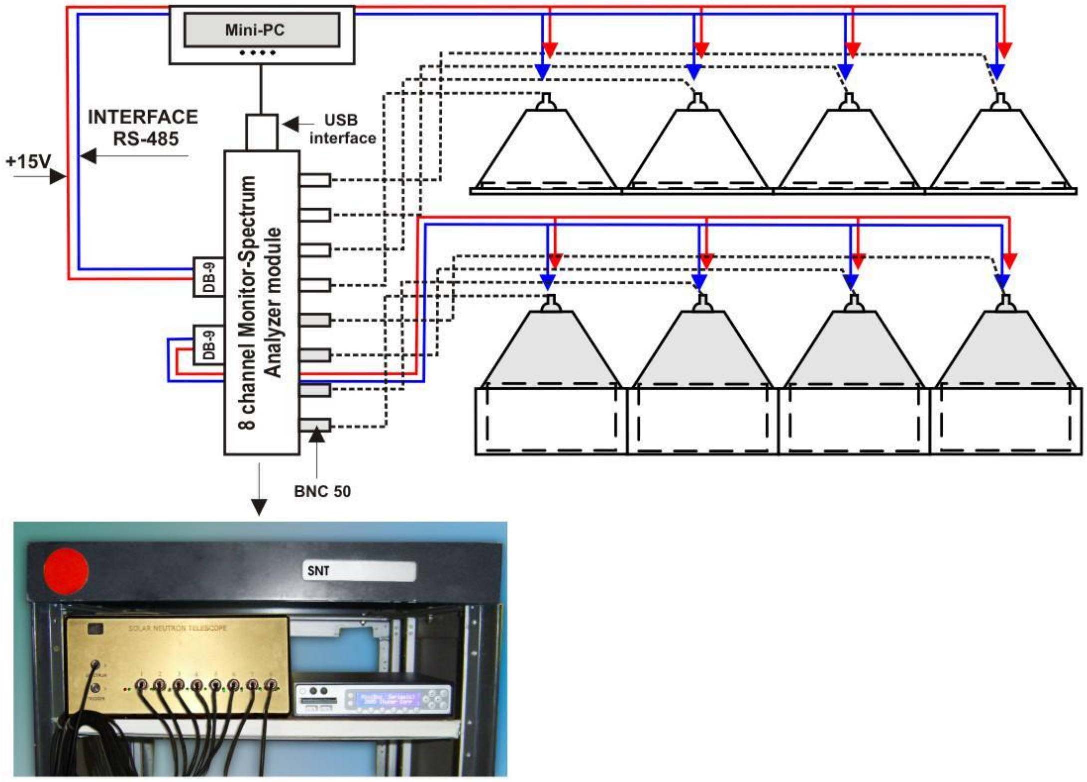

Figure 5 ASNT setup with electronics unit

The interface/power connections of the NAMMM detectors are divided into four daisy/chain lines, two to upper groups of 6 detectors and the two for lower groups.

Fig. 6 shows the charts of the metal case of the PMT tube with the PMT and electronics boards inside. There are three connectors placed on the case, A and C for the system interconnections and B for the high voltage manual measurement.

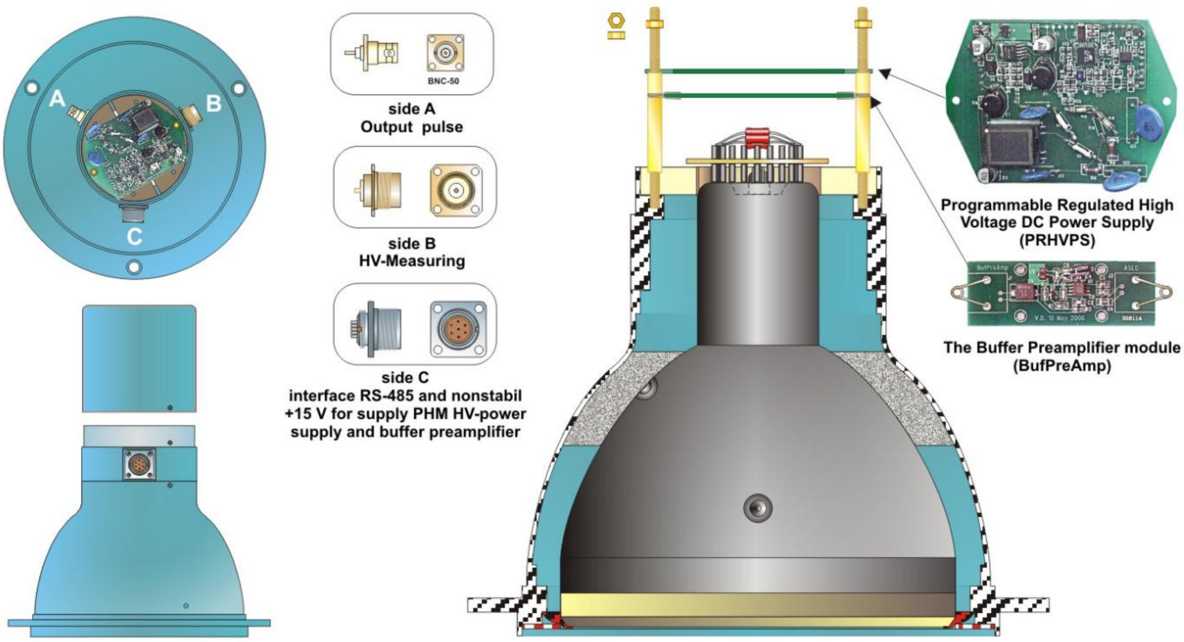

Figure 6 PM installation guide with housing, connectors and electronics

The High Voltage Power Supply (**Figure 7**) is based on a current fed push-pull topology DC/DC converter, working in a sinusoidal mode, to reduce the Electromagnetic Interferences (IMI) influence on the weak PMT output signal. To reduce the HV pulsations to sub-mvolt level, a two-stage RC filter is used. The HV Converter is powered by the switching regulator, controlled by the 8-bit ATMEL microcontroller chip. The microcontroller is integrated into the whole DCS by the RS-485 interface. The microcontroller receives the value of the HV setting from the RS-485 line and sends the measured value of HV to the line by request. The necessary HV value, sent by command from DCS is stored in the microcontroller permanent memory, so at microcontroller restarts, caused by power spikes, watchdog reset, etc., the HV value is restored without additional setting. The 6 presents as well the Buffer Preamplifier schematics. It is powered from the same +15V unregulated line as the HV Power Supply through the local linear voltage regulator. The preamplifier is based on the wideband repeater chip LMH6559. Its purpose is to match impedances of the PMT anode load resistor and the 50 Ohm coaxial line. Along with a wide frequency band of preamplifer, another requirement is high dynamic range of output pulses. The polarity of pulses is negative, therefore initial working point of the repeater is chosen close to the upper saturation limit of the chip output voltage. The rest of electronics is placed inside the ASNT Electronics Unit. The output pulses from the preamplifier are feed through coaxial cables and BNC connectors to the Logarithmic ADCs inputs.

1.2 Logarithmic Amplitude-to-digital converter

The principle of logarithmic ADC operation is based on the measurement of decay time of oscillation in the parallel RLC tank. The oscillations are caused by current pulses in the parallel RLC tank with a well known Q-factor [49]. We are aware of several realizations of this principle [50, 51, 52, 61]. In all these cases the Photomultiplier Tube (PMT) of the scintillation detector, which can be considered as an almost perfect current source, was used as the generator of current pulses. The entire electronics of the logarithmic ADC was mounted inside the PMT case and the output signal was the sequence of standard pulses with ~1 MHz frequency and the quantity proportional to the logarithm of the area (charge) of the measured current pulse [61]. The advantage of this approach is the simplicity and the high noise tolerance provided by the complete shielding of the low-signal circuit in the PMT case. Building large experimental setups with a large number of different particle detectors requires universal data processing schemes. Our overall strategy was to detect simultaneously with one and the same particle detectors both solar modulation effects and high energy galactic cosmic rays. This implies precise timing measurements (3-5 nanoseconds) and requires installation of the fast preamplifiers. LADCs cannot provide necessary time precision. Since number of incident particles can reach 10^4 per 1 m^2 scintillator LADC can generate pulse sequences with duration 80-90 microseconds, respectively. It is possible to decrease the dead time value by increasing the tank resonance frequency. However, this frequency is limited by the 1.5 - 2 MHz value because if the duration of the input pulses exceeds the quarter of resonance frequency period, the proportionality of the number of output pulses to the logarithm of input signal is disrupted.

The voltage pulse from the PMT anode load resistor is amplified by the current by the buffer pre-amplifier with a +1 voltage gain. The amplifier with the output resistance of 50 Ohm sends the pulse signal, completely repeating the shape of PMT anode current pulse, through the impedance matched 50 Ohm coaxial transmission line to the control room for further processing. Thus, the whole information about the event enters the DAQ electronics input practically without any losses. It can be subjected to various forms of processing, depending on the requirements of a particular physical experiment. To guarantee operation of electronics under different requirements, we use following scheme of signal processing, see Figure 7.

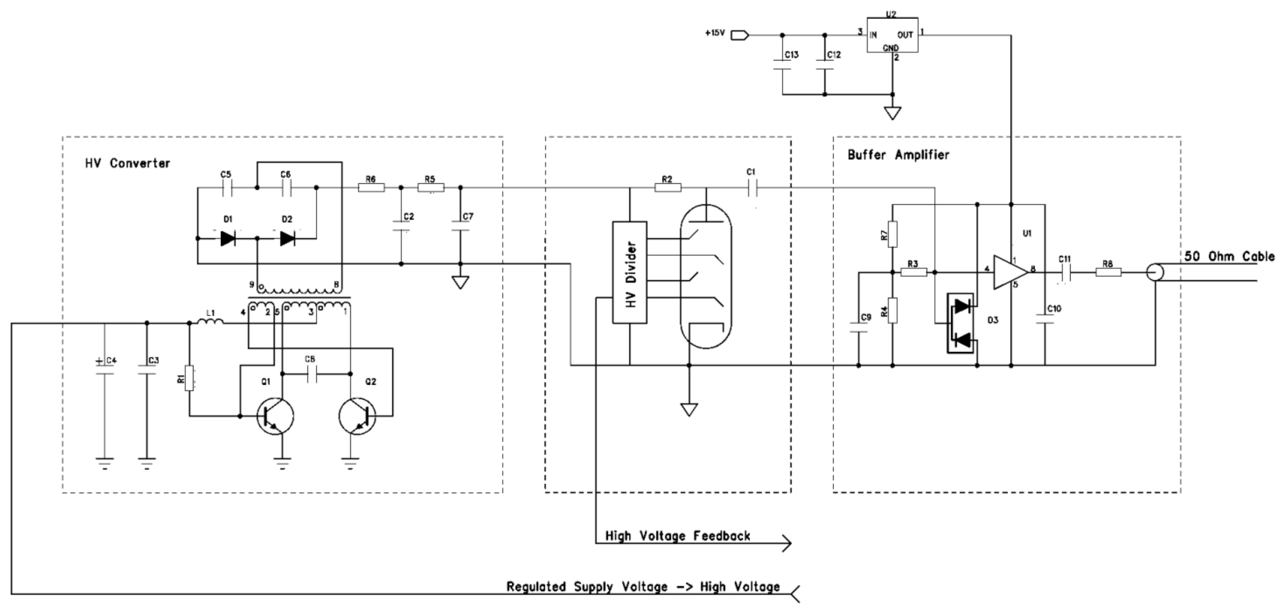

Figure 7 The PM output readout scheme

The one and the same PM output signal can simultaneously enter different electronic devices. For example, to undergo processing with short dead time, it can enter the discriminator with a fixed threshold   and for the amplitude analysis to Analog-to-Digital Converter (ADC). Different types of ADC can be used simultaneously: inexpensive logarithmic ADC (LADC) with low amplitude resolution, and the complex universal multi-channel amplitude analyzers.

The simplified schematic diagram of logarithmic LADC front-end is presented in **Figure 8**.

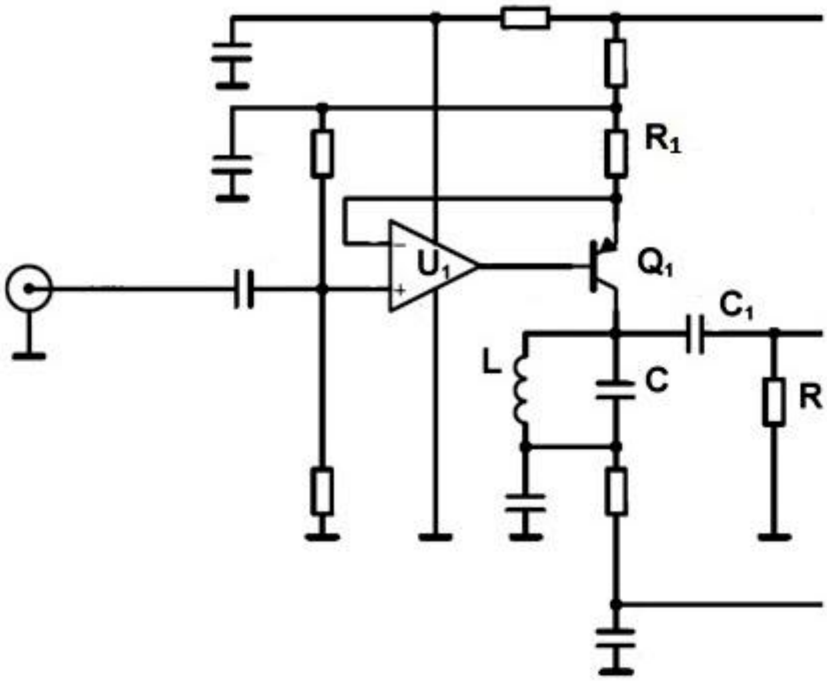

Figure 8 LADC_Frontend

The voltage-to-current converter is assembled on the elements U1, Q1, R1, its conversion gain is

$$Gain_{vi} = \frac{1}{R_1} = 2\frac{mA}{V}$$

This value is selected so that for the standard shape of PMT pulse, the peak voltage of the first half-wave on the oscillating LRC tank would be equal to the amplitude of the input pulse. Since the maximum amplitude of the input pulse is set in the preamplifier to the level of approximately 7V, the same amplitude is obtained at the input of Operational Amplifier (OA) U2. The greater maximal voltage values cause the limitation of oscillations amplitudes due to the sharp increase of the U2 input current, whereas with the smaller values the dynamic range of converter decreases due to an increase in the portion of OA inherent noise, the Radio-Frequency Interferences (RFI) from the radio stations and other kinds of Electromagnetic Interferences (EMI). As it was already mentioned, the oscillation amplitude on the RLC tank is proportional to the area of the pulse shape, if its duration is shorter, than one fourth of the tank resonance period, i.e.

$$V_0 = \frac{1}{C}\int I_{pulse}\, dt$$

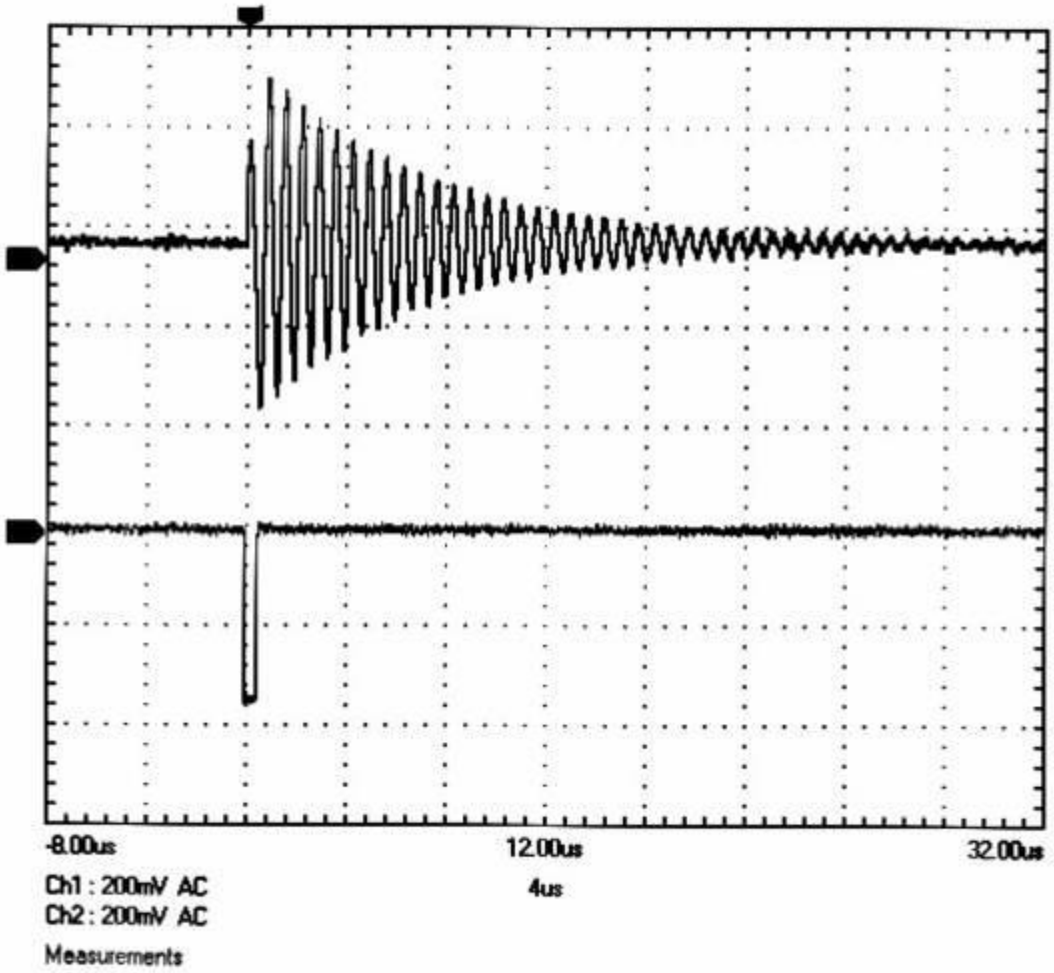

Figure 9 An input signal (lower) and damping oscillations (upper)

The current pulses from the Q1 collector cause oscillations damping in the LCR tank. The fact that R is connected to the tank through the capacitor C1 (not directly) is not relevant for the work of the circuit, since the C1 value is considerably higher than the C tank capacity. Figure 9 presents the input pulse and the damping oscillations it causes. These oscillations are further amplified by the two-stage amplifier-limiter on OA U2 and U3 in **Figure 10**. The amplifier-limiter consists of two identical non-inverting stages. The gain of each amplifier stage at 1.5 - 2 MHz operating frequency is equal to:

$$Gain_{amp} = 1 + \frac{R\_FB}{R_0} = 6.1$$

Respectively, the complete gain is equal to $Gain_{full} = Gain^2_{amp} = 37.21$

The output signal from the amplifier enters the comparator U_4 non-inverting input.

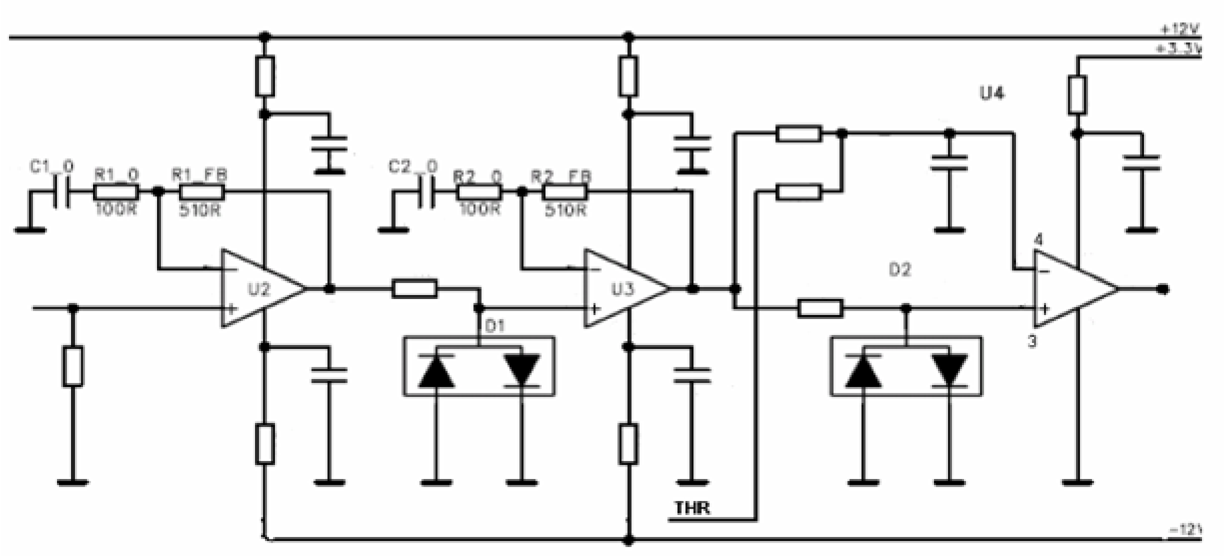

Figure 10 Amplifier-limiter

At large signal values operational amplifiers go saturated, limiting the magnitude of the half-waves of damping oscillations. The diode limiters provide an even larger level of limitation D_1, D_2. Since the threshold of the comparator is significantly lower than the limitation level, when the amplitude of oscillation decreases to the value close to the threshold, the amplifier returns to the linear work. It is very important to ensure that the operating point - the constant component of the input signal of comparator, returns to the initial level (which was before the excitation of the tank by the input pulse). In view of a certain asymmetry of levels of limitation, both of OA and of diodes, the capacitive coupling between the stages of the amplifier and the comparator can results in the displacement of operating point after large input signals, because of the recharge of coupling capacitors, which might require significant time for their discharge and operation point restoring. To avoid this, the DC connection is used between the stages of the amplifier and the comparator. At the same time, to decrease the influence of the temperature and time drift of input current of the U_2 and the bias voltages of U_2 and U_3, the DC gain of the amplifier is limited by means of capacitors C1_0 and C2_0 to the value of 1. Since even in this case the zero drift at the U_3 output can reach $20mV$ and more, the threshold of U_4 comparator is set relative not to ground, but to the DC output voltage of the amplifier U_3. The shapes of signals in different points of amplifier are demonstrated in the oscillograms presented in Figure 11. The output signal of the amplifier can be divided into 2 zones. In the zone I the amplifier works in the limitation mode, while in the zone II it works in the linear mode. To ensure the correct work of LADC, it is necessary to provide a threshold of comparator significantly lower than the limitation level, i.e., so that the comparison of the amplitude of oscillations with the threshold value would occur in the zone II, which actually occurs in our case. The threshold of the comparator is determined by the voltage entering from the output of the Digital-to-Analog Converter (DAC), signal THR1, and can be remotely programmed. While the amplitude of the oscillations entering the comparator U4: 3 exceed the threshold value of VU4: 4, each oscillation causes the generation of an output pulse of standard amplitude 3.3V, Figure 12 CompOut. The comparator IC used has input hysteresis about 4mV, which ensures the pure form of the output signal.

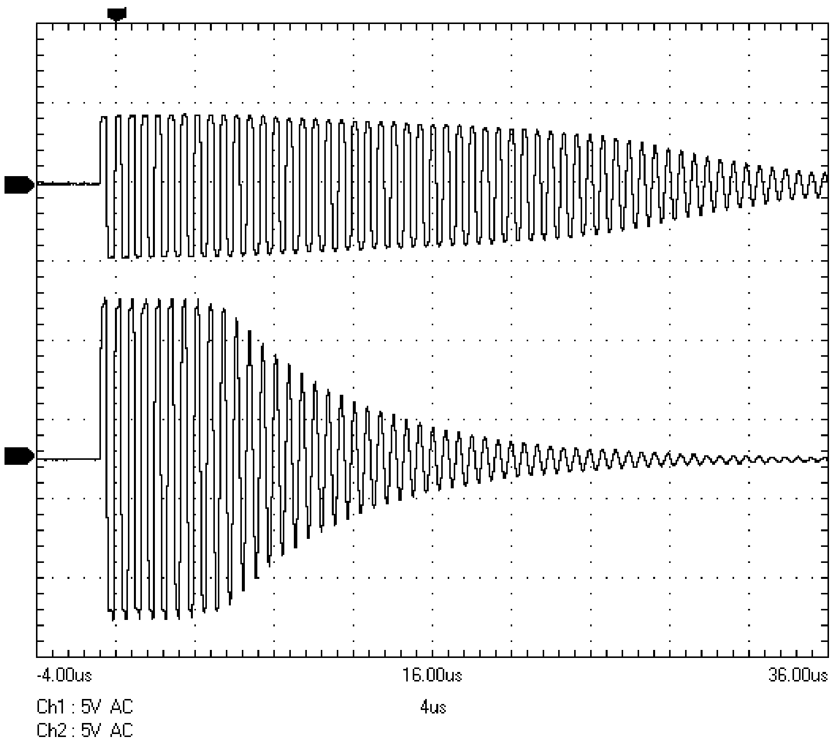

Figure 11 The output signal of the first stage of amplifier (lower) and input signal of comparator (upper)

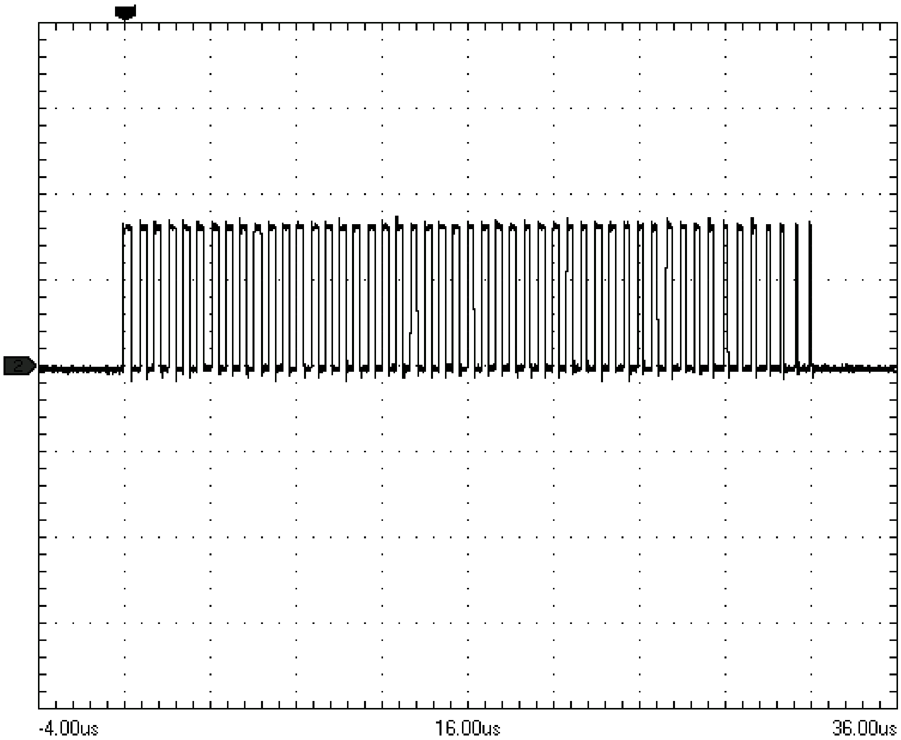

Figure 12 Comparator output signal

After the excitation of oscillations, their amplitude falls according to the law:

$$V = V_0 e^{-\frac{wt}{2Q}} \tag{1}$$

where V_0 is the initial amplitude of voltage, w the resonance frequency, Q - the quality factor of the tank. It is possible to rewrite the formula as

$$V = V_0 \cdot e^{-\frac{\pi N}{Q}} \tag{2}$$

from which

$$N = \operatorname{int}\left[\frac{Q}{\pi}\ln\frac{V_0}{V_{th}}\right], \text{ for } V_0 > V_{th} \tag{3}$$

where V_{th} – is the threshold voltage of comparator.

The (3) shows, that for providing the necessary conversion coefficient, it is necessary to have the stable Q-factor and a possibility to choose its value. In the previous versions of LADC the home-made induction coils with screw core from soft iron for the introduction of the necessary quantity of losses were used as L. The regulation of Q-factor was produced by the rotation of screw, which simultaneously changed the resonance frequency of the oscillatory tank. However, we implemented a different approach to guarantee the ease of fabrication, high reliability and stability. A highly reliable industrial inductor with the high Q-factor initial value is used as L. The desired resulting Q-factor is hard set by shunting LC tank with a stable and precise resistor R. Since the resistance of resistor depends on the temperature and other destabilizing factors much less than losses in iron core, this solution allows to choose the necessary Q-factor, simply by selecting the resistance of R, and high stability of its value. In our case the Q-factor is selected so that the change of the amplitude to 10 times, produce a change in the number of pulses of output sequence equal to 23. Respectively, (3) is changed into:

$$N_1 = \mathrm{int}[\frac{Q}{\pi} \ln \frac{V_0}{V_{th}}]$$

$$N_2 = \mathrm{int}[\frac{Q}{\pi} \ln 10 \cdot \frac{V_0}{V_{th}}]$$

where $N_2 = N_1 + 23$.

$$\frac{Q}{\pi} = \frac{23}{\ln 10} = 10$$

where $Q = 10\pi = 31.4$

Hence, the required value of the tank Q-factor is approximately 31.

As (2) demonstrates, the total conversion factor is affected by the PMT pulse shape and amplitude, which, in turn, depends on the efficiencies of the scintillator, photo-collection, photoelectric cathode, on the PMT feedings voltage and so on. In the described device the controlled parameters are the feeding voltage of FEU and the threshold of LADC comparator. These parameters are remotely preset and they can be re-set in the process of the experiment. However, tuning of these two parameters is insufficient to guarantee the complete identity of the channels and, ideally, additional adjustments are required (PMT anode load, resonant frequency, Q factor). Since the absolute calibration of the entire chain from scintillator to the output sequence is completely stored for calibration and stability monitoring purposes in the off-line mode, we decided not to use in the hardware design such additional adjustment components as potentiometers and trimming capacitors, which significantly worsened the reliability and maintenance. Structurally, all 8 LADC are located on one printed-circuit board. To simplify the installation and decrease the cost, the channels are not separated from each other by external screens; the problem of the channel interaction is solved as follows. First, the inductors of the oscillatory tanks of adjacent channels are chosen in a mutually perpendicular fashion, which sharply decreases the magnetic coupling. Secondly, by alternating the capacitances of contour capacitors, the resonance frequencies of adjacent channels are relatively shifted according to each-other approximately by 10-15%. In case of maximum amplitude values of input pulses, low oscillations can be observed in the adjacent channels. However, because of the sufficiently high values of the Q-factor, the oscillations decrease gradually and up to the moment of the end of time gates (see below) they do not reach the lowest threshold level**.** The comparator threshold is set by the output signal of programmable DAC. One eight-channel DAC IC is used for threshold setting of all eight channels of the LADC board. The output pulses of the comparator are taken to the IC of Complex Programmable Logic Device (CPLD) of the XILINX CoolRunner-II type that is used for identifying the event, counting the pulses of LADC outputs and sending the counters data to the microcontroller module. All signals from the detectors, received during the specific interval of time, named gate, are considered as belonging to the same physical event. The gate value is set by CPLD and indicated as a logical signal GATE. The identification of the event and the corresponding trigger of the gate are initiated by the pulse, received in any of the 8-channels. The information about detectors which pulses where received during the gate interval is read out and stored at the end of the gate. Information is stored in the CPLD as a bite mask, named EVENT, in which one bit corresponds to the one input channel. The 1 in this bit means, that the pulse from the detector entered this channel during the gate period. The gate duration is fixed with the binary code (N_{Gate}) hard soldered on the input pins GWIDTH0-GWIDTH3 of CPLD and is equal to

$$T_{Gate} = \frac{N_{Gate}+1}{12}\mu s$$

In our case N_{Gate} is selected as equal to 7, which corresponds to the gate duration of 0.666 micro-seconds (us). On the one hand, this value ensures time sufficiently large to register all pulses caused by one physical event, taking into account the spread of detector parameters, the lengths of cables and so on. On the other, it reduces the probability of registering two different events as one to the negligibly low value. In addition, the parasitic oscillations in the tanks, induced by the large amplitude pulses from the adjacent channels, mentioned above, do not manage to increase to the threshold values. With the beginning of the time gate, the inputs of all eight counters in CPLD opened and counter start counting the pulses of the packets, entering from the LADC outputs. The signal DURATION, reporting to the microcontroller that the process of event registering goes on is also generated when the event starts. This signal is removed approximately in 1 microsecond after the longest pulse packet ends. After the signal ends, the inputs of all counters are closed and the microcontroller begins reading out the information accumulated in CPLD: EVENT bite and one bite of counter for each of eight channels. After registering channel information, the microcontroller issues the RESET pulse on CPLD, indicating the end of event. Receiving this pulse, CPLD resets all counters and EVENT byte into the initial (zero) state. Thus, the system is ready to register the following event. The total dead time of system consists of the count time of the longest pulse packet plus the information processing time of the microcontroller (see below) and is about 100us long for the worst case of the maximal input pulse amplitude. For signals, corresponding to the maximum of the so called “one-particle distribution” tuned for 5-th channel of spectrum, value of the dead time is about 20us. The LADC module is designed in such a way that up to four LADC boards can be connected to one microcontroller, thus, forming the 32- channel DAC system. Figure 13 demonstrates such connection carried out with flat cables with 5 connectors on each. To simplify the construction, all connectors are fixed to the cable directly, without any over-twisting for the selection of the device number (practice standard for PC). Instead, each of four boards is identified by the address set on the board collected with the jumpers J10, J14.

The accepted scheme of jumper setting is as follows:

1 board (ASNT)– do not install,

2 boards (NAMMM) – do not install on the lower board, install both jumpers on the upper one,

4 boards- from bottom to top: 0,0; J10,0; 0, J14; J10, J14

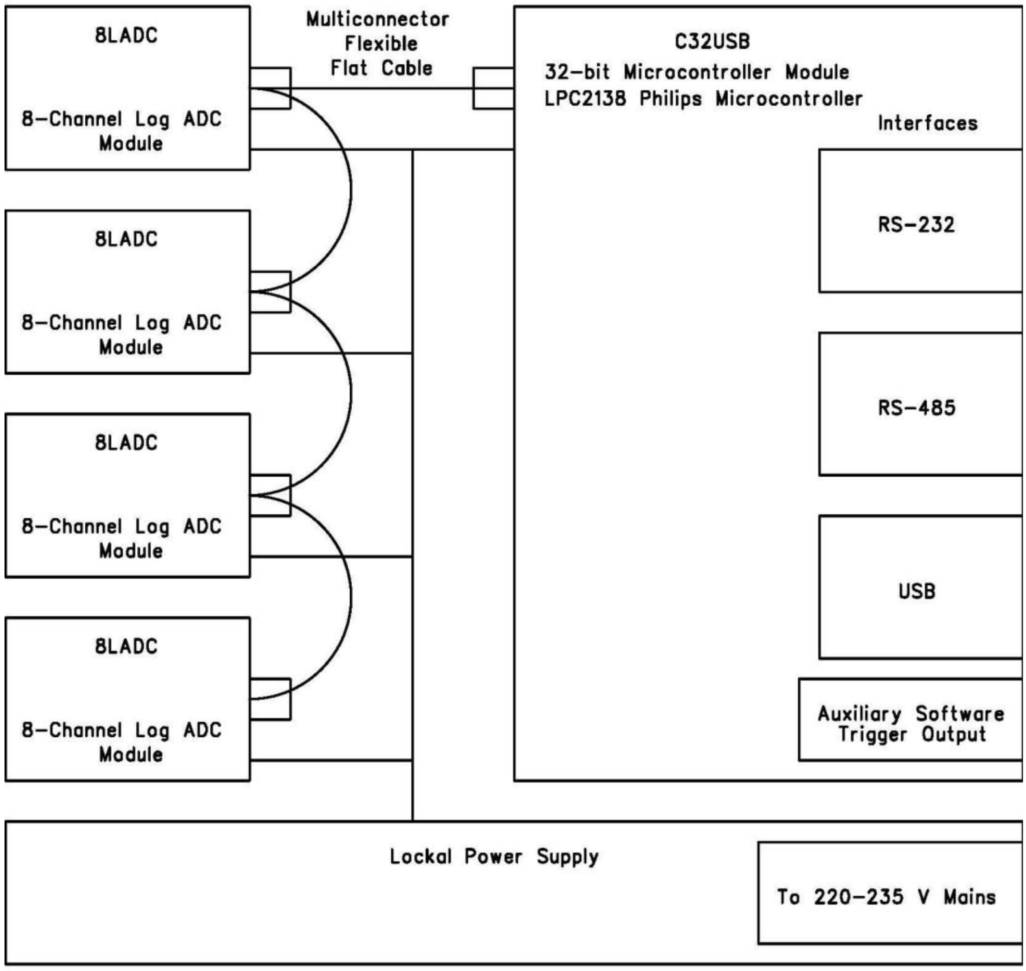

Figure 13 Assembling 4 LADC and microcontroller modules in one unit

The setting of the addresses serve both for the selection of internal information of CPLD (EVENT byte + 8 counters) and for determination of the thresholds. In case of erroneous setting of the cross connections DAC is not programmed and the threshold values are set as equal to zero, which is easily detected by the continuous counting (the LED burn) along all channels, no matter whether the cables are plugged or not. When cascading, it is important to satisfy the following condition: the impulse arrival on the entrance of any of the LADC boards is considered as an event, whereas completion of longest of the pulse packets of all boards is viewed as the end of an event. Therefore, the CPLD outputs for the signals GATE and DURATION are programmed as outputs with the open collector and the logical inputs connected to it. This allows combining these signals as a wired OR.

The readout of information from CPLD of the 8LADC boards into the module of microcontroller C32USB is provided by the parallel code on the 8- bit bus. Eight 8-bit pulse counters of LADC and

8- bit EVENT register, total 9 registers, are addresses inside CPLD. To address them, it is necessary to have the 4-bit address, presented by the microcontroller at the lines SEL0-SEL3. The addresses from 0 to 7 are used to select each of 8 counters, while any address in range 8-15 selects one and the same register - the register of event mask (EVENT). The C32USB module is based on the NXP company LPC2138 microcontroller of the ARM. It is designed as a multifunctional embedded data processing device for the initial on-line processing of data of arbitrary nature. The flexibility of the module application is provided by the possibility to work with any one of interfaces included in the system. The following interfaces are realized:

1. RS-232 for the connection to PC COM port. The rate of exchange is up to 115200 Baud. This port can be used also for the microcontroller IC firmware reprogramming.
2. USB 1- for connection to PC with virtual COM port driver. The exchange is provided through the UART micro-controller interface. The rate of exchange is up to 115200 Baud. This port can be used also for the microcontroller IC firmware reprogramming.
3. USB 2- for the high-speed exchange of information between PC and the microcontroller. Uses the parallel exchange of information between the USB interface IC and the microcontroller. The program access from the PC is provided with the driver of virtual COM port with the speed of exchange up to 115200 Baud and with DLL driver, which, in theory, can ensure the rate of exchange approaching the maximum speed, full USB2 - 10 MBaud.
4. RS-485. It is used for connecting the microcontroller to the local detector control system DCS network.

As the electronic devices, assembled on the basis of C32USB module can be used for the detector setups placed in distant places with difficult maintenance, it is very important to have WEB interface not only for the installation of the detector parameters (thresholds, the voltage of PMT supply), but also for the reprogramming of microcontroller itself. This possibility is necessary for the software modernization at changing conditions of physical experiments, i.e. for changing of so called “software triggers”, selecting data for different physical problems. Software triggers are altered by replacement of the consequences of coincidence and anti-coincidence, replacement of the conditions of the program-generated triggers and so on. Two of the realized interfaces make it possible to remote reprogramming the microcontroller by WEB interface. The micro-controller software consists of system and problem-oriented parts. The system part includes initialization of I/O ports, watchdog and interval timers, interruption handlers and main input-output, local network managing, and other similar functions. The problem-oriented part, called Aragats Data Acquisition System [56] includes pre-processing, storage and sending to the host PC data, collected from the detectors. In particular, the amplitude spectrum for each of the detectors is accumulated, coincidences and anti-coincidence are processed, the particle arrival directions statistics is accumulated, the program triggers are generated and so on. The software is written in the C language, using the free distributed GNUARM software. Some fragments of the code are written on the assembler to achieve the peak output. As an example of the DAQ electronics and software operation we present in Figure 14 histograms of the energy releases in thin and thick scintillators of the ASNT. Maximums of both distributions correspond to the mean energy release in 5 and 60 cm. scintillators (see details in [11]).

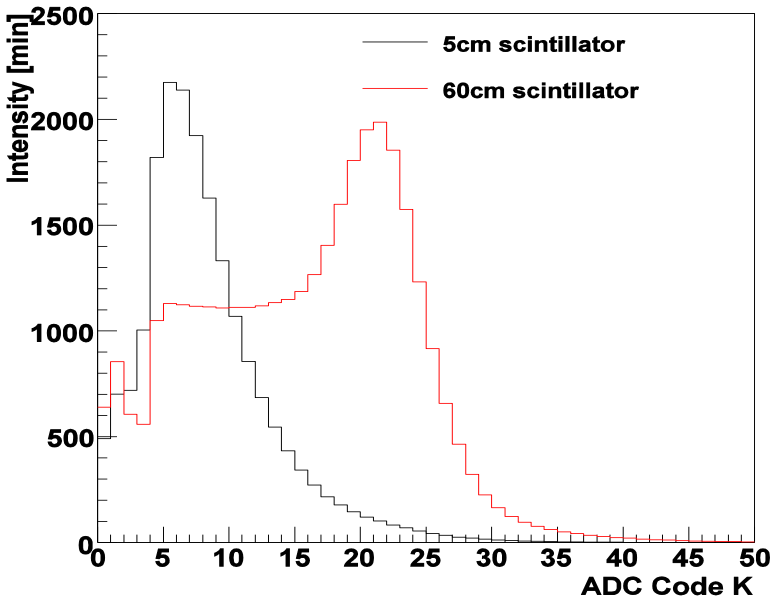

Figure 14 The histogram of the energy releases (pm amplitude spectra) as measured by the ASNT layers during a day.

1.3 24-Channel Neutron Monitor (NM) Readout Module

The main function of the 24 Channel Readout Module is receiving and counting of the 18-channel Neutron Monitor signals. It also has 6 auxiliary universal counter channels.

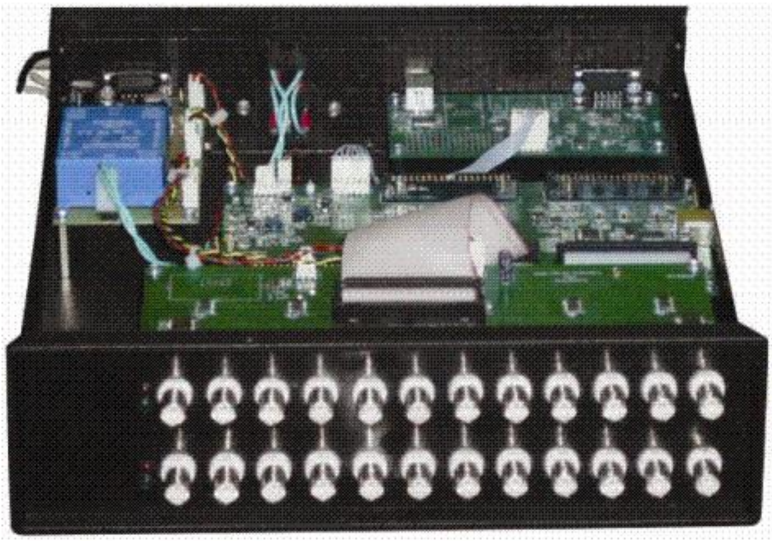

Figure 15 24-Channel Neutron Monitor (NM) Readout Module

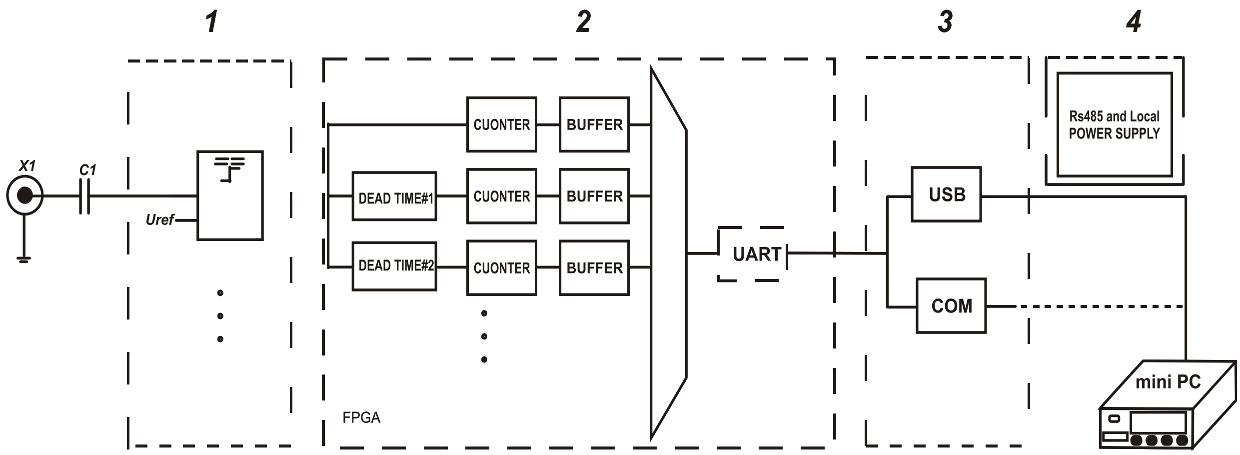

Figure 16 Functional diagram of the NM readout electronics

In **Figure 16** we present the diagram of the NM readout electronics. It consists of:

1. **Two Programmable Threshold 12-channell Discriminator/Counter boards.**
2. **Universal Multichannel Event Counter (UMEC) board.**
3. **Universal Microcontroller Interface module (MultiIFC) board.**
4. **RS-485 and Local Power supply module.**

Pulses from the detector preamplifier are discriminated and shaped in the unit 1. The discrimination threshold can be programmed in range 4mV-1000mV with 4mV step. Duration of the output TTL pulses is 400ns. The shaped pulse enters the input of Xilinx Spartan 3E FPGA (Field Programmable Gate) in the unit 2. Inside module, the FPGA pulse is applied to three counters: to the first – directly, and to other two through programmable dead time circuits. The dead time values are preset to values of 250us (#2) and 1250us (#3) (see **Figure 17**). The last value coincides with one used for both Neutron Monitors at Aragats and Nor-Amberd during 23rd solar activity cycle (1996-2007). Along with 18 programmable channels with 3 dead times (total 3x18 counters), the unit has 6 inputs for direct counting (without dead time circuits). The contents of all 60 (3*18 + 6) counters are downloaded each second in plane ASCII code to the PC through USB (or COM) interface. After downloading, all counters are instantly zeroed and start to count again. Along with the main output connection, the unit has a RS-485 interface for connecting to the Detector Control Local Net of experimental setup for the on-line programming of the thresholds.

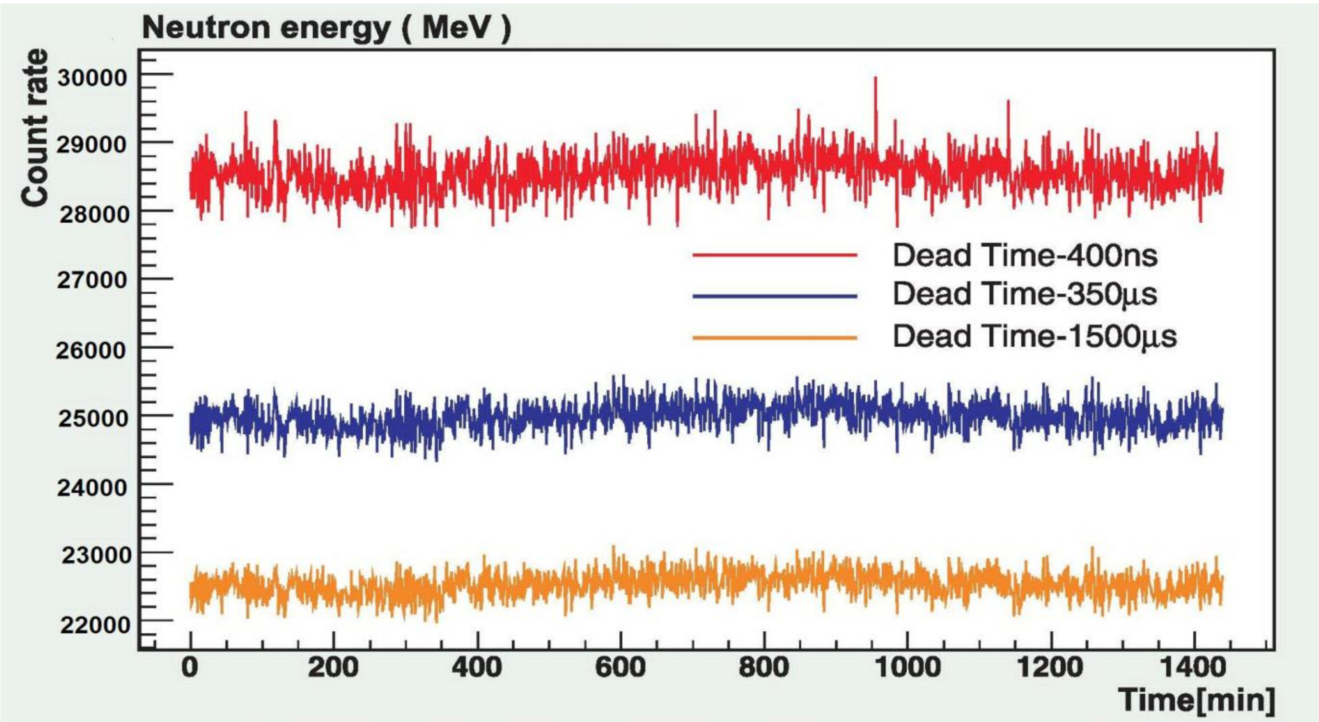

Figure 17 Tree time series from Aragats Neutron MonitoR

1.4 Electronics of large undergraound muon detector

The Aragats Multichannel Muon Monitor was equipped with scalers (electrical pulse counters) based on the old descrete elements of soviet-times. The Pentiun-1 computers were used for data acquisition. To provide stable operation of the AMMM during 24th solar activity cycle (2008 – 2019) we have designed compact and reliable DAQ electronics based on FPGA Xilinx Spartan3E chips. **Figure 18** demonstrates a single unit of new electronics. It is comprised from 2 boards containing 60 counters each, power supply, and ATNGW100 Network Gateway Kit equipped with AVR32 Digital Signal Processor (ATMEL AT32AP7000). The ATNGW100 is equipped with 32 MB SDRAM, 8 MB data flash and 2 GB SD flash memory (see Figure 19). The communication is feasible through two Ethernet ports, UART, USB, and JTAG. The external storage can be connected using SD and MMC card reader.The FPGAs are programmed to realize 60 asynchrony counters to the serial port. In the preloaded LINUX system the serial ports are attached to /dev/ttyS1 и /dev/ttyS2. The system console port is attached to /dev/ttyS0. To provide access to third serial port we have recompiled a LINUX kernel. The port parameters are 8/n/1 115200 b/c. Each second the counters are transferred to ATNGW100 and are stored in hexadecimal format in 120 bite portions. Once a minute the data are archived to the /media directory which reside on the mounted flash card. If the flash card is not installed, the /media directory is mounted to the embedded flash memory. The time synchronization is performed by the NTP client installed on NGW. FTP server is configured to serve the data to data acquisition software. Remote control is enabled by means of SSH and Telnet servers. The data transfer software twice a second read out serial ports buffers and integrate it up to 1 minute. Then 1- minute data are transferred to ATNGW100 in 120 bit portions and are stored in hexadecimal format. The number of blocks is checked and in the case if it's not equal to 60 (number of seconds in a minute) the minute count is proportionally scaled.

Figure 18 120-channel FPGA-based counter with under control of ATNGV100 network gateway kit

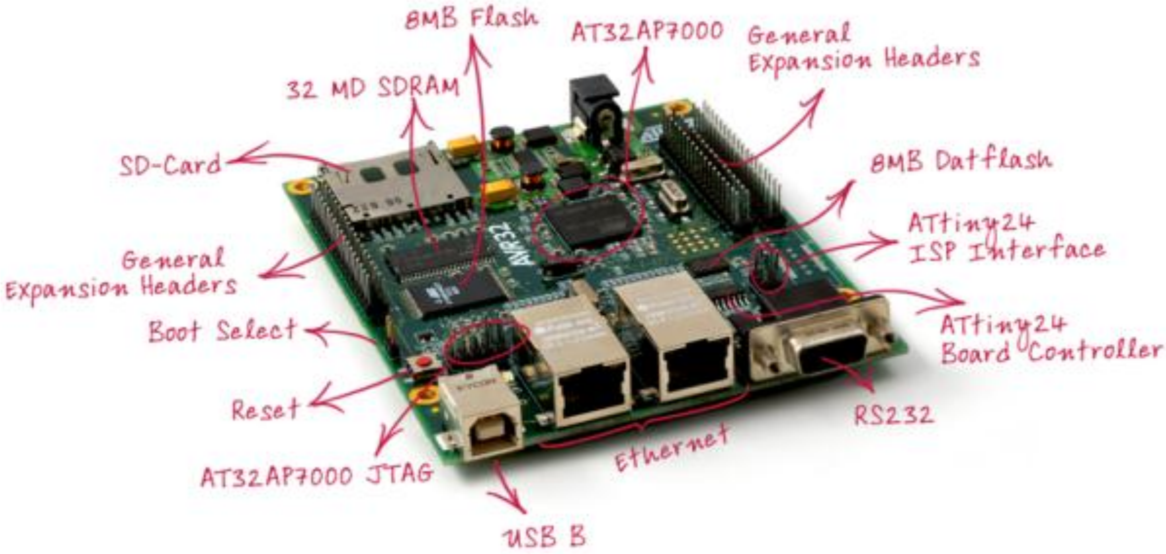

Figure 19 ATNGW100 Network Gateway Kit

During exploitation the new DAQ electronics failed to fulfill requirements of stability and accuracy. The a-synchronous counters discharge due to instability of FPGA clock lead to overflow and system often hangs. To overcome this difficulty the synchronous discharge was established; additional 20 nsec (2 ticks) time delay was introduced after discharge.

Distortions were detected due to noise in the connections of FPGA boards with ATNGW100. Several checks and consequent corrections were introduced in software as remedy.

1.5 SEVAN DAQ Electronics

A network of middle to low latitude particle detectors called SEVAN (Space Environmental Viewing and Analysis Network) [15] is planned in the framework of the International Heliophysical Year (IHY), to improve fundamental research of solar accelerators and space weather conditions. Besides the main DAQ function, the unit also acts as a master for the detector control Local Area Network (LAN) which is used for programming and monitoring high voltage values and for programming the ADC thresholds. Data Acquisition electronics implementing registration of the charged and neutral fluxes of secondary cosmic rays consists of 8-Channel Discriminator/Counter Unit (8DCU) and 3 High Voltage supplies with presetting and automatic control, which are located in the corresponding PMT cases. 8DCU parts are: The 8-channel Programmable Threshold Comparator and Counter board (8CNT) Universal RS232/RS485 interface/power supply module - IFCC, Power transformer - 220V50Hz to 2x8V 0.5A + 2x15V 1.25A (**Figure 20**)

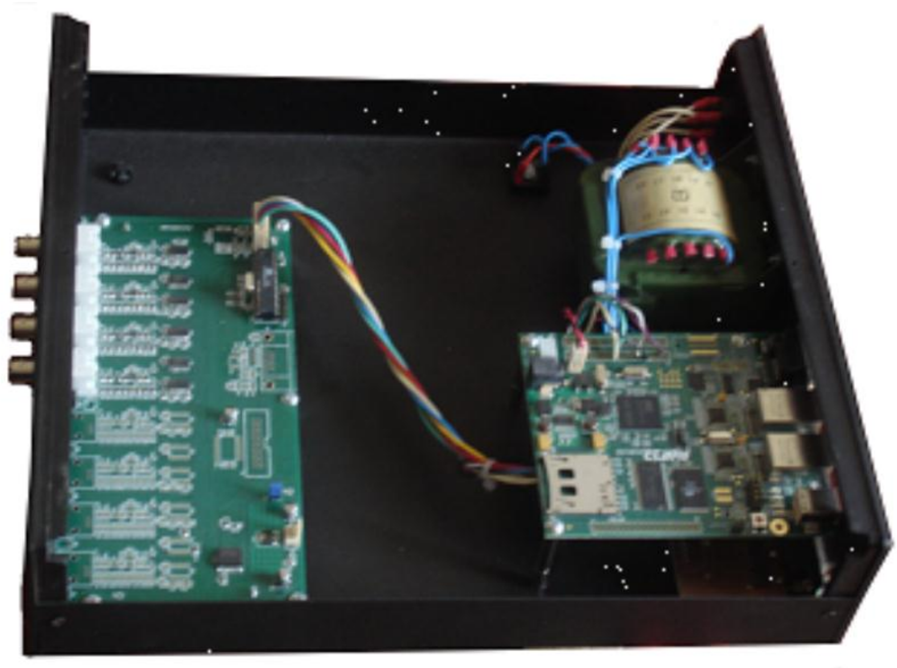

Figure 20 SEVAN DAQ module

The main features used in 8DCU are:

8 programmable threshold analog input,

Threshold programming range 4mV-1000mV with 4mV step, Powered by AC 50-60Hz 220V, 30W

Maximal counting frequency – 60kHz,

LEDs to indicate the input pulses in each of 8channels, module power and programmable trigger condition, 8 input BNC connectors, 8CNT board is used as a standalone 8-channel counter (scalar) with a programmable threshold. For the threshold programming and the output data readout, it can communicate with the host PC (local network) through the IFCC module by any of RS-232 or RS-485 interface ports. The module counter and interface logic is based on the Atmel AVR Atmega88 [53] 8-bit microcontroller. The same ATNGW100 Network Gateway Kit equipped with AVR32 Digital Signal Processor CPU (see previous section) is used as on-line PC for SEVAN modules. DAQ software consists of the host PC program and the microcontroller program (firmware). The firmware for the DAQ and control is written in C language and stored in the microcontroller reprogrammable flash memory. Below is presented the functionality, implemented for the SEVAN detector setup. In this case the microcontroller operates both for the thresholds presetting and control and as a main DAQ controller, with functions listed below:

1. Counting of signals in each of 8 channels,
2. Counting of all types of coincidences of signals in channels 1-3.

The data collection time is set by the microcontroller firmware, so any other value can be chosen. The IFCC interface module has three connections: to the microcontroller, to the RS232 connector (DSUB9F) and RS485 connector (DSUB9M). The signals propagate from each of the mentioned connections to both of others. The power for the PMT High Voltage supplies (15V unregulated, 1.2Amax) is supplied from the 8DCU through the RS485 interface connector. The counters' contents are sent out via RS232 or/and RS485 interfaces each second in the format:

Cnt1 Cnt2 Cnt3 Cnt4 Cnt5 Cnt6 Cnt7 Cnt8

Co12 Co13 Co23 Co123

<blank line>,

where CntX – is the count of pulses in channel X in 1 second, CoXY(Z) – is the count of coincidences in channels X, Y. For example, Co12 is a number of coincidences in channels 1 and 2, without signals in channel 3. The gate for the coincidences registration is in the range 0.6us - 1us. If signals in two channels come with a delay of more than 1us, they are not considered as coincident. The dead time of the counters is 10us. The data collection time is set by the microcontroller firmware, so any other value can be chosen.

1.6 Programmable Regulated High Voltage DC Power Supply (PRHVPS)

The Programmable Regulated High Voltage DC Power Supply is designed to supply high voltage to different electrodes on photomultipliers and various elementary particle detectors (see Figure 21). Industrial DC-DC power supplies usually need for the remote control ADC-equipped cards [54]. Our solution consists in high voltage power supply with build in controlled Via serial interface RS-485. Using the ATNGW100 Network Gateway Kit it is possible to remote tuning of the thresholds of discriminators and high voltage values for detector channels via Ethernet port. The PRHVPS consists of:

- Current-driven, low-noise sine wave DC/DC converter, with up to 2 stage RC output ripple
- Pulse Width Modulated programmable DC regulator
- Local +5V linear voltage regulator
- Atmel microcontroller
- RS485 interface chip
- Optional temperature sensor

The Printed Circuit Board (PCB) can be assembled with various options for different output polarity, programmable voltage range, and so on.

Specific Features:

- Voltage programming in two hardware selectable ranges ± 900V to 2100V and ±1500 to 3000V in 2V steps
- Output voltage ripple less than 5mV
- Max. output current 1.2 mA for ± 900V to 2100V range; 0.8 mA for ±1500 to 3000V range
- Input voltage from +12V to +15V
- Absolute output voltage regulated to accuracy ±1V
- Optional temperature sensor

- RS-485 half-duplex 2-wire 9600 baud interface for programming and monitoring the output voltage

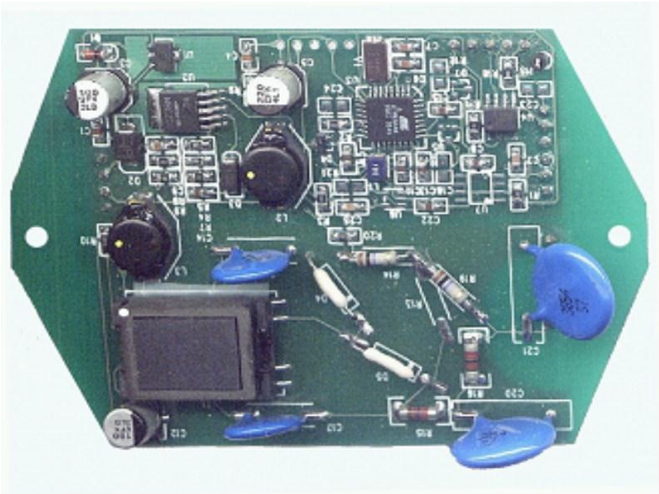

Figure 21 Programmable Regulated High Voltage DC Power Supply

After one year operation of most components of the ASEC DAQ it proves reliability and multifunctional possibilities. Several papers are published based on the new physical results enabled by flexible and powerful DAQ system. System is still under extensive testing and tuning to be ready for uninterruptable operation during started in 2008 24^{th} solar activity cycle. Work was supported by ISTC Grant A1554 and INTAS Grant 8777.

1.7 Atmospheric Pressure Measurements at the Aragats Space Environmental Center

Cosmic Ray flux incident on the terrestrial atmosphere and measured elementary particles on the Earth surface comprise very different entities although genetically connected with each other. Primary particles interactions with atmospheric nuclei and different methodological effects can hide genuine variations of the primary flux and prevent from understanding of dynamics of ongoing physical processes in solar-terrestrial chain. To recover the primary particles fluxes incident on the Earth's atmosphere it is necessary to know the relationship between observed count rates of the detectors and the primary particles fluxes, as well as the influence of the meteorological effects on the flux of secondary particles reaching the Earth surface. Dorman's theory of meteorological effects (Dorman, 2004) gives detailed classification of the effects; mentioned the barometric one as a major influencing particle fluxes (at least for highest energies – 10-100 GeV). Therefore, it is of greatest importance to accurately measure the atmospheric pressure to “unfold” the solar modulation effects. And, consequently, the precise sensors equipped with automatic readout systems are the essential part of each monitoring system. The secondary component of the cosmic ray intensity is sensitive to variations in the atmospheric column density above the particle detectors. This leads to a change in absorption of the secondaries, and a consequent change in the counting rate. Local station pressure is a generally accepted measure for this column density. These pressure effects must be taken into account before the neutron monitor data can be used for cosmic ray studies. A period of high pressure is associated with more absorber above the detector and a lower detection rate results. The purpose of this investigation is to determine the relationship between barometric pressure and cosmic ray intensity.

Pressure measuring device is a general purpose microcontroller unit, designed for environmental measurements: pressure, temperature and humidity (see **Figure 22**). In addition to the main sensors mounted on the board, it has two auxiliary connectors with pinned out microcontroller input/output port pins, which can be used for other measurement and control purposes.

- It has two alternative interfaces to integrate it into a system: RS232 and half-duplex RS485. It has Frequency Modulated (FM) output TTL for compatibility with the existing Cosmic Ray The microcontroller software (firmware) supports all the mentioned sensors and interfaces and can be easily upgraded for additional measurements and control options.

Specific Features:

- Pressure sensor Motorola MPXA6115 [55] has 15 to 115 kPa measurement range with 1.5% maximum error in the 0 to 85°C temperature range. Using an external calibrating procedure, the error can be significantly decreased. The sensor is connected to a 16-bit ADC. The measured data is averaged in software to minimize the noise. The real pressure resolution depends on the averaging time and can be as good as 15-bit (~1/32000 of full scale).
- The ATMEL Atmega8-16AI microcontroller can be easily reprogrammed using the ATMEL standard serial programming protocol.

- The board has built-in +5V regulator, thus it can be powered by any regulated or unregulated power supply with 100mA current.

The digitized data enter microcontroller Atmega8 and then via serial interface RS-385 – one of channels of 24-channel Neutron Monitor readout module. The code (or frequency) is converted in the output voltage and then to pressure (see *Figure 23*).

The sensor output is linear with respect to the pressure in the 780 to 820 mbar range. The correlation line equation is P(mbar) = 0.1429 N + 112.46 with a $\chi 2$ fit of 0.9999

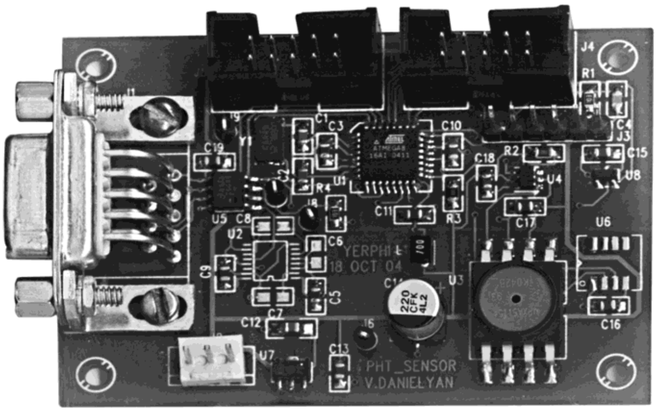

Figure 22 The Atmospheric Pressure measuring board

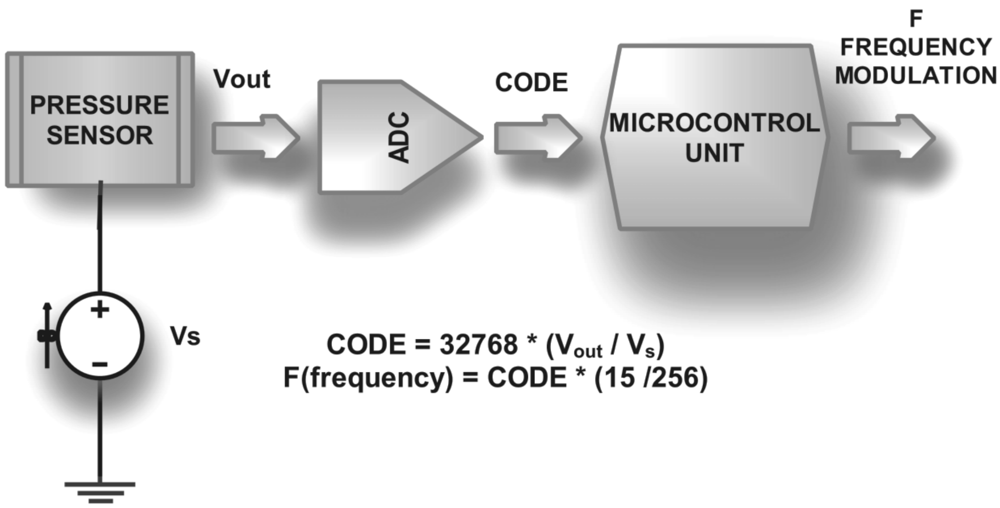

Figure 23 The scheme of Pressure measuring device

The atmospheric pressure is calculated from the sensor measurements by the following equations:

$$P = \frac{\frac{V_{out}}{V_s} + 0.095}{0.009} \pm \mathrm{PressureError}$$

$$\frac{V_{out}}{V_s} = \frac{code}{32768} = frecuency \times \frac{256}{15}$$

$$P \approx \frac{frecuency \times \frac{256}{15} + 0.095}{0.009}$$

Without calibration the atmospheric pressure measurements obtained from individual sensors can deviate from “true” value, according to the producer by 15 mbar. To calibrate the pressure device, we place the PHT sensor in a special chamber in which we can vary and measure the pressure with high accuracy (0.05mbar) using a mercury barometer. In Figure *24* the calibration curve for PHT sensor is depicted. The sensor output is a linear function of varying pressure in the range of 780 to 820 mbar. The correlation equation is P(mbar) = 0.1429 N + 112.46 with a χ 2 fit of 0.9999; where N is the sensor output. To check the factory parameters and to obtain relative accuracy of the measurements (the one needed to calculate the accuracy of, so called, barometric coefficient) we locate at each research station 2 identical sensors. As we can see from Figure 25 and Figure 26 the measured atmospheric pressure by both sensors is highly coherent shifted from each other by a constant value 4 – 7 mbar, consistent with producer’s data.

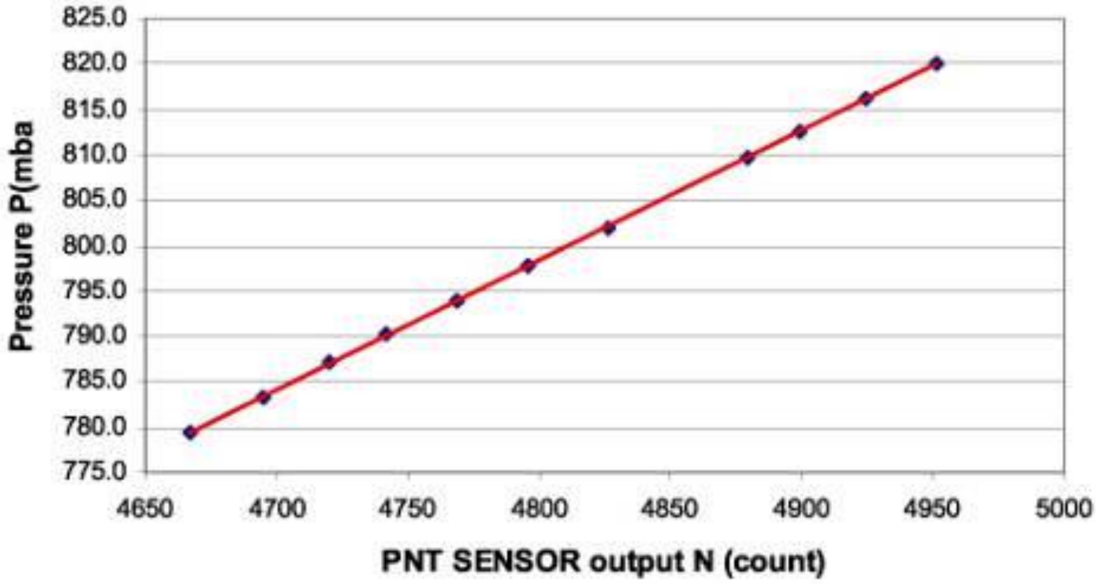

Figure 24 Calibration curve of the pressure sensor performed at Nor Amberd research station

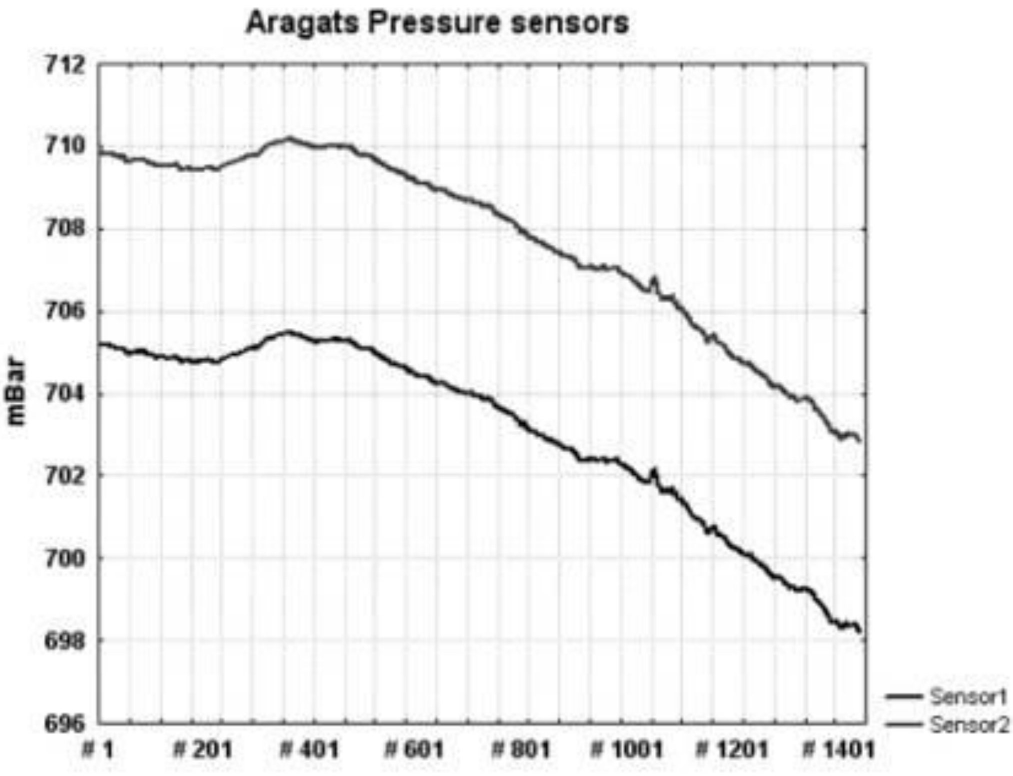

Figure 25 The daily variations of the atmospheric pressure measured at altitude 3200 m. by 2 independent pressure sensors of the same type.

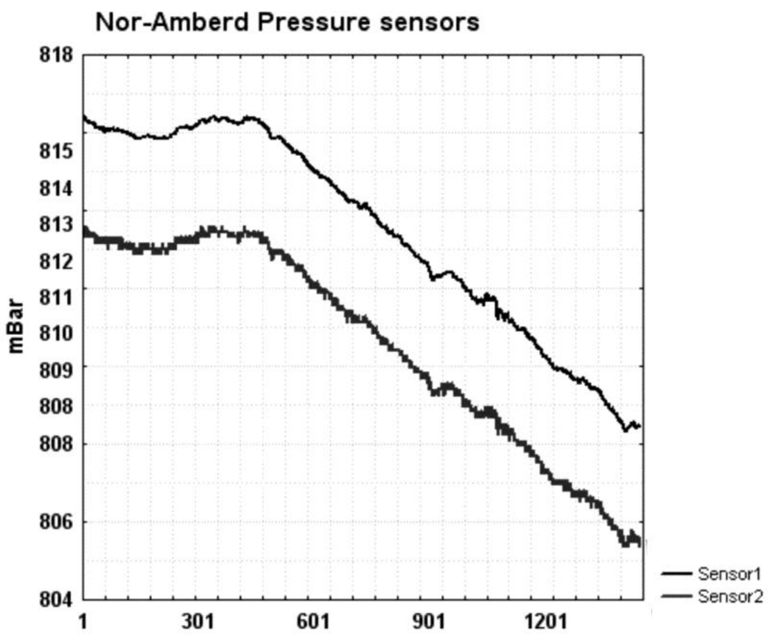

Figure 26 The daily variations of the atmospheric pressure measured at altitude 2000 m. by 2 independent pressure sensors of the same type

The bias can be eliminated by taking into account the calibration with etalon precise sensor described in the beginning of section.

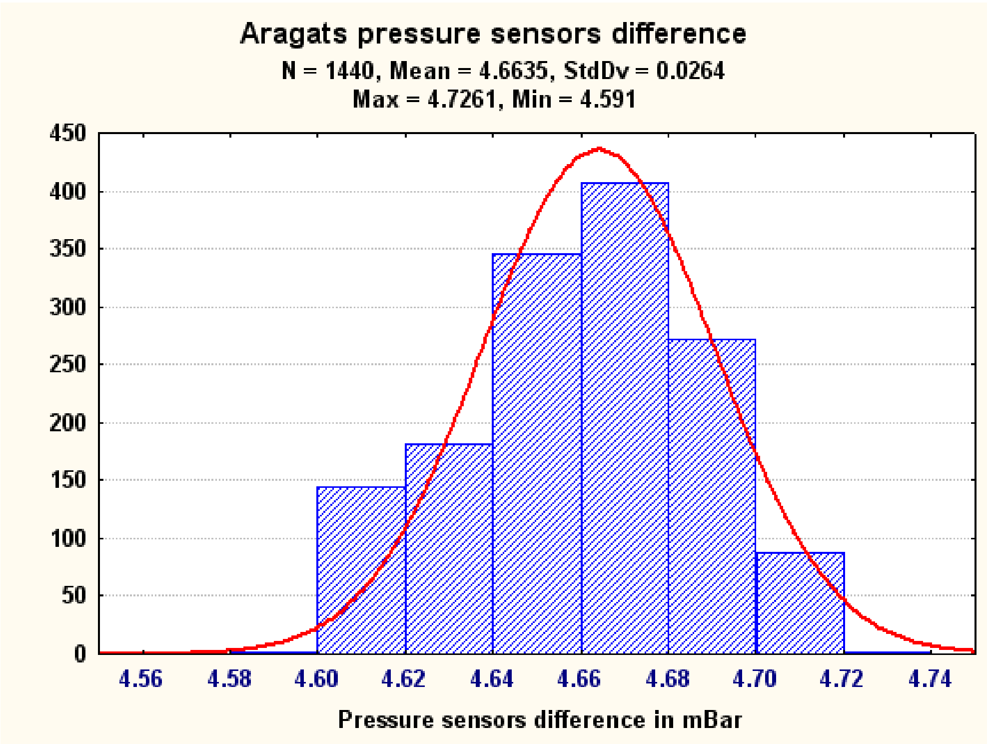

Figure 27 The distribution of the differences of measurements of 2 similar pressure sensors located at altitute 3200 m.

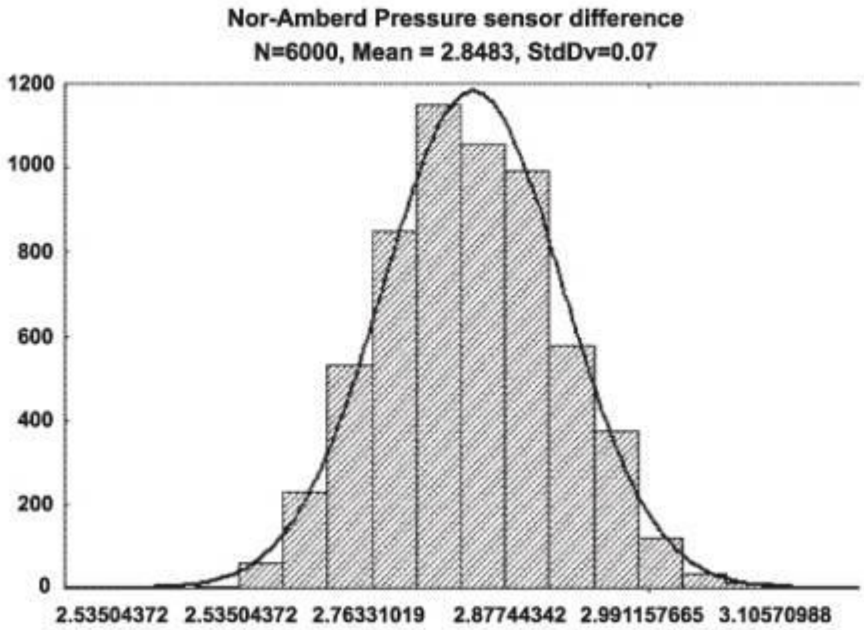

Figure 28 The distribution of the differences of measurements of 2 similar pressure sensors located at altitude 2000 m.

As we can see in **Figure 27** and **Figure 28**, the discrepancies (mean width on mean height) between sensors, located at the same altitudes is rather stable and doesn't exceed 0.07 mbar. Therefore, the accuracy of the single pressure measuring device can be estimated as not worse than 0.05 Mb (see details in [5]). As the barometric coefficients of both monitors located at Mt. Aragats are approximately -0.7 %/mbar (increasing of atmosphere pressure by 1 mbar, leads to decrease of monitor's count rate by ~0.7%) and that accuracy of 1 minute count rate of monitors is ~ 0.6% we can conclude that obtained accuracy of the atmospheric pressure measuring device is far enough for performing pressure correction of the neutron monitor count rates. To estimate the absolute accuracy of pressure measurements we should take into account also the accuracy of the calibration. The final absolute accuracy according to the measurements performs at Aragats and Nor Amberd with 4 serial sensors is not worse than ~0.05 mbar.

Starting from 2007 the count rates of the particle detectors belonging to the Aragats Space Environmental Center [1, 2] are routinely corrected for pressure before physical analysis. Among the brightest ASEC results is the discovery of the highest energy protons accelerated in the vicinity of the Sun on January 20, 2005 [14, 17]. High precision of the pressure sensors allows also meteorological research. In Figure 29 we post the atmospheric pressure curves measured at 3 different latitudes in Armenia.

Pressure correction should be made also in studies of the diurnal variations of cosmic ray flux. The amplitude of diurnal variations at minimum of solar activity is not greater than 0.5%; therefore very precise analysis of the atmospheric pressure variability is needed to disentangle atmospheric pressure and solar-terrestrial connections effects. In Figure 30 and Figure 31 we can notice periodicity in the daily pressure variations, better expressed in Nor Amberd at altitude of 2000m. Harmonic variations of pressure peaked at ~ 7 and 20 UT with amplitude of ~0.05%. Taking into account the atmospheric pressure variation allows, as we can see in Figure 30 and Figure 31, to emphasize the diurnal variations and estimates its amplitude and phase.

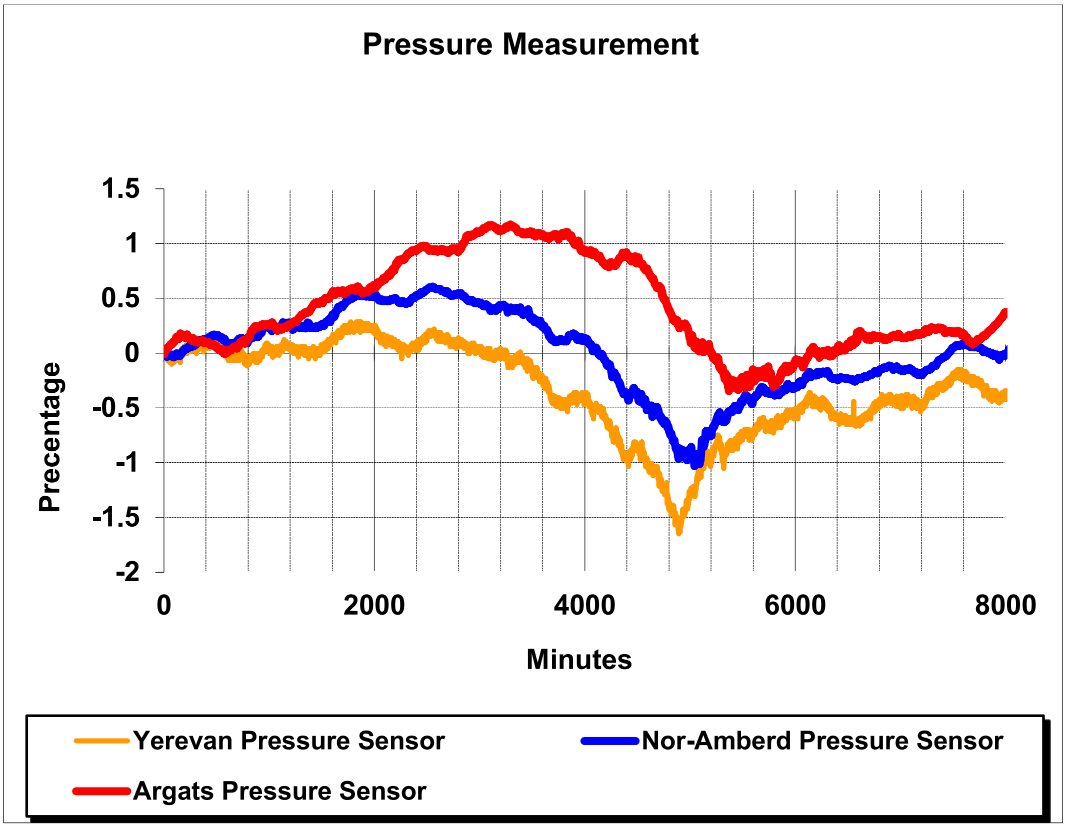

Figure 29 Measurements of pressure at different altitudes at 03 March 2009 till 09 March 2009

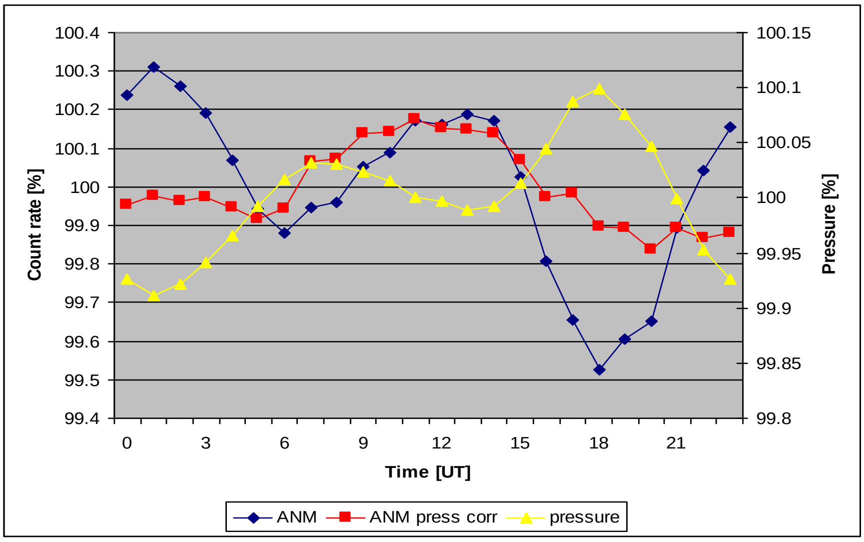

Figure 30 Daily variations of the atmospheric pressure and Aragats Neutron Monitor count rates. Note that correction to the pressure effects improves the shape of the daily count rates.

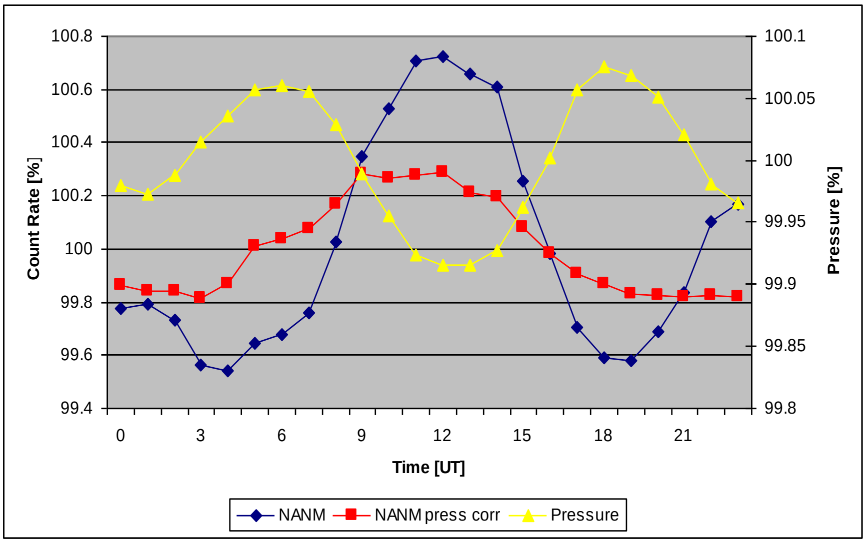

Figure 31 Daily variations of the atmospheric pressure and Nor Amberd Neutron Monitor count rates. Note that correction to the pressure effects improves the shape of the daily count rates

PHT sensor designed and fabricated in the Yerevan Physics Institute on basis of the pressure sensor Motorola MPXA6115. The device operates and supplies digitized data to the data acquisition systems of the Aragats Space Environmental Center at altitudes 1000, 2000, and 3200 m a.s.l. The accuracy of pressure measurements are not worse than 0.05 mbar, that is fully sufficient for the studies of the solar-terrestrial connections via variations of the secondary fluxes of the elementary particles detected on the Earth's surface. The device is reliable and simple in operation and can be recommended for the world- wide networks of particle detectors.

CHAPTER 2

SPACE ENVIRONMENTAL VIEWING AND ANALYSIS NETWORK (SEVAN)

INTRODUCTION

The sun influences Earth in different ways by emissions of electromagnetic radiation, interplanetary plasma structures and high-energy particles. Although the entire energy of the high-energy particles comprises very small fraction of the visible light energy, nonetheless the study of these particles gives clues about fundamental and universal processes of particle acceleration and their interactions with interplanetary magnetic field; thus providing information about the consequences of the huge solar explosions affecting the near-Earth environment, space born and surface technologies, i.e. space weather issues. During billions of years of its evolution, the Earth was bombarded by the protons and fully stripped ions accelerated in the Galaxy during tremendous explosions of the supernovae and by other exotic stellar sources. This flux was may change on the passage of the sun through the four galactic arms during its path around the center of Galaxy and was affected several times by huge explosions of nearby stars. Nonetheless, on the shorter time scales the intensity of the Galactic Cosmic Rays (GCRs) is rather stable. In turn, our nearest star –is capable of changing radiation and fluxes of the Solar Cosmic Rays (SCR) by 3–4 orders of magnitude in the span of a few minutes. Existing networks of particle detectors are unable to reliably detect very low fluxes of the SCR above 10 GeV; low statistics experiments often demonstrate fake peaks with high significances. Thus, for predicting upcoming radiation storm it is necessary to monitor changing fluxes of the different species of secondary cosmic rays with various energy thresholds. To cover wide range of SCR energies we need networks of particle detector at different latitudes longitudes and altitudes. A network of particle detectors located at middle to low latitudes known as SEVAN [15], [22] was developed in the framework of the International Heliophysical Year (IHY-2007) and now operates and continue growth within International Space Weather Initiative (ISWI). SEVAN detectors measure time series of charged and neutral secondary particles born in cascades originating in the atmosphere by nuclear interactions of protons and nuclei accelerated in the Galaxy and nearby the sun. The SEVAN network is compatible with the currently operating high-latitude neutron monitor networks ‘‘Spaceship Earth’’ [25], coordinated by the Bartol Research Center, the Solar Neutron Telescopes (SNT) network coordinated by Nagoya University [26], the Global Muon Detector Network (GMDN) [27, 28], the Eurasian Neutron Monitor Data Base [29, 30] and a new muon–neutron telescope constructed at Yangbajing, Tibet, China [31]. SEVAN modules are operating in Armenia (4 one m^2 standard modules and 2 super modules of 12 identical SEVAN units each arranged above and below 2 standard sections of Nor Amberd neutron monitor 6NM-64; both super modules are capable of muon direction estimation), in Croatia (Zagreb observatory), Bulgaria (Mt. Moussala, India (New-Delhi JNU Univ.) and are under construction in Slovakia (Mt. Lomnicky Stit).The potential recipients of SEVAN modules are Israel, Germany and Costa Rica (Figure 32). The similar detector is in operation in Tibet [31].

Figure 32. SEVAN network; World map with operating (red) and planned (blue) particle detectors.

SEVAN network provides reliable monitoring of the Sun by ~16 h per day. The particle fluxes measured by the new network at medium to low latitudes, combined with information from satellites and particle detector networks at high latitudes, will provide experimental evidence on the most energetic processes in the solar system and will constitute an important element of the global space weather monitoring and forecasting service. In the paper we present the description of SEVAN modules, its possibility to measure charged and neutral fluxes; excepted purities and efficiencies of secondary cosmic ray registration, as well as the first results of the SEVAN network operation. Also we demonstrate the ability to measure energy spectra of the solar protons by registering the GLEs; possibilities to distinguish between neutron- and proton-initiated ground level events (GLEs), and some other important properties of hybrid particle detectors. Separate chapter is devoted to registration of the Thunderstorm ground enhancements, new high-energy phenomena in the atmosphere. SEVAN modules, operated at slopes of Mt. Aragats in Armenia during recent years detect many TGE events in fluxes of gamma rays and high-energy muons, proving existence of the strong electrical fields in the thunderclouds initiating relativistic runaway electron avalanches in the thunderstorm atmospheres [23, 24]. SEVAN detectors was calibrated by the gamma ray flux of the most powerful TGEs and furthermore, the time series of the high energy muons detected by SEVAN open possibility to estimate the electrical structure of the thunderclouds, the key parameter for creating models of both TGE and lightning occurrences.

2.1 Design of SEVAN Particle Detectors

The basic detecting unit of the SEVAN network (see Figure 33) is assembled from standard slabs of 50 x 50 x 5 cm^3 plastic scintillators. Between two identical assemblies of 100 x 100 x 5 cm^3 scintillators (four standard slabs) are located two 100 x 100 x 5 cm^3 lead absorbers and thick 50 x 50 x 25 cm^3 scintillator assembly (5 standard slabs). A scintillator light collecting cone and photo multiplier tube (PMT) are located on the top, bottom and the intermediate layers of detector. The detailed detector charts with all sizes are available from http://aragats.am/SEVAN. Incoming neutral particles undergo nuclear reactions in the thick 25 cm plastic scintillator and produce protons and other charged particles. In the upper 5 cm thick scintillator charged particles are registered very effectively; however there is not enough matter for the nuclear interactions of neutral particles. When a neutral particle traverses the top thin (5 cm) scintillator, usually no signal is produced. The absence of the signal in the upper scintillators, coinciding with the signal in the middle scintillator, points to neutral particle detection. The coincidence of signals from the top and bottom scintillators indicates the traversal of high-energy muons. Lead absorbers improve the efficiency of the neutral flux detection and filtered low energy charged particles. If we denote by ‘‘1’’ the signal from a scintillator and by ‘‘0’’ the absence of a signal, then the following combinations of the 3-layered detector output are possible:

111 and 101—traversal of high energy muon; 010—traversal of a neutral particle;100—traversal of a low energy charged particle stopped in the scintillator or in the first lead absorber (energy less than 100 MeV).110—traversal of a higher energy charged particle stopped in the second lead absorber. 001—registration of inclined charged particles.

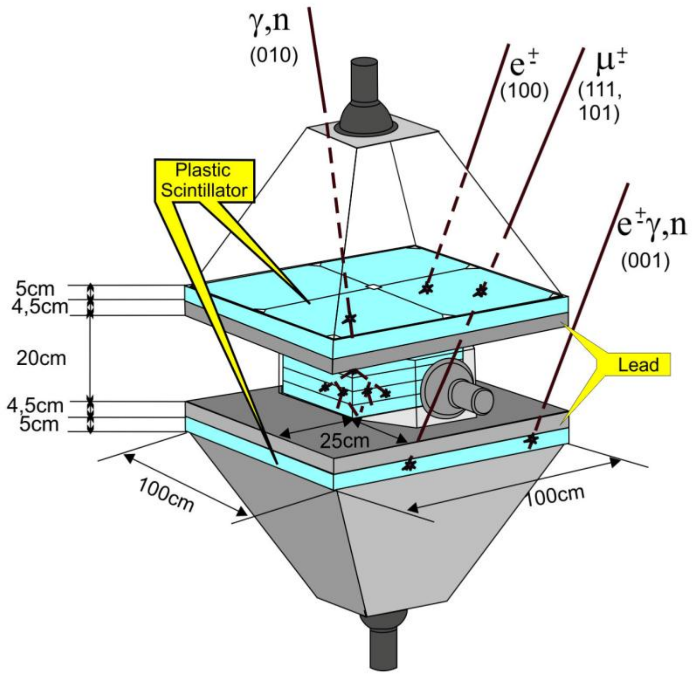

Figure 33.Basic detecting unit of the SEVAN network.

2.2 Characteristics of secondary cosmic ray fluxes detected by SEVAN modules

The modules of the SEVAN network located on different latitudes, longitudes and altitudes are probing different populations of primary cosmic rays. The SEVAN modules measure fluxes of neutrons and gammas, of low energy charged particles and high-energy muons. To understand the response of the new network to SEP events we calculate using CORSIKA code [32] most probable energies of primary protons to which the SEVAN modules, located at different latitudes, longitudes and altitudes are sensitive ([33], see Table 1). The calculations were made for different values of the spectral index of the power low energy spectrum of the primary cosmic ray: for the GCRs (γ = -2.7); for the SEP events (γ = -4, -5, and -6). From the table we can see that SEVAN network provides registration of the SEP events in broad energy range included very poorly researched energies above 10 GeV. For instance, neutron fluxes measured at Lomnisky Stit, Slovakia are sensitive to 4 GeV solar protons and high energy muon flux measured at Delhi is sensitive to 18 GeV solar protons. Taking into account intermediate energies measure at Aragats, Armenia, Zagreb ,Croatia and Moussala, Bulgaria we can reliably recover SEP energy spectrum with unprecedented accuracy.

Table 1.The range of most probable energies (in GeV) of primary protons producing secondary fluxes at different SEVAN sites.

Station	GCR (γ=2.7)				SCR (γ=4,5,6)			
	Charged particles	Muons(E > 250 MeV)	Muons (E > 5 GeV)	Neutron	Charge particle	Muons (E > 250 MeV)	Muons (E > 5 GeV)	Neutron
Yerevan (Armenia)	14.6	18.4	38.4	7.1	8.2–1.2	10–11.6	21.2 - 31.9	7.1
Nor-Amberd (Armenia)	13.1	14.9	41.2	7.1	7.6–10.6	9.7–11.3	20.5–31.3	7.1
Aragats (Armenia)	10.9	14.3	37	7.1	7.4–10	7.6–10.6	21.2–27	7.1
Moussala (Bulgaria)	10.6	13.3	–	7.4	6.6–7.4	7.1–9.5	–	7.6–9.4

Zagreb (Croatia)	17.4	17.3	–	7.6	9.4–12.9	9.1–13.4	–	5.1–5.7
Lom-niskyStit (Slovakia)	11.5	14.5	–	4.1	4.1 −6.5	5.2–8.3	–	4
Delhi JNU (India)	18.1	18.1	–	16.5	14.2–15.1	14.3–15.3	–	14.3–14.4

To quantify statements about the detection of different types of particles by the SEVAN modules, we need to perform detailed simulation of the detector response. We use simulated cascades of the charged and neutral secondary particles obtained with the CORSIKA (version 6.204) Monte Carlo code [32]. All secondary particles were tracked until their energy dropped below the predetermined value (50 MeV for hadrons, 10 MeV for muons and 6 MeV for electrons and photons) or reached all the way to the ground level. The spectra of primary protons and helium nuclei (99% of the flux at energies up to 100 GeV) are selected to follow the proton and helium spectra reported by the CAPRICE98 balloon-borne experiment [34]. Among the different species of secondary particles, generated in nuclear-electromagnetic cascades in the atmosphere, muons, electrons, γ-rays, neutrons, protons, pions and kaons were followed by CORSIKA and stored. These particles were used as input for the GEANT4 package [35], implemented for detector response simulation. Also, we take into account the light absorption in the scintillator [16]. The efficiency of the charged particle detection by all 3 layers of the SEVAN detector is above 95%; the neutron detection efficiency in the middle “thick” scintillator reaches 30% at 200 MeV, the efficiency of the γ-quanta detection reaches 60% at the same energies. The purity (relative fraction of different species registered) of 3 SEVAN detecting layers is presented in Figure 34.

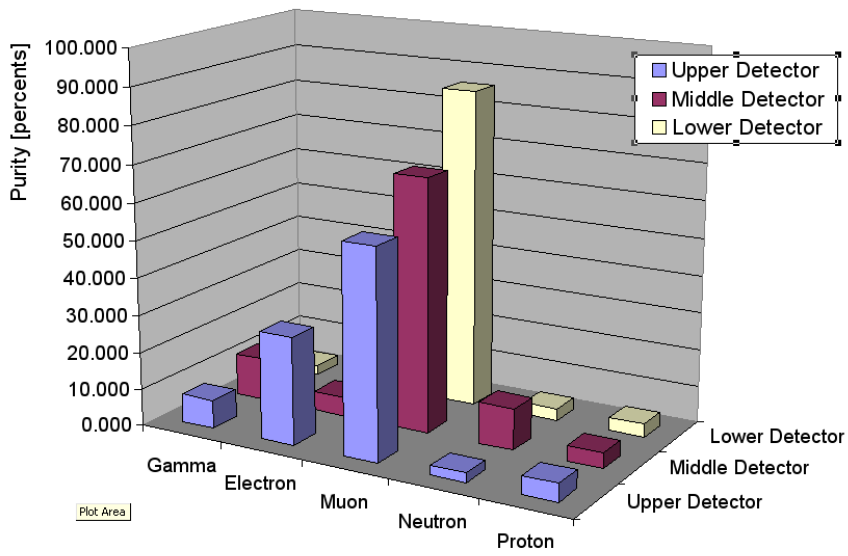

Figure 34. The purity of 3 SEVAN layers.

The pattern is significantly improved: fraction of electrons in events selected by combination 100 is above 40%; fraction of neutral particles selected by combination 010 – is larger than 85% and fraction of high energy muons in events selected by combinations 111 and 101 reaches 95%. Therefore, by analyzing combinations, instead of layer counts we can get clues how 3 types of secondary cosmic rays are influenced by meteorological and solar modulation effects. The data from Figures 34 and 35 are summarized in Table 2. The figures show that different layers are sensitive to different particles.

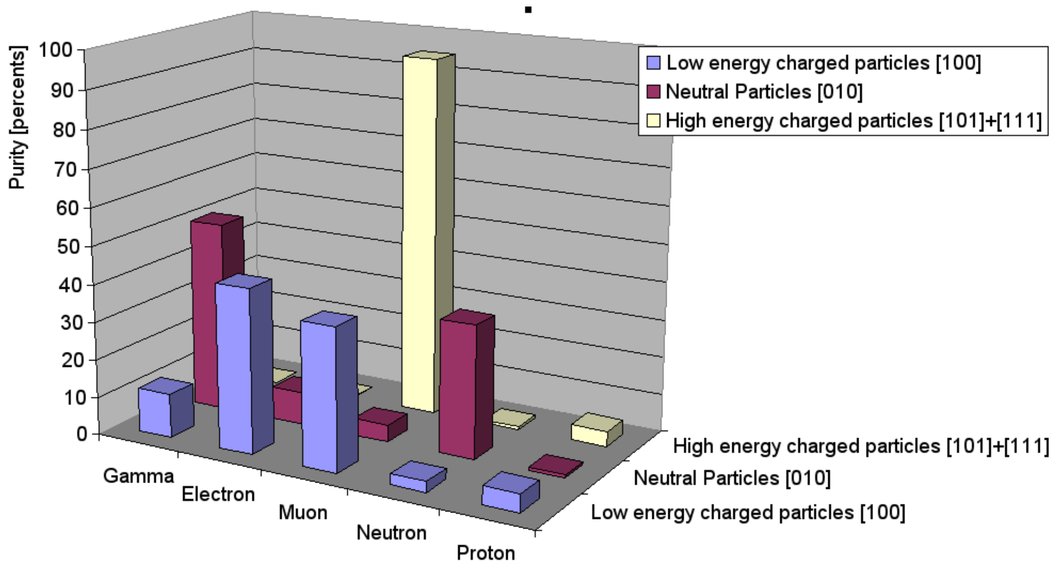

Figure 35. Purity of SEVAN combinations.

Table 2.Summary of particle selection purity by SEVAN layers and combinations.

	Gamma	Electron	Muon	Neutron	Proton
Registered particles Purity by special combination					
Low energy charged particles [100]	11.605	43.300	37.380	2.838	4.804
Neutral Particles [010]	50.612	8.837	4.494	35.071	0.972
High energy charged particles [101]+ [111]	0.002	0.106	94.904	0.808	4.077
Registered particles Purity by count rate of the detectors					
Upper Detector	7.616	28.952	56.080	2.448	4.814
Middle Detector	11.550	5.223	67.913	11.038	4.167
Lower Detector	2.696	4.438	85.873	3.267	3.634

Of course, the purity is not only parameter we are interested in; the efficiency of particle registration is also of upmost interest in detector design and operation. In **Figure 36** we post the purity-efficiency diagram explaining which fraction of primary flux will contribute to different combinations. In **Figure 36** we see that the high-energy muons are registered with both high efficiency and purity.

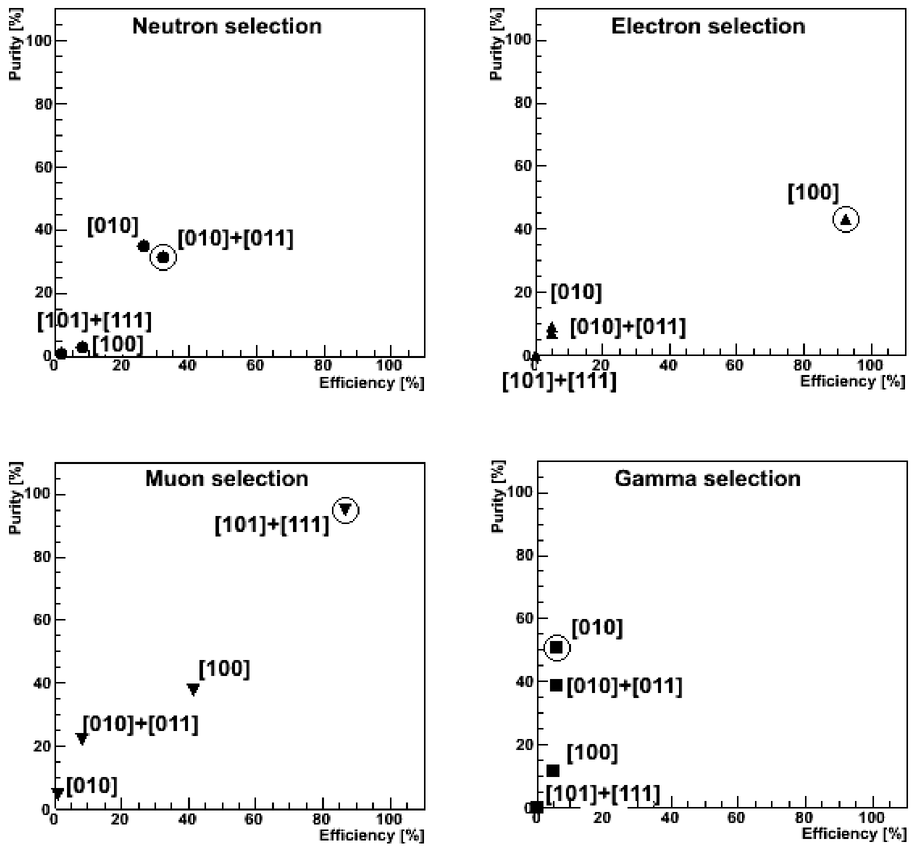

Figure 36. The purity-efficiency diagram of the SEVAN combinations registering ambient population of the secondary cosmic rays generated by interactions of GCR with atmosphere.

Neutrons are registered with rather high efficiency and purity (both ~30%). It is worth to mention that efficiency of neutron monitor is reaching 30% only for highest energy neutrons. However NM can distinguish neutrons from the gamma rays (NM has excellent purity to select primary hadrons). Gamma rays are selected with lower efficiency by all possible combinations of SEVAN layers; nonetheless efficiency of electron registration is above 90%; therefore, the low energy electromagnetic component is registered efficiently by SEVAN. For the particles registered by SEVAN we can obtain from simulation the most probable energies of primary GCR responsible for their origination. In Table 3 we post the most probable energies (medians of the energy distribution of the parent protons) producing different elementary particles in the terrestrial atmosphere. From the table we can see that the higher energy protons produce secondary muons and electrons compared with ones producing secondary neutrons.

Table 3. Modes of the GCR energy spectra corresponding to different species of secondary particles registered by the SEVAN detector at 3200 m above sea level.

Layers of detector located at 3200 m	Most probable energy of GCR (GeV)
Upper Layer	11.5
Middle 25 cm layer	8.5
Bottom Layer	14.5

As we can see in Table 2 and in Figure 36, SEVAN can register the low energy charged component, neutral component and high-energy muons. In Table 4 we compare the simulated and measured one-minute count rates of these particles. Low energy charged particles, as well as neutrons and gamma rays, are attenuated very fast as they penetrate deep in atmosphere. High-energy muons did not attenuate so fast as one can see in third row of **Table 4.**

Table 4.Experimental and simulated one-minute count rates measured by three scintillators of the SEVAN.

	Yerevan (1000m)		NorAmberd (2000m)		Aragats (3200m)	
Type of Secondary particle	Measured count rate	simulated count rate	Measured count rate	simulated count rate	Measured count rate	simulated count rate

Low energy charged particles	8862±108	7202	11593±161	10220	16010±130	17330
Neutral particles	363±19	359	690±27	795	2007±46	1680
High energy muon	4337±67	5477	4473±99	5548	4056±64	8051

2.3 Response of SEVAN particle detectors to GLEs initiated by the solar protons and neutrons

The arriving from the sun neutrons contains essential information about the ion acceleration, because they are not affected by the magnetic fields. Charged particles, trapping in the interplanetary magnetic usually arrive at the Earth later than gamma rays from solar flares. By observing the neutrons, we can directly probe the energy spectrum of the accelerated ions and also find the production time of the solar particles. Thus measurements of the time series of the solar neutrons and their energy spectra will shed line on operation of the solar accelerators. However, neutron events are very rare and it is not easy to distinguish them from more frequent proton events. The comparison of the count rate enhancements in the layers of the SEVAN module (measured in standard deviations – "sigmas") allows one to distinguish the GLE's originated from solar neutrons incident on terrestrial atmosphere. Table 5 shows that for neutron primaries there is a significant enhancement in the SEVAN thick layer and much less enhancement in thin layer. For proton primaries the situation is vice-versa: the significant enhancement is in the thin layer, and much less in the thick layer.

Table 5. Simulated enhancements (in standard deviations) of the "5-min" count rates corresponding to GLEs initiated by primary neutrons, energy spectrum adopted from Watanabe et al, 2006) and primary protons (Energy spectrum adopted from Zazyan, Chilingarian, 2009).

Detector layer	Solar Protons	Solar Neutrons
Upper 5 cm scintillator	4.8 σ	2.6 σ
Middle 25 cm scintillator	1.7 σ	6.4 σ

2.4 Forbush decrease events detected by the SEVAN network in the beginning of the 24-th solar activity cycle

The Solar Cycle 24 will peak in May 2013 with a below-average number of sunspots, predicts the panel of experts led by NOAA. Experts predict that Solar Cycle 24 will have a peak sunspot number of 90, the lowest of any cycle since 1928 when Solar Cycle 16 peaked at 78. However, even a below-average cycle is capable of producing severe space weather, all time greatest GLE and geomagnetic storm of 1859 occurred during a solar cycle of about the same size as is predicted for 2013. Now waiting till Sun accumulates energy for another huge event the SEVAN network detects first Forbush decrease (FD) events. In the middle of February 2011 the active region AR 11158 unleashed 3 solar flares of class M6.6 (13 February, solar coordinates S19, W03), M2.2 (14 February, solar coordinates S20, W14) and strongest X2.2 (15 February, solar coordinates S19, W03S21, W18). All 3 flares were accompanied with CMEs headed to the earth direction. The worldwide network of neutron monitors detects at 18 February sizeable Forbush decrease. The SEVAN network as well detects FD by 3 monitors located in Armenia and by Balkanian monitors located in Zagreb observatory (Croatia) and Mt. Moussala (Bulgaria). The SEVAN module locates in India do not register FD due to large geomagnetic cutoff.

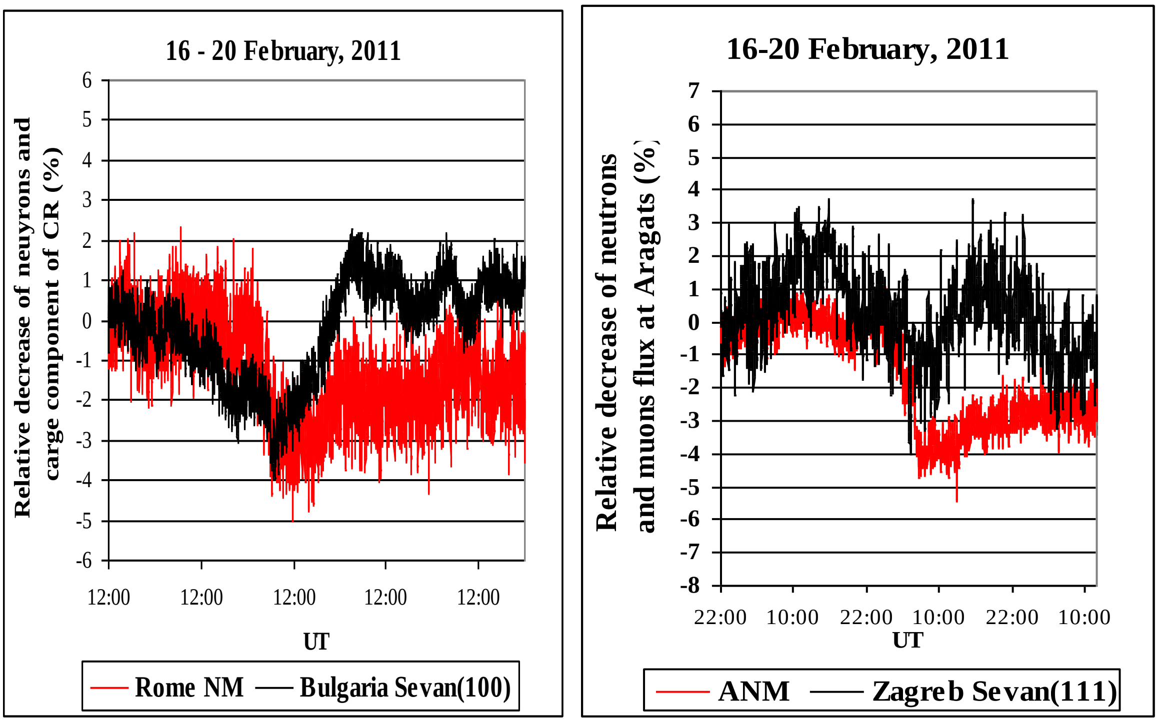

Figure 37. The time profiles of the FD on 18 February, 2011 measured by Zagreb and Moussala SEVAN monitors in comparison with Rome Neutron monitor and Aragats Neutron monitor. The low energy charged particles (combination 100) and high-energy muons (combina-

tion 111) are recovering much faster comparing with neutrons measured by Rome and Aragats Neutron monitors.

As we can see in Figure 37 the overall patterns of FD detected in charged particle fluxes are very similar to the ones measured by neutron monitors. However, there are several differences due to location of detectors at different latitudes, longitudes and altitudes. The FD phenomena is global phenomena influenced all globe (may be not the equatorial regions only where the cutoff rigidity is very large); nevertheless the detection of the local differences in time profiles of FD produced by primary particles of different energies is very important and allows to recover the event anisotropy and sometimes also the shape of the ICME. The SEVAN network located on different longitudes (from Zagreb to Delhi) gives possibility to explore FD's shape and the magnitude longitudinal dependence and character of the disturbance and its source [36, 37]. In this respect registration of FD also in low and high energy charged particle fluxes can bring additional information for the developing of the model of ICME – magnetosphere interactions. The amplitude of FD is dependent on the disturbance of the interplanetary magnetic field caused by the ICME propagation and ICME interaction with geomagnetic field. Both effects are dependent on the strength of the magnetic field "frozen" in the ICME [19]. GCRs are traversing the regions of the disturbed IMF and dependent on their energy are deflected from their path and miss encounter with earth atmosphere. Thus, the disturbed IMF is modulated the GCR flux. As we demonstrate above different components of secondary cosmic rays detected on the earth surface are generated in terrestrial atmosphere by interactions of CRs of various energies; neutrons are generated by protons of lower energies than ones generating electrons; electrons in turn are generated by protons with energies lower than ones generated high energy muons. Therefore, the amplitudes of FDs in neutron, electron and muon fluxes are expected to reflect these energies relations. In the Figure 38 and Table 6 we see that neutral component measured by Aragats SEVAN 010 combination demonstrate 4% decrease practically coinciding with FD measured by the Aragats neutron monitor (4.2%), the low energy charged component (100 combination) ~3.8% decrease and the 111 combination (high energy muons) ~3% decrease.

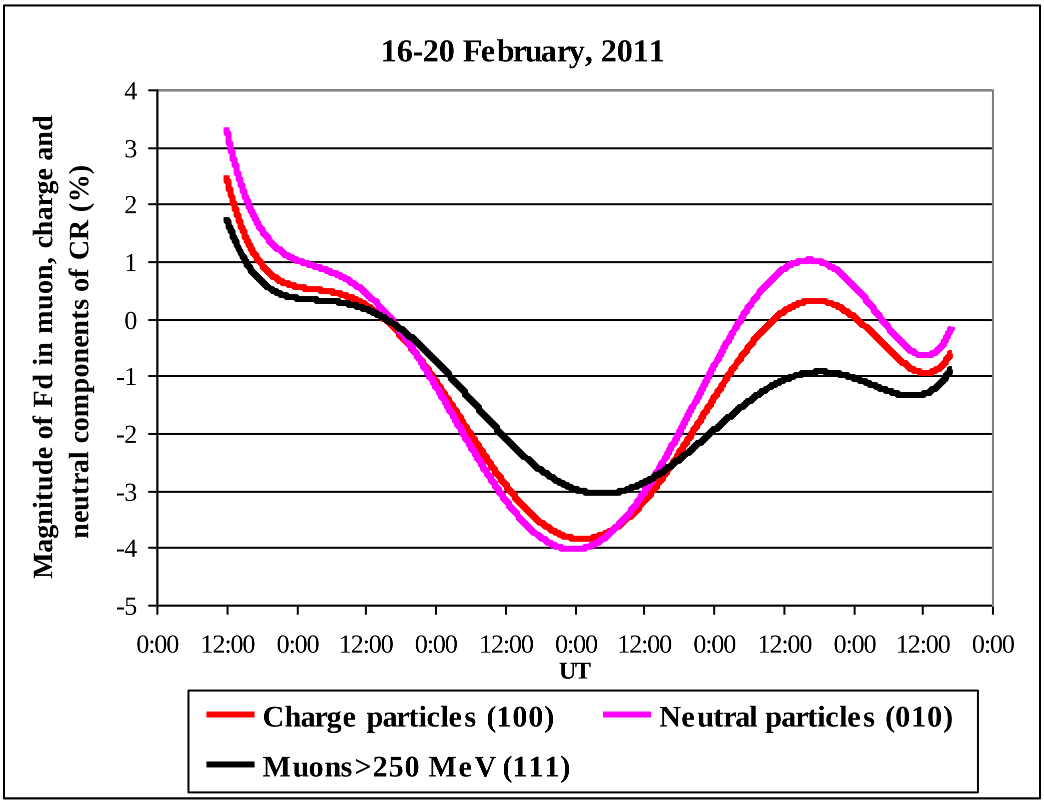

Figure 38. FD as detected by different species of secondary cosmic rays (SEVAN detector combinations).

Nor Amberd SEVAN also demonstrated biggest magnitude of FD for the neutral particles; however the magnitude of the low energy charged particles (100) is a bit lower comparing with magnitude of FD measured in the high-energy muon flux. In Zagred magnitudes of FD for all combinations are one and the same. These discrepances signalling necessity of tuning of the measuring channels operation including PM high voltage and shaper thresholds. Thus, the SEVAN detector simulations posted in the Figures 34-36 and Table 2 are confirmed by the network operation. Another solar eruption from active region AR1402 on 23 Jan at 03:38 UT, unleashed a M8.7 flare in associated with [full halo CME](#) of 2000 km/s speed reaches earth at 24 January and as we can see in the Figure 39 and Table 7 how the FD was detected by SEVAN modules.

Table 6. The magnitudes of FD measured by SEVAN network and Aragats neutron monitor on 18 February.

	Magnitude of FD Aragats, 3200m (%)	**Magnitude of FD by Nor Amberd, 2000 m (%)**	**Magnitude of FD by Zagreb 130m (%)**	**Magnitude of FD Moussala 2900m (%)**	**India, New Delhi JNU**
SEVAN(100)	-3.8	-2.1	-3	-3	0
SEVAN(010)	-4	-4.2	-3	-	0
SEVAN(111)	-3	-2.3	-3	-	0
Aragats NM	-4.2				

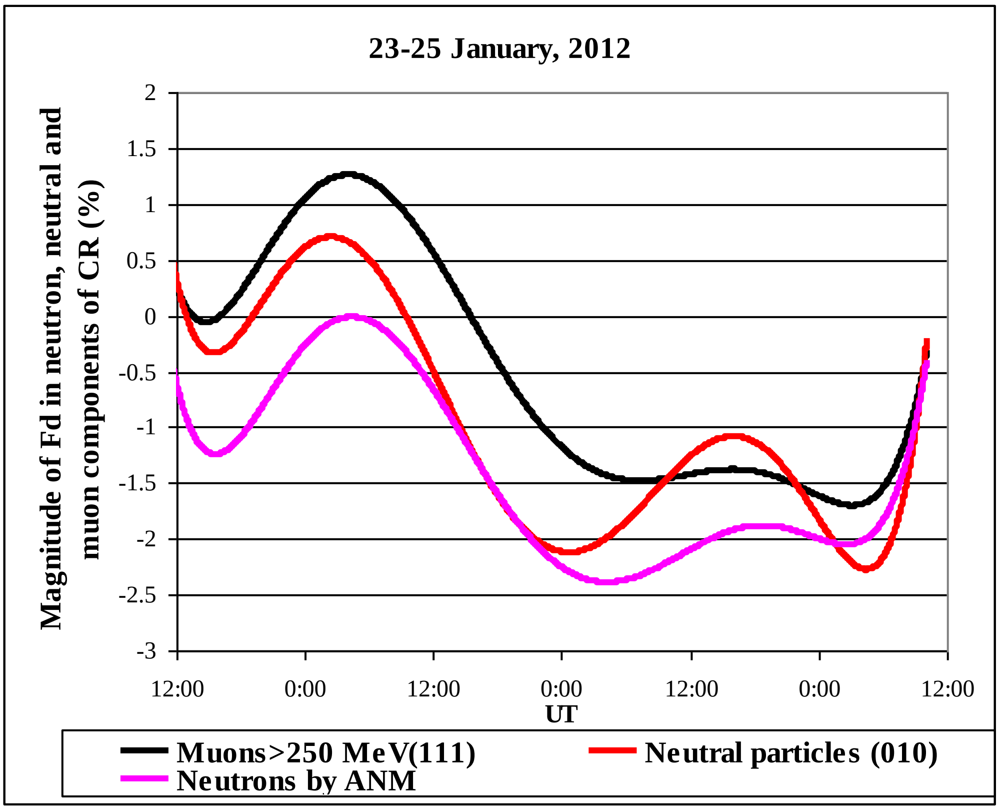

Figure 39. FD of 24 January detected by the Aragats Neutron monitor and SEVAN (010) and 111 combinations.

Table 7.The magnitudes of FD measured by SEVAN network and Aragats neutron monitor on 24 January, 2012.

	Magnitude of FD by Aragats 3200m (%)	**Magnitude of FD by Nor Amberd2000m (%)**
SEVAN(100)	-1.8	-1.7
SEVAN(010)	-2.1	-3
SEVAN(111)	-1.5	-2
Aragats NM	-2.4	

SEVAN network detects the FDs of 18 February 2011 and 24 January 2012 in the fluxes of neutrons, low energy charged particles and high-energy muons. The patterns of FD in differenct secondary particle species are very similar to ones measured by the NMs only in atmospheric neutron fluxes. However, in addition to neutron monitors SEVAN measures simultaneously FD patterns of other species of secondary cosmic rays giving additional clues for the recovering of the shape and frozen magnetic field of the ICME interacted with magnetosphere.

2.5 Thunderstorm Ground Enhancements (TGE) detected by SEVAN

Facilities of the Aragats Space Environment Center (ASEC) [1, 2] observe charged and neutral fluxes of secondary cosmic rays by the variety of particle detectors located in Yerevan and on slopes of Mt. Aragats at altitudes 800, 2000 and 3200 m. ASEC detectors measure particle fluxes with different energy thresholds as well as EAS initiated by primary proton or stripped nuclei with energies greater than 50– 100 TeV [19]. Detection of abrupt enhancements of the particle detector count rates correlated with thunderstorm activity, so called Thunderstorm Ground Enhancements (TGEs) detected during 2008-2011 years brings vast amount (343 TGE events) of small and very few large TGEs (only 6 TGE events with amplitude exceeding 20%) allowing the detailed analyses and taxonomy of new high-energy phenomena in atmosphere. Small TGEs can be explained by the modification of the energy spectra of charged particles in the electrical field of thunderclouds. Due to asymmetry of positive-to-negative flux of secondary cosmic rays in terrestrial atmosphere, peaks and deeps can arise in time series of count rates of surface particle detectors. These effects have been theoretically analyzed in [38]. Measurements at ASEC and simulation with GEANT4 package confirm additional flux of gamma rays up to 1000% in the energy range 1-10 MeV and up to 5% in the energy range up to 100 MeV. Simultaneously deeps in the muon flux at energies above 200 MeV was obtained by simulations and detected by SEVAN detectors, 101 and 111 combinations. Field meters (Boltek firm electrical mill EFM100, http://www.boltek.com/efm100.html) and lightning detectors (StormTracker Lightning Detection System powered by the software from Astrogenic systems, http://www.boltek.com/stormtracker) installed at Aragats allow correlating the measured particle fluxes with electrical field disturbances and with occurrences of lightning of different types. The electrical mill was calibrated by fair weather electrical field according to firm instructions. In database of SEVAN time series we can find significant non-random variations of cosmic ray intensity in

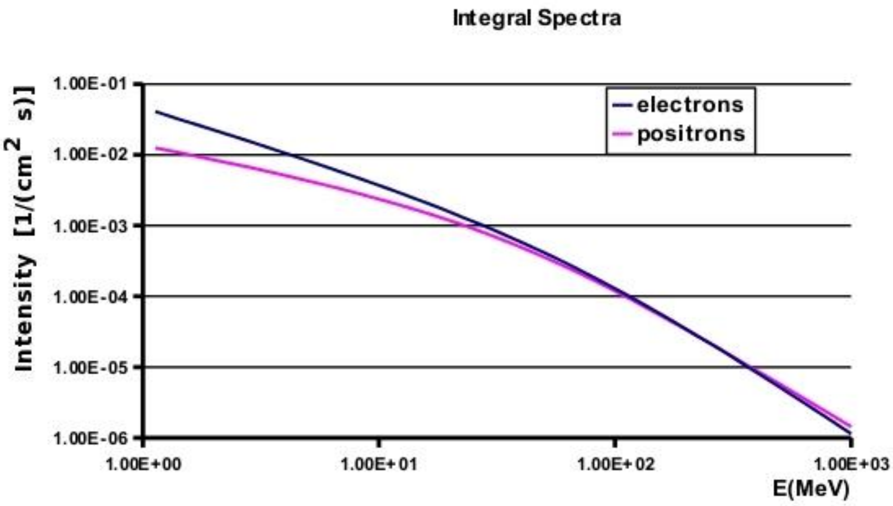

Figure 40.**Energy spectra of electrons and positrons at altitude of 5000 m a.s.l.**

absence of any lightning occurrences, signaling that the electrical field strength in the cloud is below the RREA threshold. Electrons and negative muons are accelerated downwards by lower dipole before reaching particle detector. The positrons and positive muons as well as protons will be decelerated in the lower dipole. The positive charge of primary cosmic rays (mostly protons and stripped nuclei) introduces several asymmetries between particles and antiparticles born in atmospheric cascades. The intensity of the MeV electrons is larger than intensity of positrons of the same energies in energy range 1-50 MeV; the intensity of positive muons above 100 MeV is larger comparing with intensity of the negative muons, see Figure 40 and 41. We can see in the **Figure 40** that the number of electrons with energies below 50 MeV at 5000 m altitudes is significantly larger comparing with positrons. It means that positive electrical field in the thundercloud will significantly alter the total intensity of charged particles of low energy registered by scintillators at the Earth surface. The changes of intensity will manifest themselves as peaks and deeps in the time series of count rates of particles registered by the scintillators located on the Earth surface. The energy spectrum of electrons will be shifted to the right (mean energy becoming larger) leading to the additional bremsstrahlung gamma rays; shifting to the left energy spectrum of positrons cannot compensate these enhancements because of their shortage. The attenuation length of the electrons in the energy range of 1-100 MeV is much less comparing with the one of the gamma rays. Therefore, most of TGE events are detected in the fluxes of gamma rays born by accelerated cosmic ray electrons.

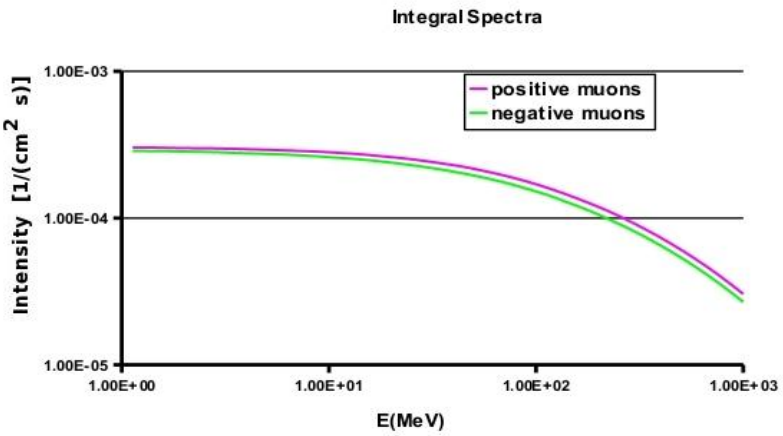

Figure 41.**Energy spectra of muons at altitude 5000 m a.s.l**

Interestingly, positive fields have opposite influence on counts of muons at energies above 200MeV. Among ASEC particle detectors there are scintillators with energy threshold greater than 200 MeV and the electron acceleration described above will not influence their count rate. Due to abundance of positive muons over negative (1.3 -1.4 times at 100-500 MeV energies, see **Figure 41**) the braking of positive muons in the positive electrical field cannot be compensated by the acceleration of the negative muons in the same field. The consequences of this asymmetry you can see in the Figure 42: on October 4, 2010 we detected ~6% deficit in the flux muons with energies greater than ~250 MeV, simultaneously detecting huge excess of low energy gamma rays and electrons. Observational data of the Aragats station's monitors obtained during 2008-2011, when solar activity was minimal and corresponding solar modulation effects were absent, demonstrates several remarkable TGE events; few of them were accompanied by the muon flux decrease. In Figure 42 one can see the count rates of the SEVAN detector on 4 October 2010. The threshold of the upper detector due the matter of the roof above is ~ 15MeV; it counts exhibits a large peak lasting ~10 minutes with maximal counting rate at 18:23. This peak is due to penetrated gamma rays (and small portion of electrons) of the Relativistic runaway electron avalanche [43, 44, 45, 46] process in the thundercloud just above the building where detector is located [40].

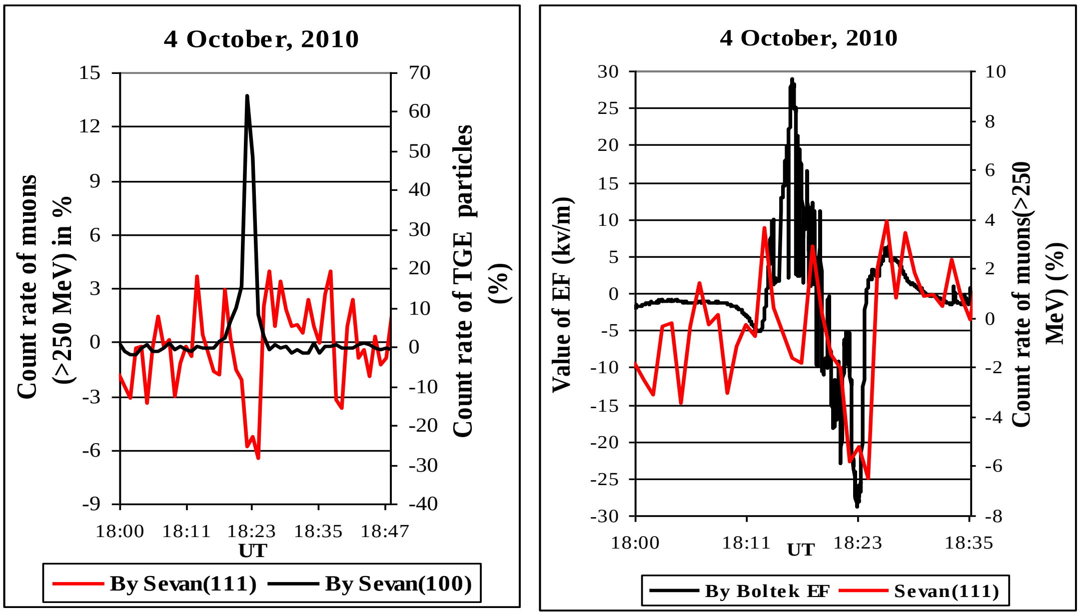

Figure 42. The count rates of SEVAN 100 and 111 combinations along with the changing near surface electrical field. The positive field in the thundercloud (electrons are accelerated downwards) is stopping positive muons; charge ratio of positive-to-negative muons is (~1.3), therefore we detect ~6% deficit of the flux of high-energy muons (energy > 250 MeV); simultaneously huge TGE in gamma ray and electron fluxes was measured.

For the same minutes the channels 111 shows pronounced decrease. Energy of particle necessary to penetrate lead filters and be detected in all three layers (combination 111) is ~250MeV.

Both increase of the RREA electron and gamma ray fluxes occur during negative near-ground electrical field. According to our model, [40] TGE event started with formation in the bottom of the cloud of the lower positive charged region (LCPR). LCPR with main middle negative charged layer compose the lower dipole accelerated electrons downward. The lower dipole is responsible for RREA process that leads to large TGEs. Unfortunately, we cannot yet perform calculations according to our model of TGE/RREA because the electrical field within lower dipole is very difficult to measure. Surprisingly the SEVAN module gives us possibility to estimate this field at least roughly. Observed deficit ~6% is caused mostly by the positive muons, which spectrum is affected significantly by the positive potential of the thundercloud. Therefore, by deriving the relationship between the measured deficit and unknown electric potential in the cloud it will be possible to estimate the electrical potential within cloud, based on observed values of high-energy muon deficit. The huge flux of the gamma rays measure at 18:23 on 4 October, 2010 was used to check the Aragats SEVAN ability to detect gamma ray flux by 010 the combination. Simulating the passage of the recovered gamma-ray flux through the roof above and detector and taking into account the detector response to gamma rays and electrons, we have estimated the expected number of gamma rays detected by the "010" combination to be 1459 respectively. This value is in a good agreement with experimentally measured value of 1452 ± 42.

In Figure 43 we post the pattern of the first TGE detected in Yerevan (800 m a.s.l.) at midnight July 18, 2011. Again during thunderstorm negative near surface electrical field was measured, although not so large as on Aragats. At the same time upper layer of Yerevan SEVAN module, located on the roof of CRD headquarters registered significant peak of ~6% (~ 7 standard deviations). With high probability it was gamma rays, though electron TGE flux should attenuate reaching the detector. The thunderclouds above Yerevan are rather high and electrons will attenuate in dense air.

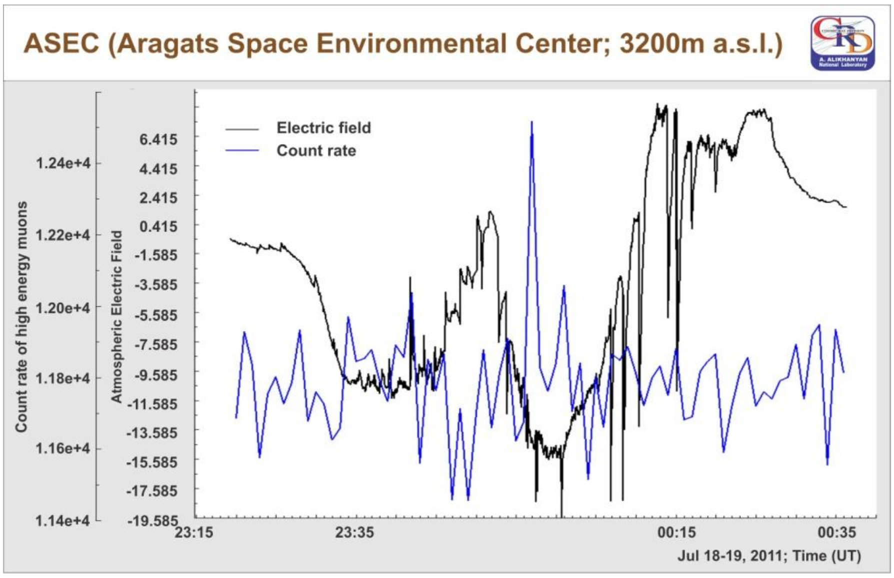

Figure 43. The first TGE registered by Yerevan SEVAN.

CHAPTER 3

THE ARAGATS SPACE ENVIRONMENT CENTER (ASEC)

INTRODUCTION

The Aragats Space-Environmental Center (ASEC), [1,2] provides monitoring of different species of secondary cosmic rays at two altitudes and with different energy thresholds. 1-minute data are available on-line from http://adei.crd.yerphi.am/adei. ASEC consists of two high altitude stations on Mt. Aragats in Armenia: "Aragats" research station (40°28'N, 44°10'E, 3250m above sea level) and. "Nor-Amberd" research station (40°22'N, 44°15'E, 2000m above sea level), cutoff rigidity: ~7.6 GeV. At these stations several monitors continuously measure the intensity of the secondary cosmic ray fluxes and send data to the Internet in real time. The specifications of the ASEC monitors are shown in Table 8. The two 18NM-64 neutron monitors **Error! Reference source not found.**, in operation at Nor-Amberd (2000m elevation), and at Aragats, (3200m elevation) research stations are called the Nor Amberd Neutron Monitor (NANM), and the Aragats Neutron Monitor (ArNM), respectively. The monitors are equipped with interface cards, providing time integration of counts from 1 sec up to 1 minute. Aragats Solar Neutron Telescope (ASNT) located on the slope of the mountain Aragats in Armenia, 3250m above sea level. Geographical coordinates are 40°28'N, 44°10'E. ASNT is formed from 4 separate identical modules, as shown in Figure 44. Each module consists of standard slabs of 100x100x5 cm^3 plastic scintillators stacked vertically on a 100x100x60 cm^3 horizontal plastic scintillator slab. Scintillator slabs are fine polished to provide good optical contact of the assembly. The slab assembly (scintillator housing) is covered by white paper from the sides and bottom and firmly kept together with special belts. Total thickness of the assembly is 60 cm. Four detectors of 100x100x5 cm3 size each located above the thick scintillator assembly as is seen in Figure 44, are used to indicate if charged particle traverse near vertically. This information is used for selecting neutral particles and "vetoing" charged particles. A scintillator light capture cones and Photo Multiplier Tubes (large cathode, FEU 49 type) are located on the top of scintillator housing in special iron shielding, where as well the Amplitude-to-digital convertor and other electronics is located.

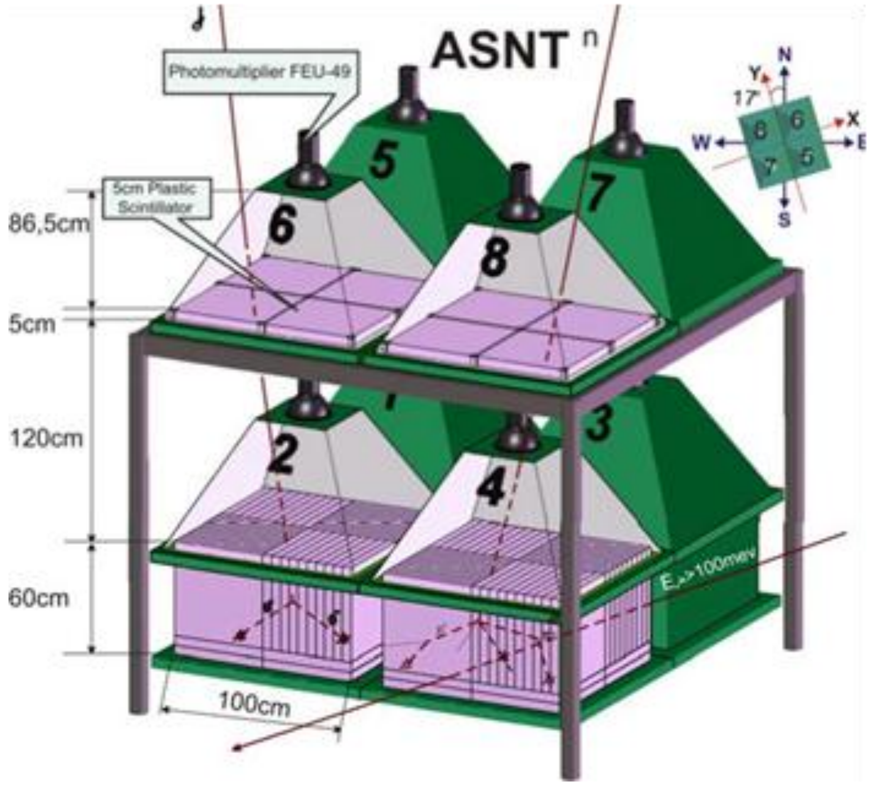

Figure 44 The assembly of ASNT with enumeration of 8 measuring channels (scintillators) and chart indicating orientation of detector axes relative to direction to the North Pole.

Table 8: Characteristics of ASEC Monitors.

Detector	Altitude *m*	Surface m^2	Threshold(s) *MeV*	Operation	Count rate (min^{-1})
NANM (18NM64)	2000	18	50	1996	2.7×10^4
ANM (18NM64)	3200	18	50	2000	6.1×10^4
ASNT 8channels	3200	4 (5cm thick) 4 (60cm thick)	7 85, 172, 256, 382	1998	1.2×10^5 $5.2\times10^{4*}$
NAMMM 24 channels	2000	10 – upper 10 – down	7 250	2006	1.8×10^5 1.1×10^5
AMMM	3200	100	5000	2002	3×10^5
MAKET-ANI 6 channels	3200	6	7	1996	1.5×10^5

*Count rate for the first threshold; near vertical charged particles are excluded

3.1 Structure of the information content from ASNT

Initial goal of the ASNT was to be a part of the worldwide network aimed to detect neutrons born in photosphere and reach Earth bringing direct information from its origin. The network is coordinated by the Solar-Terrestrial laboratory of the Nagoya University [26] and consists of seven same type detectors distributed at different longitudes to observe the sun 24 hours daily. In addition to the primary goal of detecting the direct neutron flux from the Sun, the SNT also has the possibility to detect charged fluxes (mostly muons and electrons) and roughly measure the direction of the incident muons. Also ASNT constitutes a central part of the new surface array operating at Aragats in 2009 (see MAKET section below). The main ASNT trigger reads and stores the analog signals (PMT outputs) from all 8 channels if at least one channel reports signal. The frequency of triggers is ~4 KHz due to hit of charged and neutral particles. Big advantage of ASNT is additional, so called, software triggers, exploiting the information from Amplitude-Digital-Converters (ADC) on energy releases in scintillators.This, additional information, not assessable yet from other particle detectors from world-wide networks, allows as we will see, solving additional physical problems. The software triggers are not fixed in electronics and it is possible to remote add or change them very flexible. The list of available information from modernized ASNT is as follows:

1. 1 minute count rates (easily can be changed to 10 seconds, or to another time span) of all 8 channels of ASNT (see Table 9,Figure 45);

2. Count rates from different incident directions separately, 16 possible coincidences of 4 upper and 4 bottom scintillators are related to 9 different directions (see Table 10);

3. Count rates of the special coincidences (see details in Table 11, Figure 46);

4. Estimates of the variances of count rates of each ASNT channel, variances are calculated by12 five-second count rates (see Table 12, Figure 47);

5. 8 x 8 correlation matrix of ASNT channels calculated by five-second count rates in 1 minute (see Table 13);

6. Count rates correspondent to old SNT 4 threshold on the energy release in thick scintillators (see Table 14);
7. The same as in previous point put only for particles that did not registered in upper layer (veto on charged particles to select samples enriched by neutrons) (see Table 14);
8. Histograms of energy releases in all 8 channels of ASNT (see Figure 48);
9. The same as in previous point with invoking veto option;
10. Time and values of energy releases in ASNT channels conditioned on existence of signals in all 8 scintillators, so called, EAS trigger (accuracy of time stamp is ~50 μsec), (Figure 49);
11. Energy releases in upper or bottom scintillators conditioned on absence of signal in correspondingly down and upper layers and on minimal energy release, i.e. horizontal muon trigger.

We use XML format of data, allowing metafiles with detailed information about detector location, and operation conditions. After transfer by wireless connections to CRD headquarters in Yerevan the data are archived and stored in MySQL data base. All raw data in the XML format is available from HTTP server at CRD headquarters in Yerevan from the link.

http://adei.crd.yerphi.am/adei

In the directory "DEFOULT" following information is stored:

1. SNT (columns 1-8) - the count rates of all 8 ASNT channels: first 4 columns – from 60 cm scintillators, 5-8 columns – from 5 cm scintillator. The numbering of scintillators is explained in the **Error! Reference source not found.**. The count rates are posted in the Table 9;
2. SNT (columns 9-24) – the count rates corresponding to the 16 coincidences in upper and bottom ASNT layers, i.e. – corresponding to the traversal of the single charged particle (the probability that neutron will generate energy release in 5 cm scintillator is rather small). The order of the different directions in the file is following: [1-5] [1-6] [1-7] [1-8] [2-5] [2-6] [2-7] [2-8] [3-5] [3-6] [3-7] [3-8] [4-5] [4-6] [4-7] [4-8], where the first number corresponds to the lower layer and the second – to the upper (see Figure 44) Also on the same Figure you can see the orientation of ASNT axes according to direction to the North Pole, thus we can calculate the interval of the horizontal angles of incidence related to each coincidence.

3. SNT (columns 25-31) – the count rates of the “special” coincidences different from listed above and forming the “full system” of possible configurations of the channel operation. Conditioned on the existing as minimum 1 signal in 8 ASNT channels there could be the following possibilities of number of counts in top and bottom layers (the first sign in the pair is corresponding to the bottom thick scintillator): many-many [m-m] (more than one count in 4 bottom and 4 top layers), many-zero [m-z] (more than 1 in bottom and nothing in 4 top), zero-many [z-m], zero-one [z-o], one-zero [o-z], many-one [m-o], one-many [o-m]. The fraction of the “special” coincidences relative to the “main” trigger is posted in the Table 11 the time-series of the s “special” triggers are posted in the Figure 46.
4. SNT (columns 32) - the number of the “main” triggers – at least one signal in 8 channels in preselected time span (1 minute). If we consider all logical configurations of ASNT operation outcomes, this number will be equal to sum of the columns 9-31. As we mention already the number of triggers is ~ 4 KHz, dependent on the hardware settings: PMT high voltage and threshold of channel “firing”.
5. SNT (columns 33-40) - the variances of 8 channels, see Table 12 and Figure 47;
6. SNT (columns 41-68) – the correlation matrix, see Table 13.

In the directories “spectrum” following information is stored:

1. spectrum1, … spectrum4 the histograms of the spectrum of amplitude codes in thick 60 cm scintillator; In files with extension;
2. spectrum5, … spectrum8 the histograms of spectrum of amplitude codes in 5 cm thin scintillators;
3. spectrum9,..., spectrum12 histograms of spectrum of amplitude codes in 60 cm thick scintillators (with invoking veto option on the charged particles in the upper “anticoincidence” shielding);

By integrating the histograms spectrum1,..., spectrum4 and spectrum9,...,spectrum12 we calculate the count rates according to 4 predefined thresholds on the value of the spectrum of amplitude codes (PMT output), to continue time series in the same data format as old version of ASNT started from 1996 (http://adei.crd.yerphi.am/adei). As a first (or zero- threshold) we use the sum of all channels of the histogram. To get number of particles with Threshold 1 we must calculate sum of the channels of the histogram from 16 to 127. For the Threshold 2 – sum of the 23-127 channels, Threshold 3 – 27-127 channels and Threshold 4 – 31-127 channels.

To calculate count rate of the particles with thresholds for the detector 1-4 (60cm) we us spectrums 1-4 files. To calculate count rate of the particles with veto for the detector 1-4 we us spectrums 9-12 files (see Table 14). The CRD "ARSRV" local file server contains files with following information:

The detailed information on the many-many case: the time stamp and energy releases in all 8 ASNT cannels. This case is related to the Extensive Air Showers (EAS), when energy of primary particle is high enough to generate particle cascade with numerous secondary particles reaching earth surface. By selecting different subsamples of many-many case according to the number of detected secondary particles (energy releases) we can select events with different primary energies, thus constructing the energy spectra of the primary particles. The calibration of the ASNT can be done with MAKET-ANI EAS (Extensive Air Showers).

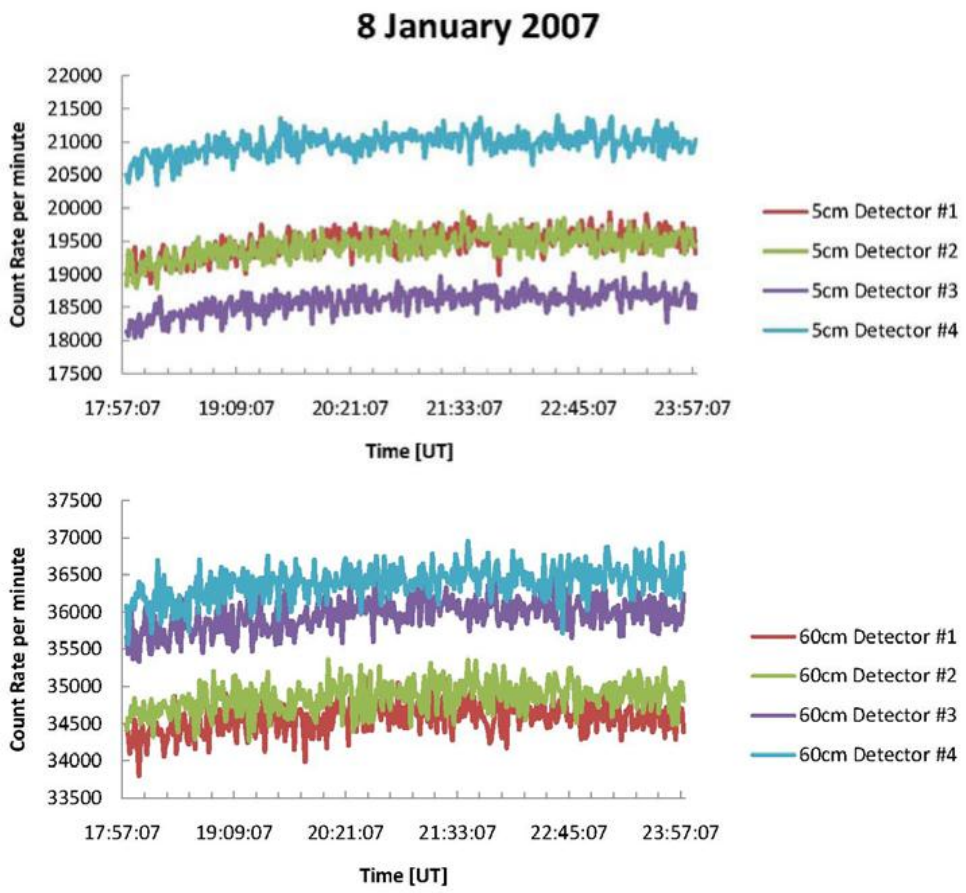

Figure 45 Time series of count rates of 8 ASNT channels. The difference of mean values is due to peculiarities of PMT used

Table 9 Count rates of the ASNT channels, Standard Deviation and relative errors

Detector	Average	Standard Deviation	Relative error [%]
60cm Detector1	34465	244	0.70
60cm Detector2	33027	238	0.72
60cm Detector3	34864	238	0.68
60cm Detector4	35235	252	0.71
SUM 60cm	**141784**		
5cm detector5	22254	178	0.80
5cm detector6	19775	201	1.01
5cm detector7	22315	178	0.80
5cm detector8	20871	209	1.00
SUM 5cm	**78459**		

Table 10: Mean count rates related to the different incident directions, Standard deviations, relative errors and fractions according the number of "main" triggers (181474/ minute). φ is true north-based azimuth angle, θ is zenith angle.

Direction		Average	Standard deviation	Relative error [%]	Fraction
Vertical Directions	[1-5]	3965	70	1.77	1.66
	[2-6]	2899	76	2.66	1.67
	[3-7]	3754	68	1.83	1.39
	[4-8]	3128	79	2.54	1.86
$\varphi=163^0\pm31^0$ E $\theta=30^0\pm11^0$	[1-6]	1278	37	2.92	0.69
	[3-8]	1306	38	2.98	0.73
$\varphi=73^0\pm31^0$ E $\theta=30^0\pm11^0$	[1-7]	1544	40	2.64	0.67
	[2-8]	1346	40	3.01	0.80
$\varphi=343^0\pm31^0$ E $\theta=30^0\pm11^0$	[2-5]	1458	38	2.64	0.74
	[4-7]	1496	39	2.63	0.67
$\varphi=253^0\pm31^0$ E $\theta=30^0\pm11^0$	[3-5]	1454	38	2.67	0.68
	[4-6]	1267	38	3.00	0.72
$\varphi=118^0\pm20^0$ E $\theta=38^0\pm10^0$	[1-8]	691	27	4.00	0.39
$\varphi=28^0\pm20^0$ E $\theta=38^0\pm10^0$	[2-7]	672	26	3.86	0.33
$\varphi=208^0\pm20^0$ E $\theta=38^0\pm10^0$	[3-6]	591	25	4.27	0.33
$\varphi=298^0\pm20^0$ E $\theta=38^0\pm10^0$	[4-5]	730	27	3.83	0.37
SUM		**27579**			**13.70**

Table 11: Mean count rates of "special" cases; variances, relative errors and fractions according the number of "main" triggers (181474/ minute).

Coincidence	Average	Standard deviation	Relative error [%]	Fraction
Many – Many	568	24	4.27	0.31
Many – Zero	5536	87	1.58	3.33
Zero – Many	759	28	3.78	0.33
Zero – One	51735	274	0.53	26.57
One – Zero	93191	345	0.37	54.55
Many – One	1551	47	3.05	0.90
One – Many	690	29	4.20	0.32
SUM	**154030**			**86.30**

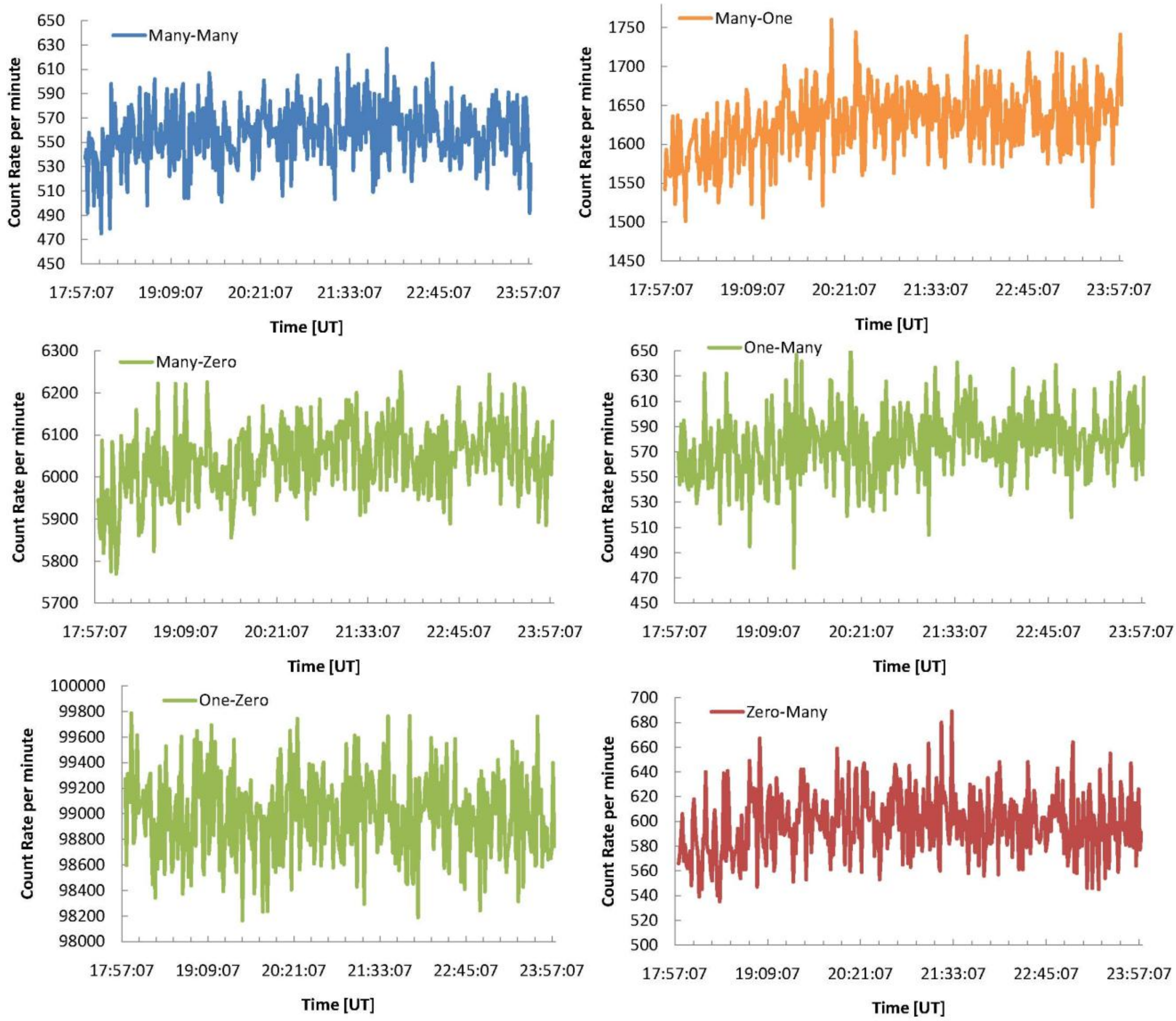

Figure 46: Time series of the "special" cases, see description in the in the text and in the Error! Reference source not found.**.**

Table 12: Mean value of the variance, its variance and relative error calculated by 5-sec count rates of 1 minute time span (total 12 5-dec count rates) (07.02.2008).

Detectors	Average	Standard deviation	Relative error [%]
60cm Detector 1	52	11	21.36
60cm Detector 2	50	10	21.36
60cm Detector 3	51	11	21.71
60cm Detector 4	52	11	21.71
5cm Detector 1	42	9	21.30
5cm Detector 2	39	8	21.00
5cm Detector 3	42	9	21.36
5cm Detector 4	40	9	21.69

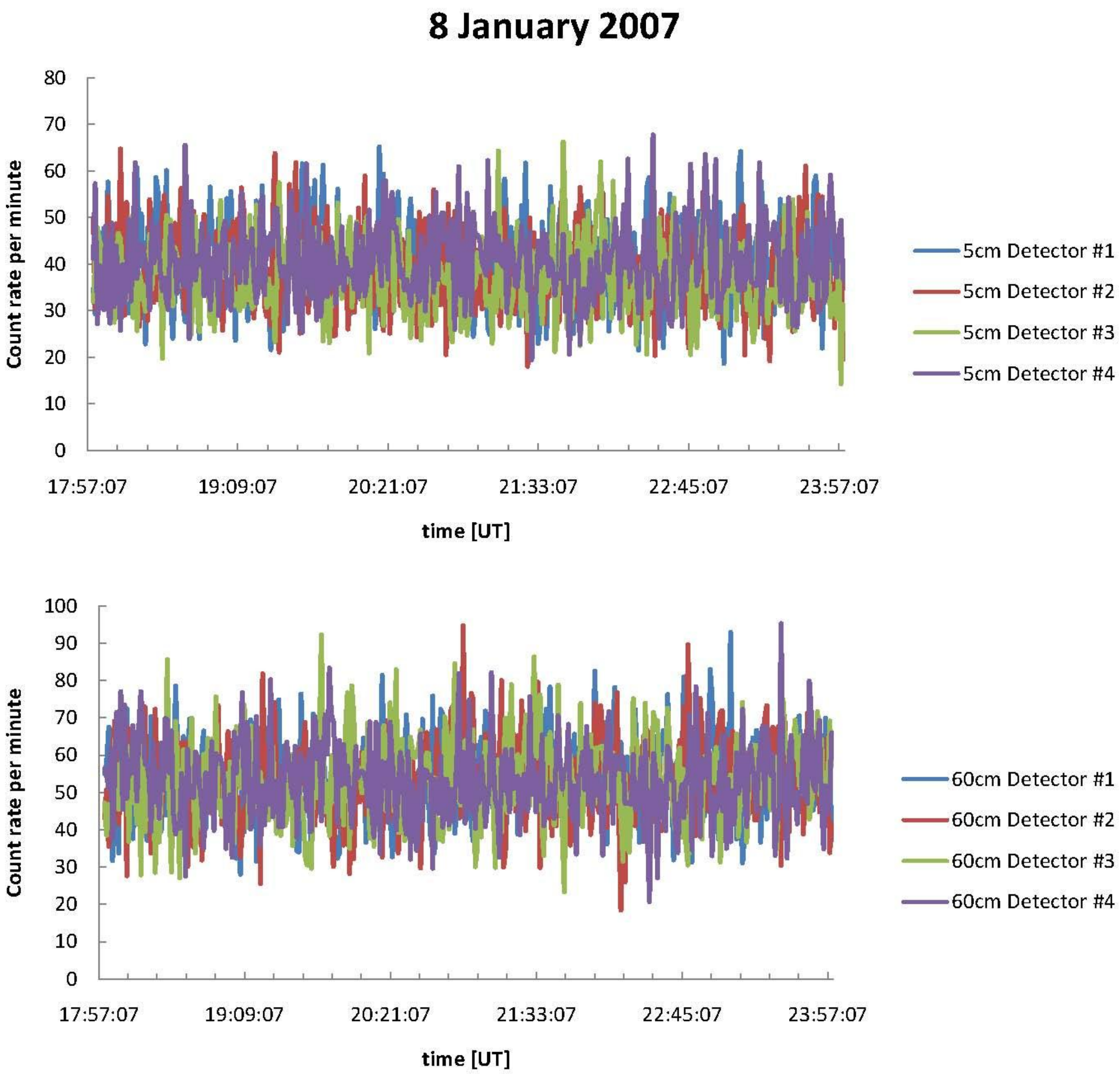

Figure 47 Time series of the ASNT channel variances. Despite the mean values of ASNT channels slightly differ, the variances are very close to each-other, thus proving uniformity of ASNT channels.

Table 13: Mean value of the correlation matrix, calculated by 5-sec count rates of 1 minute time span and averaged over time span of 6 hours at 7 January 2008. Emphasized (red) values are related to ASNT channels stacked one above another, for which correlation should be non zero.

	Det 1	Det 2	Det 3	Det 4	Det 5	Det 6	Det 7	Det 8
Det 1	1							
Det 2	0.041	1						
Det 3	0.042	-0.003	1					
Det 4	-0.003	0.032	0.042	1				
Det 5	0.154	0.067	0.049	0.024	1			
Det 6	0.066	0.118	0.006	0.053	0.015	1		
Det 7	0.053	0.027	0.135	0.049	0.022	-0.007	1	
Det 8	0.048	0.052	0.057	0.122	0.021	0.018	0.023	1

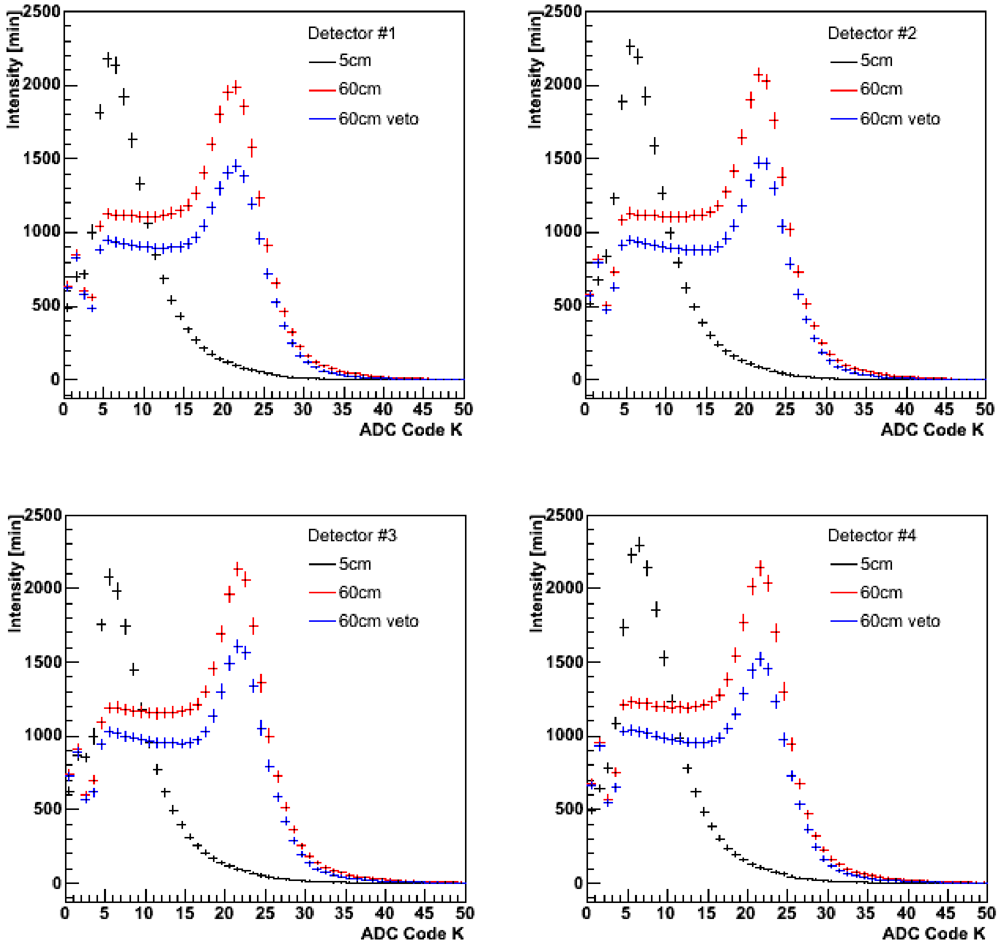

Figure 48 Spectra of the energy releases in thick and thin scintillators. Veto option suppresses contamination of the charged particles by ~25%.

Table 14: **Count rates correspondent to old SNT 4 threshold on the energy release in thick scintillators.**

Threshold	Average		Standard deviation		Relative error [%]	
		Veto		Veto		Veto
Threshold1	78586	58705	551.77	300.14	0.70	0.51
Threshold2	34460	25737	895.00	587.74	2.60	2.28
Threshold3	10550	7725	353.88	268.68	3.35	3.48
Threshold4	4410	2866	139.61	99.23	3.17	3.46

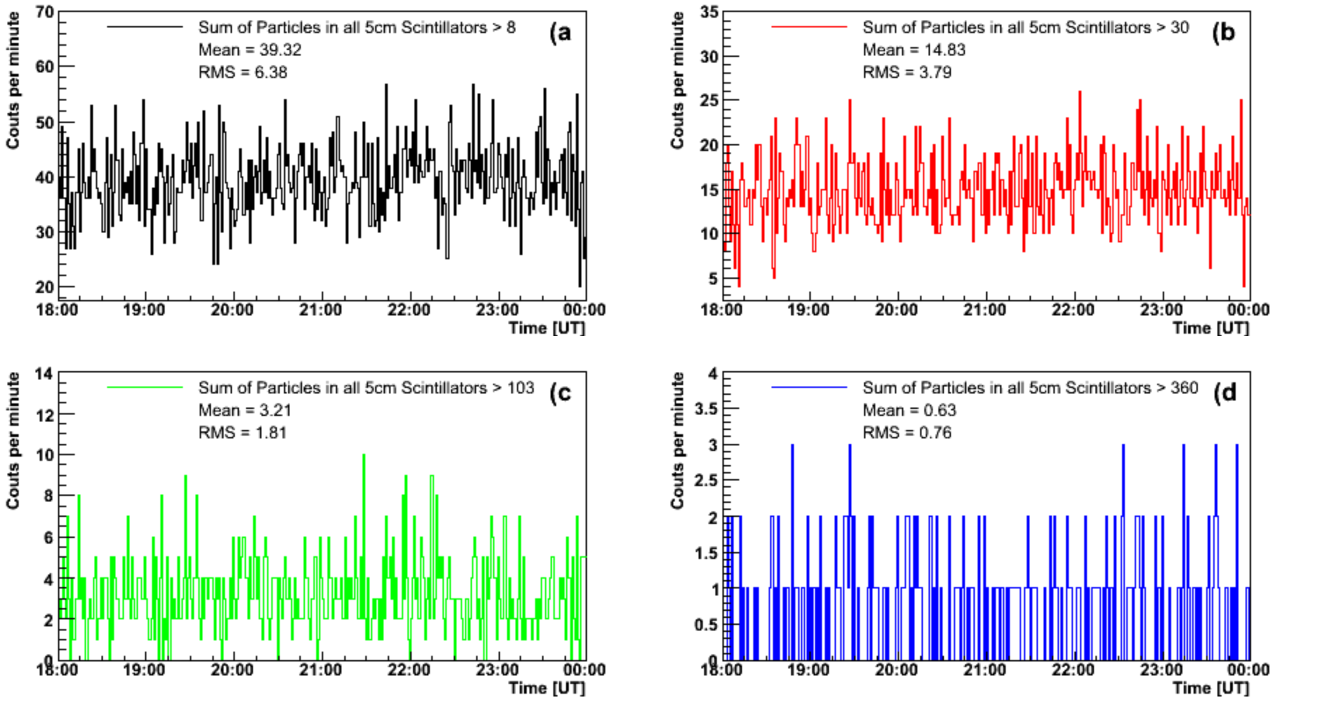

Figure 49: The time series of the EAS initiated triggers (many-many case) conditioned on the value of the minimal number of incident particles (shown in the Figures) in 5 cm scintillator.

3.2 Nor-Amberd Multidirectional Muon Monitor (NAMMM)

The Nor-Amberd Muon Multidirectional Monitor NAMMM **Error! Reference source not found.Error! Reference source not found.**, shown in Figure 50 consists of two layers of plastic scintillators above and below one of the three sections of the Nor Amberd NM. The lead (Pb) filter of the NM absorbs electrons and low energy muons. The threshold energy of the detected muons is estimated to be 350 MeV. The NAMMM consists of 6 up and 6 down scintillators, each having the area of 0.81 m^2. The distance between layers is ~ 1 m., and the mean angular accuracy is ~ 25º. The data acquisition system of the NAMMM can register all coincidences of detector signals from the upper and lower layers, thus, enabling measurements of the arrival of the muons from different directions. The signals ranging from 0.5 mV to 7.2 V, from each of 12 photomultipliers, are passed to the programmable threshold discriminators. The discriminator output signals are fed in parallel to the 12-channel OR gate triggering device and to a buffer. Two 6 bit length words are stored in the buffer, reflecting the trigger status from the 12 registering channels: the first word is for the upper set and the second word is for the lower set. The ones correspond to “fired” channels and zeros to channels that were not fired during a program selectable duration gate in the range 100-1000 nsec. The NAMMM triggered condition is defined by detecting at least one signal in the 12 data channels.

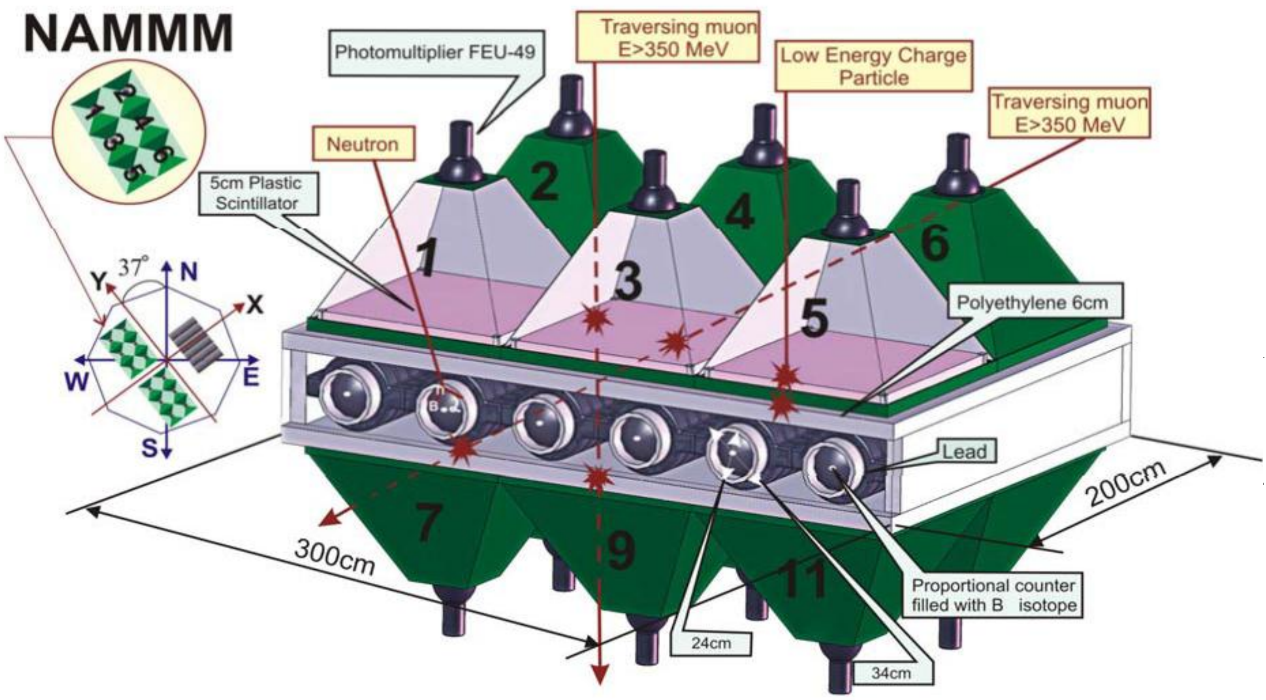

Figure 50: Nor Amberd Multidirectional Muon Monitor.

There are 43 different possibilities of so called “basic states” of detector triggers. 36 of them carry information about the direction of the incident muon. For example, trigger word configuration “001000” for the upper layer and “001000” for the lower layer corresponds to the muon traversal through third upper and third lower scintillators (zenith angle between 0 and 45º), as demonstrated in Figure 50. Upper and lower layer trigger word configuration of “001000” and “100000” respectively corresponds to the traversal through the third upper and the first lower scintillator (zenith angle between 45 and 65º). The other 7 possibilities, for example, more than one trigger in upper and lower layers such as “111100” and 110000” respectively, or one in the upper layer and many in the lower layer, can be analyzed in terms of the various physical processes, such as the extensive air shower hitting the detector setup, or particle generation in the lead (Pb) layer of the neutron detector system, neutron bursts **Error! Reference source not found.**, etc.

The raw data of the two sections of NAMMMs in the XML format available from CRD http server. http://adei.crd.yerphi.am/adei

In the directory “DEFAULT” of both mentioned links the following information is stored correspondingly for the first and second sections of detector, namely NAMMM1 and NAMMM2:

- columns 1-12 - the count rates of all channels of NAMMM: first 6 columns – from upper layer scintillators, 7-12 columns – from lower layer scintillator. The numbering of scintillators is explained in the Figure 50.
- columns 13-48 – the count rates corresponding to the 36 coincidences in upper and lower NAMMM layers, i.e. – corresponding to the traversal of the single charged particle (mostly muons with energy > 250 MeV). The order of the different directions in the file is following: [1-7] [1-8] [1-9] [1-10] [1-11] [1-12] [2-7] [2-8] [2-9] [2-10] [2-11] [2-12] [3-7] [3-8] [3-9] [3-10] [3-11] [3-12] [4-7] [4-8] [4-9] [4-10] [4-11] [4-12] [5-7] [5-8] [5-9] [5-10] [5-11] [5-12] [6-7] [6-8] [6-9] [6-10] [6-11] [6-12], where the first number corresponds to the upper layer and the second – to the lower (see Figure 50) Also on the same Figure you can see the orientation of NAMMM axes according to direction to the North Pole, thus we can calculate the interval of the horizontal angles of incidence related to each coincidence.
- columns 49-55 – the count rates of the “special” coincidences different from listed above and forming the “full system” of possible configurations of the channel operation. Conditioned on the existing as minimum 1 signal in 12 NAMMM channels there could be the following possibilities of number of counts in top and bottom layers (the first sign in the pair is corresponding to the upper scintillator): many-many (more than one count in 4 top and 4 bottom layers), many-zero (more than 1 in top and nothing in 4 bottom), zero-many, zero-one, one-zero, many-one, one-many.

- columns 56 - the number of the “main” triggers – at least one signal in 12 channels in preselected time span (1 minute). If we consider all logical configurations of NAMM operation outcomes, this number will be equal to sum of the columns 13-55.
- columns 57-68 - the variances of 12 channels.
- columns 69-134 – the correlation matrix**Error! Reference source not found.**.

In the directories “spectrum” the 127-channel histograms of the energy releases are stored for each minute, in files with extensions:

- spectrum1 - spectrum6, the histograms of the energy releases in the upper scintillators are stored.
- spectrum7 - spectrum12, the histograms of the energy releases in the lower scintillators are stored;
- spectrum13 - spectrum18, histograms of energy releases, in upper detectors are stored with condition that in lower detectors there was now signal, i.e., the energy releases of electrons and low energy muons filtered in the lead absorber.

Events corresponding to each of the 43 basic states, described above, are independently summed over a 10-second data collection period. Then the string of the 10-second averaged 43 numbers is passed to the analysis software and another cycle of 10-second summation is started. The sequence of the 10-second summation data is gathered for 5 minutes for a total of 30 number strings. The total amount of data from the 5-minute integration time (thirty sequences of 43 number strings, or 1290 numbers) is too large for storing on the chip. Therefore, we calculate 12 x 12 correlation matrices, to monitor how the correlations of count rates of the 12 detector channels are changing. The correlation matrix will provide a test for the random enhancements of the total detector count rate to spurious signals in one or more detector channels. The enhancement of the count rate in the detector due to changing geophysical conditions should be accompanied by the coherent enhancements of correlations between all (or vast majority) of the detecting channels. After completing the 5-minute cycle, the computed means, standard deviations, and the correlation matrix are transferred to the on-line computer.

All electronics are of original design, according to modern very compact and high reliable technologies, oriented for easy maintenance and production. To minimize data transmission rate, the raw data is partially processed in microcontroller before sending it to the main computer. A 32-

bit microcontroller is chosen as the basic element. Taking into account the slow data rates, and to minimize the cost, a serial data transmission is used, instead of much more expensive parallel data transmission standards like CAMAC, VME, etc.

To guarantee the data acquisition continuity, the electronics system is modernized gradually. A newly designed readout is based on the concept of full software control of the detector parameters and maximum utilization of all detector data. Each photomultiplier has its own local programmable high voltage (HV) power supply and buffer preamplifier to condition the pulses in preparation for sending them via long coaxial cables without degrading the dynamic range and signal-to-noise ratio. Counting modules are located in the counter room. They have buffer preamplifiers and programmable threshold comparators (discriminators) at the inputs. The threshold of the counter module input comparators can be programmed by voltage and polarity in the range from -0.5V to 0.5V. Besides the comparators, the buffer preamplifier output signals can be transferred to other data processing devices such as ADC's, etc., to be installed later. All electronics modules are based on using modern 8-bit and 32-bit microcontrollers, for the detector control system (HV programming and measurement) and for the main data acquisition respectively. Currently the Atmel 8-bit and Fujitsu FR 32-bit controllers are used.

The microcontroller based electronics units (HV power supply and counting modules) have optional environmental sensors. The HV power supply has only temperature sensor, counting modules also have pressure and humidity sensors.

The main pressure sensor of the whole system is placed in a special pressure-tight box with possibility of periodic calibration using a standards Hg barometer. It consists of Motorola MPXA6115 Integrated Silicon Pressure Sensor and ATMEL 8-bit microcontroller and has frequency modulated output for direct coupling with counter modules and serial asynchronous interface to connect to the PC.

3.3 Nor-Amberd and Aragats Neutron Monitors (NANM & ArNM)

Two 18NM-64 neutron monitors (see Figure 51, Figure 52) [3], are in operation at Nor-Amberd (40°22'N, 44°15'E, 2000m above sea level), and at Aragats, (40°28'N, 44°10'E, 3250m above sea level) research stations. They called the Nor Amberd Neutron Monitor (NANM), and the Aragats Neutron Monitor (ANM), respectively. The monitors are equipped with new electronics providing time integration of counts by three dead times. The first dead time equals to 400ns for collecting almost all thermalized neutrons entering the proportional chamber from the lead. The second dead time is equal to the 0.25ms and the third one equal 1.25ms (as most of NM from world-wide network). Also 2 proportional chambers without lead coverage are added to NANM.

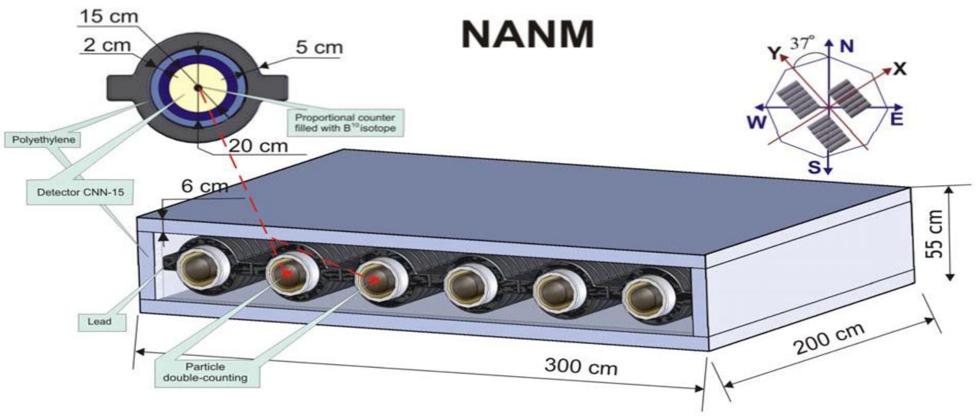

Figure 51 Nor-Amberd Neutron Monitor (NANM)

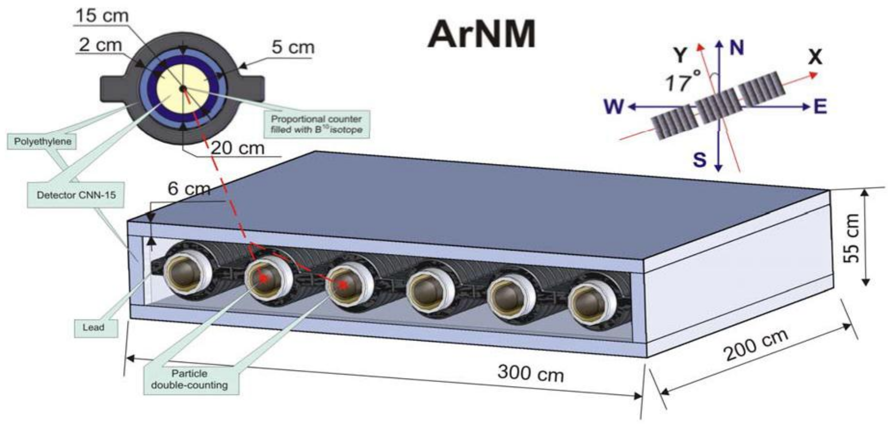

Figure 52 Aragats Neutron Monitor (ArNM).

The raw data of the NANM and ArNM is available from CRD http server by these links:

http://adei.crd.yerphi.am/adei

Table 15. Count rates of the 18 channels of the NANM .

	Number of Column	Average Count Rate (0.4us)	Std. Dev.	SUM	**Number of Column**	Average Count Rate (250us)	Std. Dev.	SUM	**Number of Column**	Average Count Rate (1250us)	Std. Dev.	SUM
Detector 1	**1**	1530	57		**2**	1312	39		**3**	1172	33	
Detector 2	**4**	1375	47		**5**	1216	37		**6**	1101	32	
Detector 3	**7**	1608	52		**8**	1405	40		**9**	1262	35	
Detector 4	**10**	1628	52		**11**	1425	39		**12**	1277	33	
Detector 5	**13**	1580	53		**14**	1379	41		**15**	1243	35	
Detector 6	**16**	1391	64		**17**	1198	37		**18**	1082	32	
Detector 7	**19**	1676	54		**20**	1455	41		**21**	1310	34	
Detector 8	**22**	1608	51		**23**	1412	41		**24**	1268	35	
Detector 9	**25**	1539	50	**27483**	**26**	1345	38	**23993**	**27**	1215	32	**21633**
Detector 10	**28**	1553	53		**29**	1361	41		**30**	1228	35	
Detector 11	**31**		54		**32**	1370	41		**33**	1232	35	
Detector 12	**34**	1417	49		**35**	1236	38		**36**	1114	32	
Detector 13	**37**	1471	51		**38**	1260	39		**39**	1133	33	
Detector 14	**40**	1369	46		**41**	1226	37		**42**	1120	33	
Detector 15	**43**	1561	53		**44**	1362	41		**45**	1234	35	
Detector 16	**46**	1620	52		**47**	1426	41		**48**	1286	34	
Detector 17	**49**	1581	51		**50**	1395	40		**51**	1260	35	
Detector 18	**52**	1374	47		**53**	1202	36		**54**	1086	31	

In the data files of the NM following information is stored (Table 15 and Table 16**Error! Reference source not found.**):

1. columns 1+3i (i=0,…,17) - the count rates of all 18 channels of NM with dead time 400ns.
2. columns 2+3i (i=0,…,17) - the count rates of all 18 channels of NM with dead time 0.25ms.
3. columns 3+3i (i=0,…,17) - the count rates of all 18 channels of NM with dead time 1.25ms.
4. column 55 – the pressure coefficient.

5. columns 56 – 60 yet unused channels, additional neutron detectors to be attached soon.

Table 16. Count rates of the 18 channels of the ArNM .

	Number of Column	Average Count Rate (0.4us)	Std. Dev.	SUM	**Number of Column**	Average Count Rate (250us)	Std. Dev.	SUM	**Number of Column**	Average Count Rate (1250us)	Std. Dev.	SUM
Detector 1	**1**	2574	72		**2**	2235	51		**3**	1997	43	
Detector 2	**4**	2521	64		**5**	2249	52		**6**	2031	44	
Detector 3	**7**	2840	68		**8**	2528	54		**9**	2259	45	
Detector 4	**10**	2800	68		**11**	2495	54		**12**	2235	46	
Detector 5	**13**	2314	59		**14**	2092	48		**15**	1907	42	
Detector 6	**16**	2335	59		**17**	2074	47		**18**	1866	40	
Detector 7	**19**	2437	64		**20**	2169	51		**21**	1938	43	
Detector 8	**22**	2648	63		**23**	2368	50		**24**	2131	43	
Detector 9	**25**	2650	62	**43261**	**26**	2392	50	**38769**	**27**	2166	44	**35055**
Detector 10	**28**	2731	63		**29**	2469	51		**30**	2239	44	
Detector 11	**31**	2459	62		**32**	2209	52		**33**	2000	45	
Detector 12	**34**	2315	62		**35**	2055	49		**36**	1852	42	
Detector 13	**37**	2145	59		**38**	1910	46		**39**	1733	40	
Detector 14	**40**	1877	51		**41**	1723	44		**42**	1589	39	
Detector 15	**43**	2069	53		**44**	1900	45		**45**	1746	39	
Detector 16	**46**	2043	54		**47**	1861	45		**48**	1709	39	
Detector 17	**49**	2396	63		**50**	2146	50		**51**	1943	44	
Detector 18	**52**	2097	58		**53**	1886	48		**54**	1705	41	

3.4 MAKET-ANI Extensive Air Shower Detector.

In the assembly of the ANI Cosmic Ray experiment **Error! Reference source not found.**, two detectors measuring the Extensive Air Showers (EAS) are operating on the Aragats research station. The main goal of the GAMMA **Error! Reference source not found.** and MAKET-ANI **Error! Reference source not found.**,**Error! Reference source not found.** detectors are to investigate the energy spectra of cosmic rays to understand the origin and accelerator mechanisms. Both detectors use the same particle density detection techniques to determine the number of electrons in the shower and infer the energy and type of the primary particle. EAS detectors are triggered arrays, but each detector counts all incident particles and an independent read-out stores the changing fluxes of charged particles. The count rates of the charged components at altitude 3200 a.s.l. are ~420 counts/m2/sec for >10 MeV electrons and ~50counts/m2/sec for >5 GeV muons. These high count-rates, combined with the large area of the electron and muon detectors on Mt. Aragats, are very attractive for establishing a monitoring facility to investigate the correlations between variations of electron and muon count rates with the enhancing flux of solar ions incident on the Earth's atmosphere.

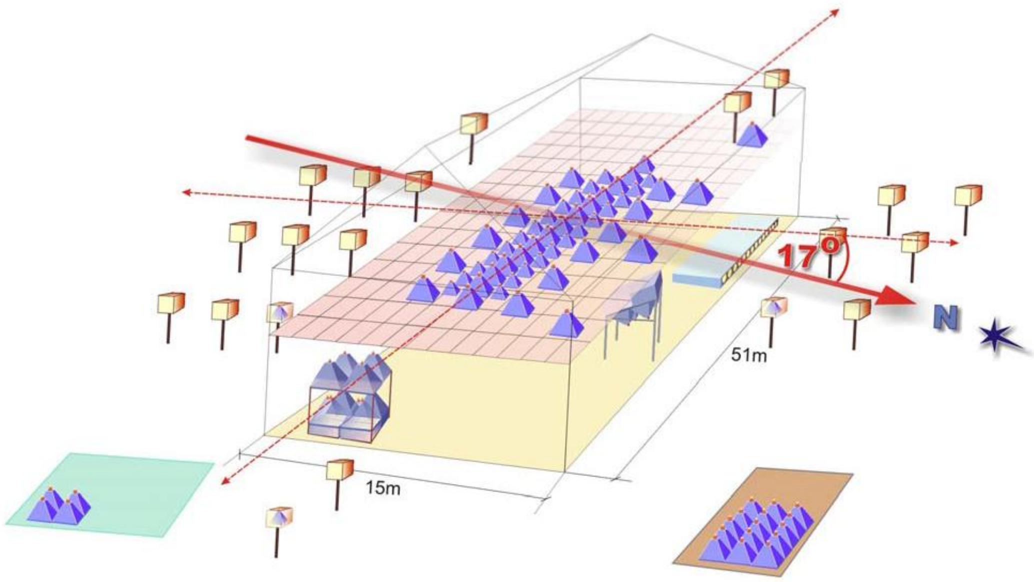

Figure 53: MAKET-ANI Extensive Air Shower Detector.

The MAKET-ANI surface array, see Figure 53, consists of 92 detectors formed from 5 cm thick plastic scintillators, with area 1m2 each, to measure particle density of the registered EAS. Twenty four of them have 0.09 m^2 area and 68 have 1 m^2 area. The central part consists of 73 scintillation detectors and is arranged in a rectangle of 85 x 65 m^2. In order to estimate the zenith and azimuthal angles, 19 detectors from the 92 are equipped with timing readout to measure the EAS front appearance with an accuracy of ~ 5 ns. The photomultipliers (FEU-49) are placed in light-tight iron boxes. Logarithmic Analog to Digital Converters (ADC) and Constant Fraction Discriminators (CFD) are placed just above the photomultiplier. The dynamic range of the registered particle number is ~ 5 x 10^3. During multiyear measurements the detecting channels were continuously monitored. Data on background cosmic ray spectra was collected for each detector. The slope of the spectra was used for detector calibration. The slope of the background spectra is a very stable parameter which did not change even during very severe Forbush decreases, when the mean count rates can decrease as much as 20%. The changing fluxes of muons and electrons incident on the MAKET-ANI detector are available from the MAKET-ANI data bank. All Forbush decreases and other geoeffective events are very well reproduced by these data with very good statistical provision, the 1- minute count ray of 1 m^2 plastic scintillator is ~ 25,000. 150 plastic scintillators with area of 1 m^2 each are located in the underground hall of the ANI experiment, to measure the muon content of the EAS. The 6 m thick concrete blocks plus the 7 m soil filter the electrons and the low energy muons. Thus, only muons with energies > 5GeV reach the detectors. After obtaining and publishing final results of the MAKET-ANI (see Figure 53) experiment [11] the experiment for collecting high energy galactic cosmic rays was stopped. Some of the scintillators were used for rearranged smaller detector. Around the ASNT detector (consisted of four 60 cm thick scintillators and four 5 cm thick scintillators another 8 5 cm scintillators were arranged and attached to the 16 channel spectrum analyzer. Meanwhile new MAKET array provides following information:

1. 1 minute count rates of all 16 channels of the MAKET; (see Table 17)

2. Count rate of the EAS triggering 8 and all 16 detectors;

3. Estimates of the variances of count rates of each MAKET channel, variances are calculated by 12 five-second count rates (see Table 19);

4. 16 x 16 correlation matrix of MAKET channels calculated by five-second count rates in 1 minute. Advanced Data Analysis System (ADAS) provides registration and storage of all logical combinations of the detector signals for further off-line analysis and for on-line alerts issuing. The slow control system of the ADAS provides the remote control of the Photo Multiplier Tube (PMT) high voltage and important parameters of the DAQ electronics.

The data is stored in

http://adei.crd.yerphi.am/adei

In the directory “DEFOULT” following information is stored:

1. Columns 1-16 - the count rates of all 16 MAKET channels: first 4 columns – from 60 cm scintillators, 5-16 columns – from 5 cm scintillator. The count rates are posted in the Table 17;

2. Columns 17-18 – the count rates corresponding to the EAS initiated triggers. 17^{th} column corresponds to the coincidence of the first 8 channels (ASNT scintillators), 18^{th} column corresponding to the coincidence in all 16 channels. The count rates are posted in the Table 18;

3. Columns 19-34 – the variances of 16 channels, see Table 19;

4. Columns 35-154 – the correlation matrix.

Table 17 Count Rates of the MAKET channels, variances and relative errors.

Detector	Average	Standard deviation	Relative error [%]
Detector 1 (60cm)	37973	201	0.53
Detector 2 (60cm)	29869	185	0.62
Detector 3 (60cm)	33244	188	0.57
Detector 4 (60cm)	32074	164	0.51
Detector 5	23732	152	0.64
Detector 6	28100	167	0.59
Detector 7	17125	146	0.85
Detector 8	24845	174	0.70
Detector 9	22956	144	0.63
Detector 10	18313	140	0.76
Detector 11	23722	159	0.67
Detector 12	18901	148	0.78
Detector 13	22589	152	0.67
Detector 14	19492	134	0.69
Detector 15	22964	152	0.66
Detector 16	21154	144	0.68

In the directories “spectrum” following information is stored:

1. spectrum1, … spectrum4 the histograms of the spectrum of amplitude codes in thick 60 cm scintillator are stored. In files with extension;
2. spectrum5, … spectrum16 the histograms of spectrum of amplitude codes in 5 cm thin scintillators are stored;

In the CRD local server available files with following information:

- In the files with “events” extension is related to the Extensive Air Showers (EAS). The logical software trigger selects events when signals are more than in 8 detectors.

Table 18 Count Rates of the MAKET EAS initiated triggers, variances and relative errors.

Detector	Average	Standard deviation	Relative error [%]
Coincidence in thirst 8 channels	20	4	21.02
Coincidence in all 16 channels	5	2	41.95

Table 19 Mean value of the variance, its variance and relative error calculated by 5-sec count rates of 1 minute time span (total 12 5-dec count rates).

Detector	Average	Standard deviation	Relative error [%]
Detector 1 (60cm)	53	11	21.46
Detector 2 (60cm)	49	10	21.06
Detector 3 (60cm)	52	12	22.63
Detector 4 (60cm)	50	11	21.37
Detector 5	44	10	21.87
Detector 6	47	10	22.18
Detector 7	37	8	20.79
Detector 8	45	11	23.28
Detector 9	43	9	20.85
Detector 10	38	8	21.16
Detector 11	43	9	20.96
Detector 12	39	8	20.66
Detector 13	42	9	20.62
Detector 14	39	8	21.22
Detector 15	43	9	21.68
Detector 16	41	8	20.50

3.5 Aragats Multidirectional Muon Monitor (AMMM)

The Aragats Multidirectional Muon Monitor (AMMM) consists of 2 layers of the scintillation detectors. 29 scintillation detectors (each detector have 1m^2 surface and 5cm thickness),are located on top of the top of ANI concrete calorimeter and 100 the same type detectors 14 m below (under 4m concrete and 7m soil), as shown in Figure 54. Zenith angle between axes of AMMM and direction to South pole is ~-17º. Count rate in the upper detectors is ~28000 counts per minute and variance ~170. Count rate of each of 1 m^2 scintillators in the underground hall(high energy muons with energy threshold 5 GeV) is ~3000 counts per minute and variance ~55. The relative accuracy of 1-minute count rates of underground high energy muon detector is ~0.2%, of the low energy muons and electrons on surface ~ 0.12%.The new electronics will be installed in the summer 2008.

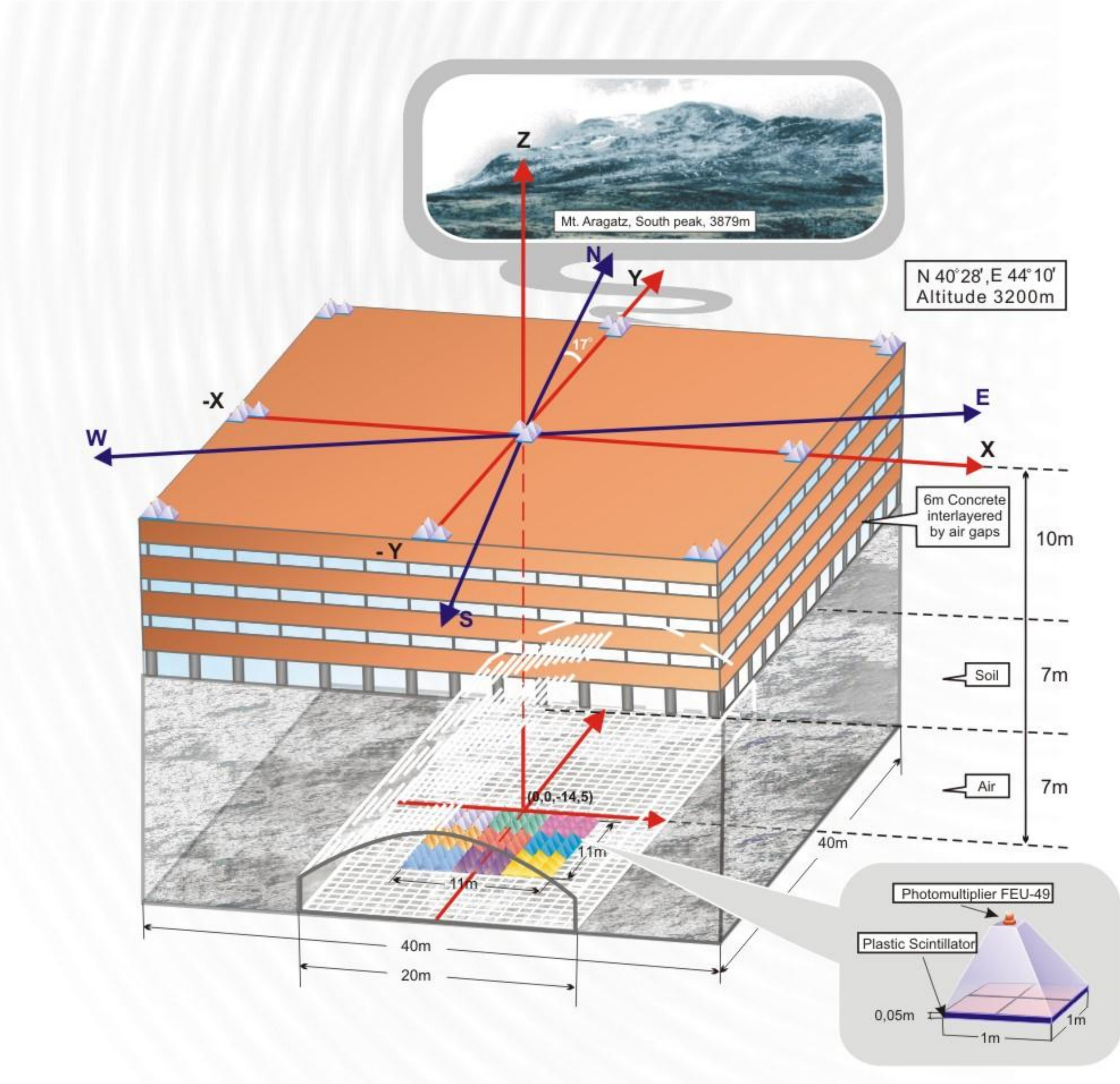

Figure 54 Aragats Multidirectional Muon Monitor (AMMM).

In tables 20 and 21 we present averaged count rates as measured at 8 December 2008 and total number of muons measured by each detector per day. Total 248,292,843 muons were detected.

Table 20 Average minute count rates and standard deviations of 5 GeV muons measured at 8 December 2008

Nº	Average	Standard deviation	Relative error [%]	Nº	Average	Standard deviation	Relative error [%]	Nº	Average	Standard deviation	Relative error [%]
1	2914	43.1	1.48%	**31**	2939	52.2	1.78%	**61**	3003	54.4	1.88%
2	3052	55.9	1.83%	**32**	2875	55.7	1.94%	**62**	2883	55.6	1.93%
3	3027	56.7	1.87%	**33**	2834	56.3	1.99%	**63**	2687	54.9	2.04%
4	2804	53.5	1.91%	**34**	2749	55.0	2.00%	**64**	2854	59.5	2.08%
5	2997	56.9	1.90%	**35**	2933	55.8	1.90%	**65**	2931	56.2	1.92%
6	3013	55.0	1.83%	**36**	2704	53.6	1.98%	**66**	2674	52.4	1.96%
7	2957	54.5	1.84%	**37**	2854	55.6	1.95%	**67**	3049	63.5	2.08%
8	2829	55.5	1.96%	**38**	2834	54.8	1.93%	**68**	2832	59.9	2.12%
9	2896	53.6	1.85%	**39**	2873	52.6	1.83%	**69**	2988	52.8	1.77%
10	2930	54.7	1.87%	**40**	2768	55.1	1.99%	**70**	2837	53.9	1.90%
11	2945	55.3	1.88%	**41**	2756	53.0	1.92%	**71**	2732	55.1	2.02%

12	2912	54.0	1.86%	**42**	2683	53.6	2.00%	**72**	2708	50.8	1.88%
13	2800	53.6	1.91%	**43**	2845	58.3	2.05%	**73**	2827	51.0	1.80%
14	2785	54.1	1.94%	**44**	2773	53.4	1.93%	**74**	2844	56.1	1.97%
15	2972	55.5	1.87%	**45**	2713	55.5	2.05%	**75**	2608	52.8	2.03%
16	2815	53.5	1.90%	**46**	2771	55.2	1.99%	**76**	3042	56.7	1.86%
17	2874	55.0	1.91%	**47**	3006	56.4	1.88%	**77**	3112	58.5	1.88%
18	2904	54.5	1.88%	**48**	3105	56.4	1.82%	**78**	3061	55.8	1.82%
19	2917	56.2	1.93%	**49**	3047	56.4	1.85%	**79**	2824	56.9	2.01%
20	2753	54.1	1.97%	**50**	3087	58.5	1.90%	**80**	2988	52.8	1.77%
21	2858	54.2	1.90%	**51**	2942	49.6	1.69%	**81**	2950	56.8	1.93%
22	2824	53.7	1.90%	**52**	3053	56.9	1.86%	**82**	3014	56.6	1.88%
23	2704	53.6	1.98%	**53**	2950	56.5	1.92%	**83**	3214	57.2	1.78%
24	2833	54.3	1.92%	**54**	3148	58.8	1.87%	**84**	3069	59.4	1.94%
25	2765	53.8	1.94%	**55**	2813	54.7	1.94%	**85**	3063	57.7	1.88%
26	2810	55.7	1.98%	**56**	2871	55.4	1.93%	**86**	3133	58.5	1.87%
27	2686	50.7	1.89%	**57**	2964	55.8	1.88%	**87**	2934	58.1	1.98%
28	2706	53.2	1.96%	**58**	3070	55.3	1.80%	**88**	3048	54.7	1.79%
29	2799	54.6	1.95%	**59**	2785	55.0	1.98%	**89**	2847	52.3	1.84%
30	2883	54.7	1.90%	**60**	2717	54.4	2.00%				

Table 21 One day count rates and standard deviations of 5 GeV muons measured at 8 December 2008

№	$\sum_{n=1}^{1440}$	$\sigma_i = 1/\sqrt{\sum}$	№	$\sum_{n=1}^{1440}$	$\sigma_i = 1/\sqrt{\sum}$	№	$\sum_{n=1}^{1440}$	$\sigma_i = 1/\sqrt{\sum}$
1	4196468	0.0488%	**31**	4232101	0.0486%	**61**	4324100	0.0481%
2	4395304	0.0477%	**32**	4139766	0.0491%	**62**	4150894	0.0491%
3	4359005	0.0479%	**33**	4080938	0.0495%	**63**	3869546	0.0508%
4	4037325	0.0498%	**34**	3958483	0.0503%	**64**	4109263	0.0493%
5	4315526	0.0481%	**35**	4222960	0.0487%	**65**	4219990	0.0487%
6	4338958	0.0480%	**36**	3893592	0.0507%	**66**	3851007	0.0510%
7	4258254	0.0485%	**37**	4110259	0.0493%	**67**	4390325	0.0477%
8	4073309	0.0495%	**38**	4081318	0.0495%	**68**	4077850	0.0495%
9	4169796	0.0490%	**39**	4137306	0.0492%	**69**	4303104	0.0482%
10	4218662	0.0487%	**40**	3986352	0.0501%	**70**	4085042	0.0495%
11	4240291	0.0486%	**41**	3968941	0.0502%	**71**	3933727	0.0504%
12	4192812	0.0488%	**42**	3863947	0.0509%	**72**	3900099	0.0506%
13	4032229	0.0498%	**43**	4096364	0.0494%	**73**	4071561	0.0496%
14	4010753	0.0499%	**44**	3992580	0.0500%	**74**	4095402	0.0494%
15	4279079	0.0483%	**45**	3907415	0.0506%	**75**	3754887	0.0516%
16	4053002	0.0497%	**46**	3989798	0.0501%	**76**	4381165	0.0478%
17	4138683	0.0492%	**47**	4328704	0.0481%	**77**	4481856	0.0472%
18	4181801	0.0489%	**48**	4471243	0.0473%	**78**	4408270	0.0476%
19	4199887	0.0488%	**49**	4387797	0.0477%	**79**	4066982	0.0496%
20	3963823	0.0502%	**50**	4445565	0.0474%	**80**	4303104	0.0482%
21	4115385	0.0493%	**51**	4236352	0.0486%	**81**	4248538	0.0485%
22	4067173	0.0496%	**52**	4396528	0.0477%	**82**	4340346	0.0480%
23	3894107	0.0507%	**53**	4247376	0.0485%	**83**	4628072	0.0465%
24	4079820	0.0495%	**54**	4533420	0.0470%	**84**	4420002	0.0476%
25	3980961	0.0501%	**55**	4050083	0.0497%	**85**	4411247	0.0476%
26	4046710	0.0497%	**56**	4134758	0.0492%	**86**	4511576	0.0471%
27	3868109	0.0508%	**57**	4268051	0.0484%	**87**	4225168	0.0486%
28	3897071	0.0507%	**58**	4420483	0.0476%	**88**	4389114	0.0477%
29	4031055	0.0498%	**59**	4010297	0.0499%	**89**	4099514	0.0494%
30	4152082	0.0491%	**60**	3912626	0.0506%			

In Table 22 we present analogical characteristics for 29 plastic scintillators located on the top of ANI calorimeter. Along with 1-minute data from ASEC monitors available from MSQL data base, the summary of daily plots can be observed from http://adei.crd.yerphi.am/adei/.

Table 22 Averaged 1 minute and dayly count rates of surface low energy charged flux measured at 8 December 2007

№	Average	Standard deviation	Relative error [%]
1	29279	180	0.62%
2	28238	249	0.88%
3	28721	261	0.91%
4	29703	223	0.75%
5	29283	181	0.62%
6	28333	256	0.90%
7	29948	247	0.82%
8	28859	301	1.04%
9	29119	244	0.84%
10	29076	178	0.61%
11	28789	282	0.98%
12	28460	166	0.58%
13	29077	178	0.61%
14	29895	229	0.77%
15	28972	250	0.86%
16	28734	245	0.85%
17	29056	240	0.83%
18	27832	248	0.89%
19	29461	230	0.78%
20	29767	236	0.79%
21	28782	229	0.80%
22	27445	247	0.90%
23	29092	238	0.82%
24	29076	177	0.61%
25	28207	281	0.99%
26	29053	224	0.77%
27	28370	257	0.91%
28	28111	175	0.62%
29	28491	248	0.87%

№	$\sum_{n=1}^{1440}$	$\sigma_i = 1/\sqrt{\sum}$
1	42161758	0.0154%
2	40662397	0.0157%
3	41357704	0.0155%
4	42772070	0.0153%
5	42167188	0.0154%
6	40799310	0.0157%
7	43124876	0.0152%
8	41557256	0.0155%
9	41931409	0.0154%
10	41870013	0.0155%
11	41455964	0.0155%
12	40982046	0.0156%
13	41871011	0.0155%
14	43049245	0.0152%
15	41719295	0.0155%
16	41377597	0.0155%
17	41840189	0.0155%
18	40078730	0.0158%
19	42423917	0.0154%
20	42864930	0.0153%
21	41446634	0.0155%
22	39520922	0.0159%
23	41891844	0.0155%
24	41868918	0.0155%
25	40618066	0.0157%
26	41835649	0.0155%
27	40853231	0.0156%
28	40480268	0.0157%
29	41026404	0.0156%

3.6 Correlation analysis of ASEC monitors recordings.

The biggest Forbush decrease from 29 October 2003 was detected by all ASEC monitors.

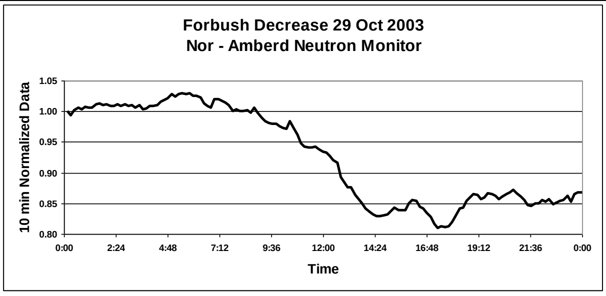

Figure 55 **Forbush decrease; Neutrons, 2000 m.a.s.l.**

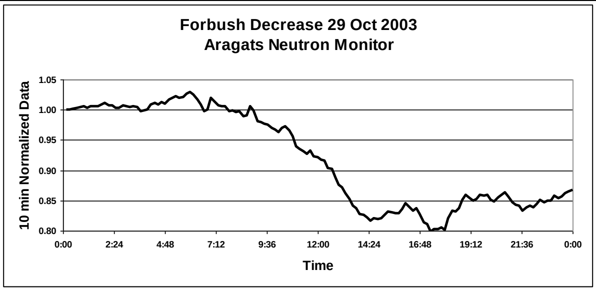

Figure 56 Forbush decrease; Neutrons, 3200 m.a.s.l.

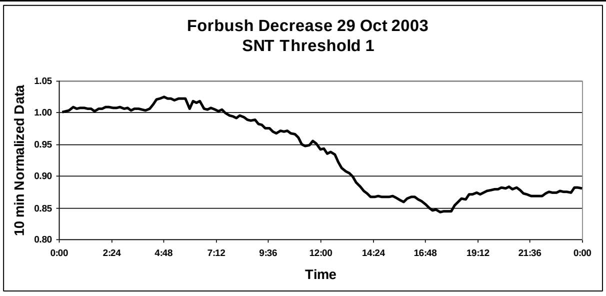

Figure 57 First threshold of SNT

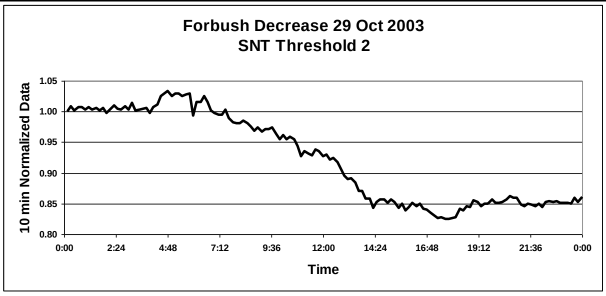

Figure 58 Second threshold of SNT

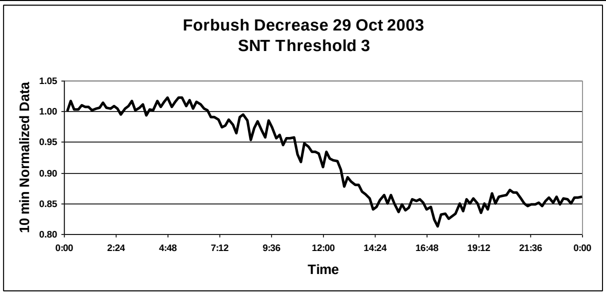

Figure 59 Third threshold of SNT

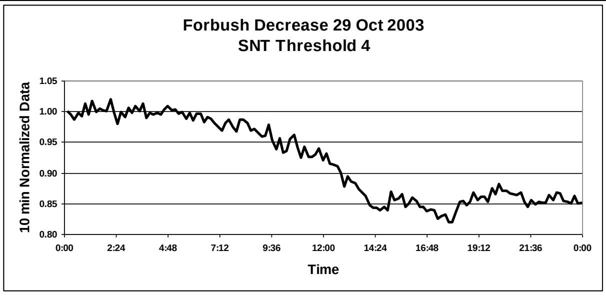

Figure 60 Forth threshold of SNT

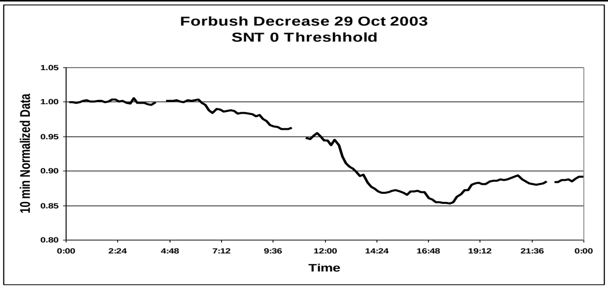

Figure 61 Fd in low energy charged particles; 60 cm thick scintillator

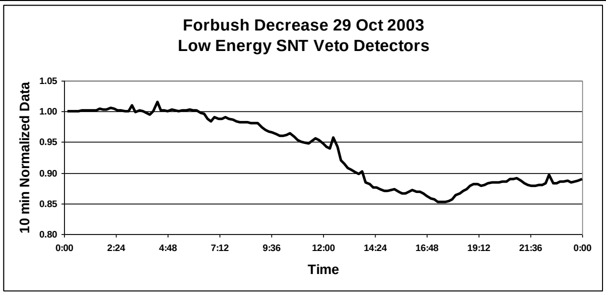

Figure 62 Fd in low energy charged particles; 5 cm thick scintillator - VETO detector

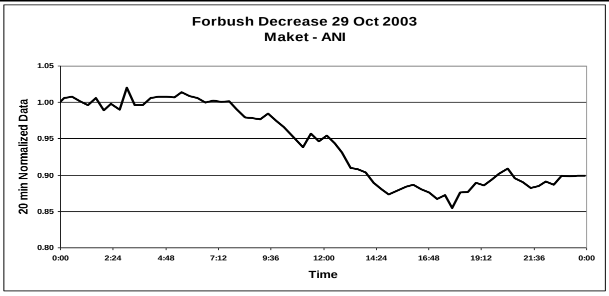

Figure 63 Fd in low energy charged particles; 5 cm thick scintillators, MAKET ANI detector

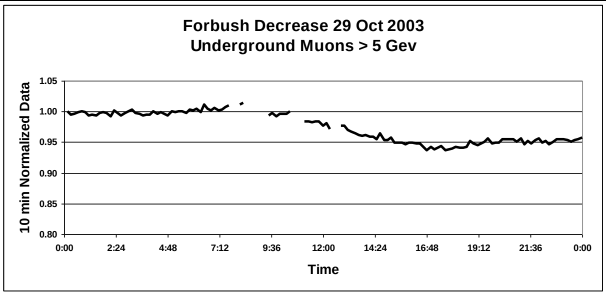

Figure 64 Fd in 5 GeV muons; 5 cm thick scintillator

From Figure 55**Error! Reference source not found.** - Figure 64 we can see that on 29 October, 2003 the neutron flux is attenuated by 20%, low energy charged particle flux – by 15% and high energy muons by 7-8%. The relative values of flux attenuation in different components of the secondary cosmic ray flux can be used as a characteristic of the Fd magnitude. For the investigation of parameters of secondary fluxes, which are the most sensitive to the geoeffectiveness of the event, we select 4 distinct test cases: one corresponding to the silent phase of the geomagnetic disturbance, and others corresponding to the Fd of different magnitudes - from modest, to strongest. The selected cases are: 25 January 2004, 20 November 2003, 27 July 2004, 29 October 2003. Correlation matrices of these events are presented in Tables 23 – 26. Correlations between different particle fluxes calculated for 25 January 2003, when no geomagnetic activity was detected are presented in Table 23. As it is expected, there are no correlations between different monitor recordings. Only SNT of different thresholds display correlation with each other's, because if the particle has enough energy to trigger threshold 4, it triggers all lower thresholds as well, and all thresholds react on the one and the same particle.

For 29 October 2003 Fd, very strong correlations between all monitors are seen (Table 23), which indicates that the magnetic field of the CME has influence on the particles of all energies (up to ~50GeV - the median value of the primary proton energy generating 5GeV muons), so that all monitor count rates are decreasing similarly. For smaller events of 27 July 2004 and 20 November 2003 (Tables 24, 25) it is seen that the correlations between monitor count rates are large for the low energy particles and they are decreasing with energy. Correlation with 4 energy thresholds of SNT is gradually decreasing from 0.75 down to 0.32. Now we will try to illustrate how the calculated correlation coefficients are related to the geoeffectiveness of the event. As a geoeffectivess characteristic we choose the Disturbance storm time (DST), which is a geomagnetic index, indicating the world magnetic disturbance level. The index is constructed by averaging the horizontal component of the geomagnetic field from mid-latitude and equatorial magnetometers from all over the world.

In Table 27 we present the correlation coefficients of above-mentioned four events with corresponding detected minimal values of the DST.

Table 23 Correlations between different ASEC monitor recordings for January 25, 2003 (the case of absence of any geomagnetic activity).

	ArNM	NANM	SNT thr0	SNT thr1	SNT thr2	SNT thr 3	SNT thr4	Muons > 5Gev
ArNM	1							
NANM	0.01	1						
SNT thr0	0.02	-0.01	1					
SNT thr1	0.05	0,03	0,06	1				
SNT thr2	0.04	-0,04	-0,05	0,43	1			
SNT thr3	0.03	0,03	-0,01	0,31	0.42	1		
SNT thr4	0.03	0.02	0.01	0.22	0.24	0.21	1	
Muons > 5Gev	0.03	0.02	0.12	0.08	-0.04	0.00	0.01	1

Table 24 Correlations between different ASEC monitor recordings for the Forbush decrease of November 20, 2003 event (from 10:00 UT to 12:00 UT).

	ArNM	NANM	SNT thr0	SNT thr1	SNT thr2	SNT thr 3	SNT thr4	Muons > 5Gev
ArNM	1							
NANM	0.72	1						
SNT thr0	0.75	0.76	1					
SNT thr1	0.69	0.72	0.88	1				
SNT thr2	0.62	0.63	0.75	0.81	1			
SNT thr3	0.41	0.47	0.52	0.56	0.68	1		
SNT thr4	0.32	0.37	0.36	0.40	0.48	0.68	1	
Muons > 5Gev	0.38	0.43	0.48	0.45	0.42	0.28	0.12	1

Table 25 Correlations between different ASEC monitor recordings for the Forbush decrease of July 27, 2004 event (from 0:00 UT to 24:00 UT).

	ArNM	NANM	SNT thr0	SNT thr1	SNT thr2	SNT thr 3	SNT thr4	Muons > 5Gev
ArNM	1							
NANM	0.93	1						
SNT thr0	0.92	0.89	1					
SNT thr1	0.89	0.86	0.94	1				
SNT thr2	0.75	0.72	0.83	0.90	1			
SNT thr3	0.62	0.59	0.66	0.71	0.79	1		
SNT thr4	0.45	0.43	0.47	0.50	0.56	0.70	1	
Muons > 5Gev	0.85	0.84	0.83	0.81	0.66	0.52	0.37	1

Table 26 Correlations between different ASEC monitor recordings for the Forbush decrease of October 29, 2003 event (from 6:00 UT to 14:40 UT).

	ArNM	NANM	SNT Thr 0	SNT Thr 1	SNT Thr 2	SNT Thr 3	SNT Thr 4	Muons > 5Gev
ArNM	**1**							
NANM	**1.00**	**1**						
SNT Thr 0	**0.99**	**0.99**	**1**					
SNT Thr 1	**0.99**	**0.99**	**1.00**	**1**				
SNT Thr 2	**0.99**	**0.99**	**0.99**	**1.00**	**1**			
SNT Thr 3	**0.98**	**0.98**	**0.99**	**0.99**	**0.99**	**1**		
SNT Thr 4	**0.98**	**0.98**	**0.99**	**0.99**	**0.99**	**0.99**	**1**	
Muons > 5Gev	**0.97**	**0.97**	**0.97**	**0.97**	**0.97**	**0.96**	**0.95**	**1**

Table 27 Correlation coefficients and minimal values of DST for different event

Event	Correlation coefficient between ArNM and AMMM	Correlation coefficient between ArNM and SNT_0	Dstmin (nT)
25 January 2004	0.03	0.02	-20
20 November 2003	0.38	0.75	-84
27 July 2004	0.85	0.92	-236
29 October 2003	0.97	0.99	-360

From Figure 65 it is apparent that a strong association exists between selected correlation coefficients and corresponding values of Dstmin. Thus, the correlation matrixes contain valuable information on the geoeffectiveness of the event: the higher correlation coefficient between ArNM and AMMM, and/or between ArNM and SNT, the stronger is the geomagnetic disturbance. We performed also correlation analysis of 20 November 2003 huge geomagnetic storm. In Figure 66 we see large enhancement of the Neutron Monitor count rates accompanied by much smaller enhancement of the low energy charged component and - stable count rate of the high-energy muons.

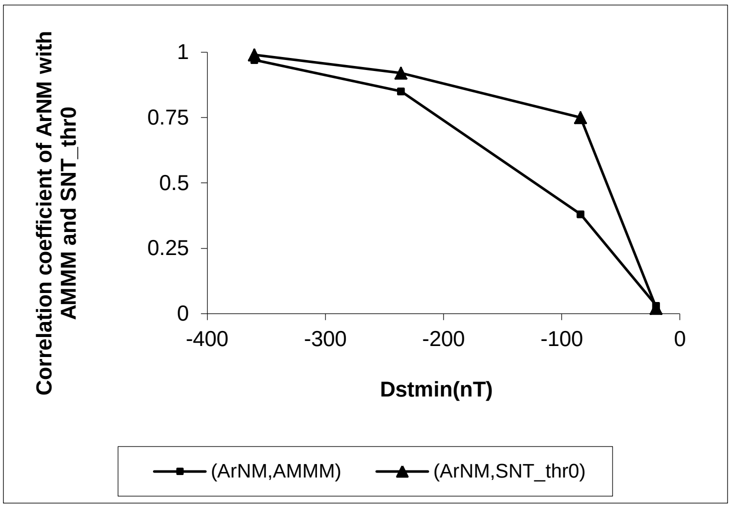

Figure 65. Correlation coefficients between neutrons and high energy muons (ArNM, AMMM) and between neutrons and low energy charged particles (ArNM, SNT_0-threshold) versus minimal value of Dst.

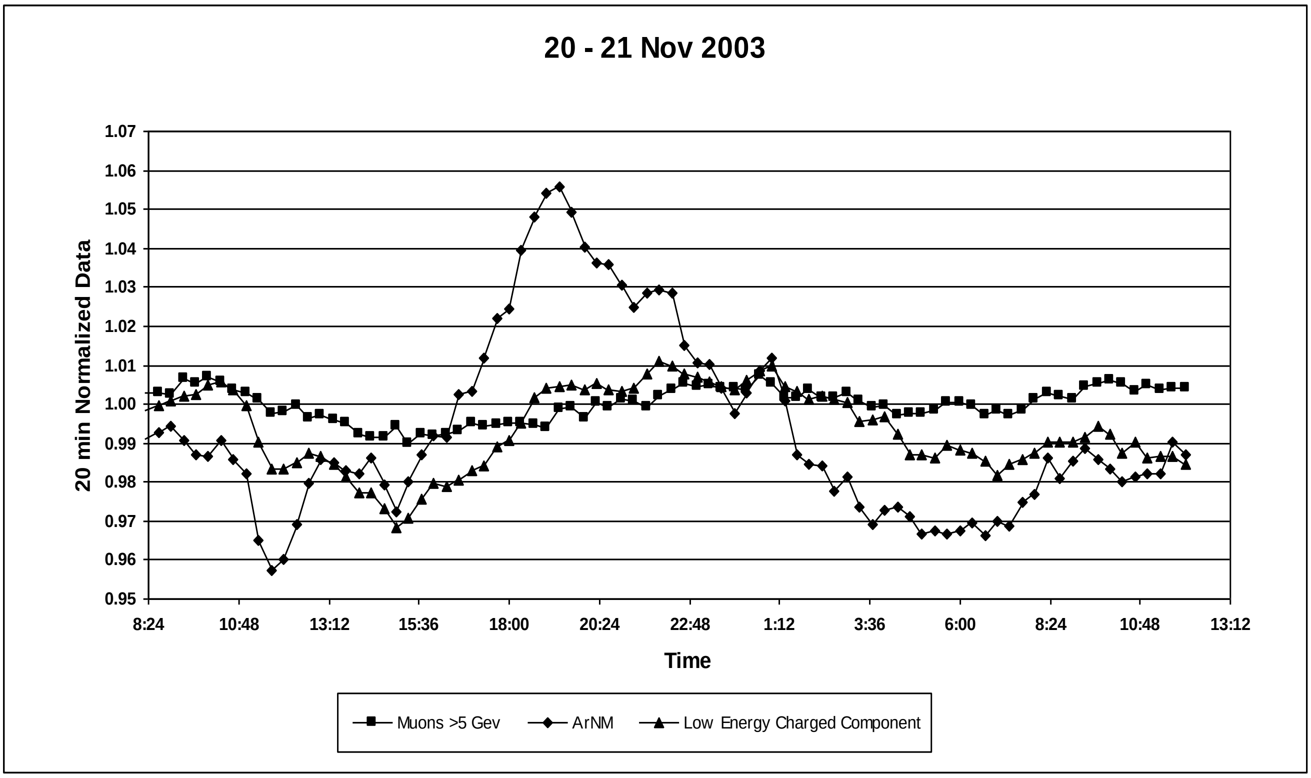

Figure 66 Time profile of particles observed by ASEC monitors on November 20, 2003.

To characterize the magnitude of the geoeffectiveness of the event, we again use the Dst index. During this storm the Dst index decreased by as much as a record value of –472 nT. Interaction of the arriving shock with the geomagnetic field leads to the significant reduction of geomagnetic cut-off at the Mt. Aragats latitude. The correlation matrix for this event is presented in Table 28. One can see that for the geomagnetic storm of November 20, 2003 the correlation between ArNM and NANM is strong (~0.9), because these two instruments of the same type are registering neutron flux, originated by low energy primaries. The different location levels cause the differences in these monitors' recordings. Some secondary neutrons from low energy primaries, which are registered by ArNM, are missed in NANM, because they do not reach the NANM level (2000m a.s.l.). There is also a strong correlation between the neutron flux and the the charged component flux (mostly electrons and low energy muons). High energy muons didn't correlate with neutrons. To reproduce this correlation pattern we perform simulations of the time series of different secondary cosmic rays. We take into account as CR propagation through the Earth's atmosphere using CORSIKA code [12] and also detector response according to [13].

Table 28 Correlations between different ASEC monitors recordings for the geomagnetic storm of November 20, 2003 event (from 14:40 UT to 6:00 UT 21 November).

	ArNM	NANM	SNT thr0	SNT thr1	SNT thr2	SNT thr 3	SNT thr4	Muons > 5Gev
ArNM	1							
NANM	0.89	1						
SNT thr0	0.47	0.44	1					
SNT thr1	0.81	0.79	0.64	1				
SNT thr2	0.85	0.83	0.34	0.82	1			
SNT thr3	0.67	0.65	0.44	0.70	0.76	1		
SNT thr4	0.38	0.35	0.34	0.43	0.43	0.67	1	
Muons>5Gev	-0.01	-0.04	0.44	0.14	-0.04	0.13	0.13	1

The median energies of primary protons, originating as minimum one neutron or low energy charged particle in the secondary fluxe are ~10 - 20GeV, while high-energy muons are originated by protons with median energy of ~50GeV. This conclusion follows from Figure 67, where three simulated distributions represent: the normalized energy spectra of primary protons originating at least one neutron, one electron or muon, and one muon of high energy at detection altitude of 3200m. Therefore, the primary protons from the left tails of the mentioned distributions will enter the atmosphere and generate additional particles detected by NMs and lower channels of SNT. The distribution of the protons generating the high-energy muons is shifted to the right on the energy scale, and decrease of the geomagnetic cutoff cannot influence the count rate of high-energy muons.

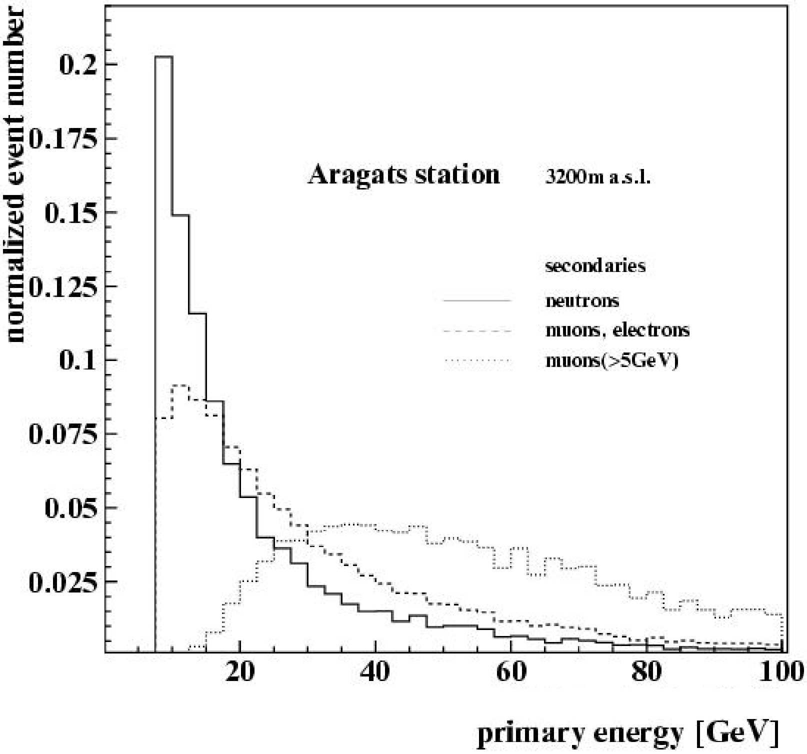

Figure 67 The normalized event numbers of primary particles originating different secondary particle fluxes.

SUMMARY

The main results expected from ASEC and SEVAN networks can be formulated as follows:

- Continuous measurement and display of fluxes of different species of secondary cosmic rays with different energy thresholds and directions of incidence;
- Measurements of the time series of the histograms of the energy deposit in “thick” scintillators;
- Reliable data transfer and storage in the data bases on high altitude stations and CRD headquarters in Yerevan.

The new electronics developed and installed in the framework of presented dissertation solve problems mentioned above. Electronics provides 24 hour, whole year monitoring of the secondary cosmic rays by networks of particle detectors. Registered data were transferred to CRD partners in real time. Most components of the DAQ system prove reliability and multifunctional possibilities. Several papers are published based on the new physical results enabled by flexible and powerful DAQ system. The first three SEVAN modules operated at Aragats Space Environmental Center in Armenia, at altitudes 1000, 2000 and 3200 m in Yerevan and on the slopes of mountain Aragats. The expansion of SEVAN networks continuous by deploying detectors in Croatia and Bulgaria; in 2010 SEVAN detector was deployed in New Delhi University, India, in 2012 in Slovakia. Data from all SEVANs is entering the CRD database. Networks of particle detectors on Earth’s surface provide timely information and constitute an important element of planetary Space Weather warning services. The big advantage of ground based particle detectors is their consistency, 24 h coverage, and multi- year operation. In contrast, the planned life of the satellites and spacecraft is only a few years, they are affected by the same solar blast that they should alert, and space-born facilities instead of sending warnings are usually set in the stand-by mode.

The multi-particle detectors provided with sophisticated electronics probe different populations of primary cosmic rays. The basic detector of the SEVAN network is designed to measure fluxes of neutrons and gammas, low energy charged particles and high-energy muons. The rich information obtained from the SEVAN network located mostly at low and middle latitudes will allow estimating the energy spectra of the highest energy SCR. The SEVAN network is sensitive to very weak fluxes of SCR above 10 GeV, a very poorly explored region of the highest energy.

The phenomenon of decreasing of the high-energy muon flux measured by SEVAN detector during TGEs can be explained by the shifting of energetic spectrums of muons in electric field. During positive flux in the lower dipole that accelerates electrons and negative muons downwards spectrum of negative muons shifts right, whereas spectrum of positive muons shift left on the amount corresponding to net potential difference of electrical field. In the result of such shifting the fluxes of muons above threshold energy of detector are changed: flux of negative muons increases, while the flux of positive muons decreases. Summary, the total particle's flux decreases (SEVAN cannot distinguish positive and negative muons) because number of positive muons is greater (~30% at energies above 100 MeV) than number of negative muons. By the measured deeps in high energy muon time series it is possible to remotely estimate the total potential drop in thundercloud; the problem that escaping the solution till now-the-days because of absence of adequate techniques.

The atmospheric pressure was measured by the PHT sensor designed and fabricated in the Yerevan Physics Institute on basis of the pressure sensor Motorola MPXA6115. The device operates and supplies digitized data to the data acquisition systems of the Aragats Space Environmental Center at altitudes 1000, 2000, and 3200 m a.s.l. The accuracy of pressure measurements are not worse than 0.05 Mb, that is sufficient for the studies of the solar-terrestrial connections via variations of the secondary fluxes of the elementary particles detected on the Earth's surface. The device is reliable and simple in operation and can be recommended for the world- wide networks of particle detectors. Mentioned tasks are realized using integrated systems of Complex Programmable Logic Devices (CPLDs), microcontrollers and Field Programmable Gate Arrays (FPGA). Incorporation of the "intellectual" elements allows fulfilling rather complicated tasks of particle detection and, also, performing remote control and tuning of most crucial parameters of the detector. ASEC system is much more complicated and flexible as compared to ones often used in particle detectors of world-wide networks monitoring fluxes of cosmic ray.

The follouing electronic devices have been developed and created in frameworks of this dissertation:

1. The Preamplifier-Discriminator-Shaper circuit using in the systems operating in counter mode. The dead time of these systems has been reduced to 0.4us using fast comparators and CPLDs.
2. Logarithmic Amplitude–to-Digital Converter (LADC) is using in systems requiring measurements of pulse amplitudes giving information about particle energy or number of incident particles. Programmable threshold and remoute control allows for combining these circuits into flexible devices. For this purpose the following electronic modules were developed.
3. The Programmable Threshold 8-channel fast Discriminator/Counter (8CNT module) designed for usage in particle counter setups after the buffer preamplifier. It can be used as a main DAQ device along the MultiIFC module (see below) and as the intermediate stage between detectors and FPGA based counter modules (UMEC, see below) in more complex experimental setups.
4. The 12-channell Discriminator/Counter with Programmable Threshold (12CNT module) is similar to the 8CNT module, but has more input channels, while being slower, delay in range 300-500ns. This module is cheaper solution for slow detectors, like proportional chambers.
5. Universal Multichannel Event Counter (UMEC) is a high-performance FPGA based programmable module to be used in different Cosmic Ray detector setups. It has 60 standard 3.3V TTL level digital inputs and can be programmed as conventional multichannel counter, trigger-driven multichannel counter, trigger generator for complex event patterns, etc. and combination of listed.
6. The MultiIFC module is universal electronic module for connecting above listed electronic modules to PC or directly to Ethernet.
7. The 32-bit universal microcontroller module with USB interface (C32USB) is designed for usage as universal data processing and interface unit for ASEC detectors DAQ and Detector Monitoring System (DMS). It is based on the NXP (former Philips) LPC2100 Advanced RISC Machine (ARM – de facto industrial standard) microcontroller.
8. The Programmable Regulated High Voltage DC Power Supply is designed to supply high voltage to photomultipliers (PMT) and other elementary particle detectors. The module output voltage can be

remotely controlled by 1-2 V steps. Remote control functions are performed by local microcontroller through RS-485 interface.

9. Additional elestronics has been desiged for the Pressure, Humidity, Temperature (PHT) SENSOR. It is a general purpose microcontroller unit, designed for environmental measurements: pressure, temperature and humidity.

Total energy consumptions including DAQ electronics for 24 channels and build-in micro-PC did not exceed 100 Wt. Therefore, accu-battery system powered by solar energy can be also used for feeding the detector, as usually is required for the CR experiments. All listed above modules are used as constructive elements to build different electronics units for ASEC and SEVAN networks.

Acknowledgement

I am grateful to my supervisor Ashot Chilingarian for suggesting the topic of the dissertation and for giving opportunity to present the results at international conferences and schools. Our work was supported by IHY-2007 initiative, and I thank H.Haubold, J.Davila, N. Gopalswami for being so instrumental in helping us to create worldwide SEVAN networks. Our work was supported by ISTC A1554 grant, INTAS Grant 8777 and EOARD grant FA 8655-07-01-3014. I also thank SEVAN instrument hosts D. Rosa, J. Stamenov, K. Kudela, S. Mukherjee for their interest to be a part of SEVAN network and for operating SEVAN modules, the staff of the ASEC for 24 hours whole year operation of the particle detectors. I am grateful to my colleagues and friends Varuzhan Danielyan, Ar**a** Daryan, Laura Melkumyan and Mary Zazyan for the useful discussions and valuable comments.

ACRONYMS

ACE	Advanced Composition Explorer
ACT	Atmospheric Cherenkov Telescopes
ADAS	Advanced Data Analysis System
ADC	Amplitude-Digital-Converters
AGN	Active Galactic Nuclei
AMMM	Aragats Multidirectional Muon Monitor
ArNM	Aragats Neutron Monitor
ASCII	American Standard Code for Information Interchange
ASEC	Aragats Space Environmental Center
ASNT	Aragats Solar Neutron Telescope
AU	Astronomical unit (distance Sun-Earth, $1{,}5 \times 10^{11}$m)
CME	Coronal Mass Ejection
CMOS	Complementary Metal–Oxide–Semiconductor
CPLD	Complex Programmable Logic Device
CR	Cosmic Rays
CRD	Cosmic Ray Division, Yerevan Physics Institute
DAQ	Data Acquisition
DCS	Detector Control System
DST	Disturbance Storm Time
DVIN	Data Visualization Interactive Network
EAS	Extensive Air Showers
ESA	European Space Agency
Fd	Forbush decrease
GAMMA	EAS installation on Mt. Aragats
GCR	Galactic Cosmic Rays

GLE	Ground level Enhancement (Excess, Event)
GOES	Geostationary Operational Environmental Satellite
GPS	Global Positioning System
IACT	Imaging Atmospheric Cherenkov Telescope
IHY	International Heliophysical Year
IMF	Interplanetary Magnetic Field
IP	Interplanetary
LADC	Logarithmic ADC
LAN	Local Area Network
LEP	Large Electron-Positron Collider
MAKET ANI	EAS installation on mt. Aragats
NAMMM	Nor Amberd Multidirectional Muon Monitor
NANM	Nor-Amberd Neutron Monitor
NM	Neutron Monitor
NS	North-South
nT	nano Tesla
PMT	Photo Multiplier Tube
SCR	Solar Cosmic Ray
SEP	Solar Energetic Particles
SEVAN	Space Environmental Viewing and Analysis Network
SF	Solar Flare
SN	South-North
SNR	Supernova Remnants
SNT	Solar Neutron Telescopes
SVG	Scalable Vector Graphics
TTL	Transistor-Transistor Logic
URCS	Unified Readout and Control Server

VHE	Very High-Energy
WE	East-West
WE	West-East
XML	eXtensible Markup Language

BIBLIOGRAPHY

1. Chilingarian, A., K. Avakyan, V. Babayan et al. (2003), Aragats Space-Environmental Center: Status and SEP Forecasting Possibilities, Journal of Physics G, 29, 939-952.
2. Chilingarian, A., K. Arakelyan, K. Avakyan et al. (2005), Correlated Measurements of Secondary Cosmic Ray Fluxes by the Aragats Space- Environmental Center Monitors, Nucl. Instrum. and Methods in Phys. Res., Sect A 543, 483-496.
3. H. Moraal, A. Belov, J.M. Clem, Space Sci. Rev. 93 (2000)285.
4. A.S. Beglaryan, S.P. Bujukyan, et al., Scientific publication of YerPhI 1197(74) 1989.
5. L.L. Dorman, Variations of the Galactic Cosmic Rays, Publishing house of the Moscow State University, Moscow, 1975.
6. Y.V. Stenkin, J.F. Valdes-Galicia, et al., Astroparticle Phys. 16(2001) 157.
7. T.V. Danilova, et al., Nucl. Instr. and Meth. A 323 (1992) 104.
8. A.P. Garyaka, R.M. Martirosov, et al., J. Phys. G 28 (2002) 2317.
9. V.V. Avakian, E.B. Bazarov, et al., VANT, ser. Tech.Phys. Exp. 5 (31) (1986) 1.
10. A.A. Chilingarian, et al., Proceedings of the 24th Interna- tional Cosmic Ray Conference, Salt Lake City, vol. 1, 1999, p. 240.

11. A.Chilingarian et al, (2007) Study of Extensive Air Showers and Primary Energy Spectra by MAKET-ANI Detector on Mountain Aragats, Astroparticle Physics 28, p. 58-71.
12. Heck D. et al., Forschungszentrum Karlsryhe, FZKA Report 6019, 1998
13. Clem J.M. and Dorman L.I.,(2000) Space Sci.Rev., **93**,335.
14. Bostanjyan, N., Chilingaryan A., Eganov V., Karapetyan g., On the production of higest energy solar protons on 20 January 2005. Adv. Space res. 39, 1454-1457, 2007
15. A. Chilingarian and A. Reymers, Investigations of the response of hybrid particle detectors for the Space Environmental Viewing and Analysis Network (SEVAN), Ann. Geophys, 26, (249-257), 2008.
16. A.A. Chilingarian, A.E. Reymers, Particle detectors in Solar Physics and Space Weather research, Astroparticle Physics (2007), Astropart. Phys., 27, 465-472
17. A. Chilingarian, R. Mirzoyan and M. Zazyan, Cosmic Ray research in Armenia, Advances in Space Research Volume 44, Issue 10, 16 November 2009, Pages 1183-1193
18. Leerungnavarat K., D. Ruffolo,The Astrophysical Journal, 593, 587–596, 2003.
19. A. Chilingarian and N. Bostanjyan, On the relation of the Forbush decreases detected by ASEC monitors during the 23rd solar activity cycle with ICME parameters, Advances in Space Research, Volume 45, Issue 5, 1 March 2010, Pages 614-621
20. Haurwitz et al., 1965 M.W. Haurwitz, S. Yoshida and S.I. Akasofu, Interplanetary magnetic field asymmetries and their effects on polar cap absorption effects and Forbushdecreases. J. Geophys. Res., 70 (1965), pp. 2977–2988
21. Bagrat Mailyan , Ashot Chilingarian, Investigation of diurnal variations of cosmic ray fluxes measured with using ASEC and NMDB monitors, Advances in Space Research 45 (2010) 1380–1387
22. A. Chilingarian, G. Hovsepyan, K. Arakelyan, S. Chilingaryan, V. Danielyan, K. Avakyan, A. Yeghikyan, A. Reymers, S. Tserunyan, Space Environmental Viewing and Analysis Network (SEVAN), Earth, Moon and Planets: Volume 104, Issue 1 (2009), page 195
23. Chilingarian, A.Daryan, K.Arakelyan, et al., Ground-based observations of thunderstorm-correlated fluxes of high-energy electrons, gamma rays, and neutrons, Phys.Rev. D., 82, p. 043009, 2010
24. Chilingarian, G. Hovsepyan, and A. Hovhannisyan, Particle bursts from thunderclouds: Natural particle accelerators above our heads, Physical review D 83, p. 062001, 2011

25. Kuwabara, T., et al. (2006), Realtime cosmic ray monitoring system for space weather, Space Weather, 4, S08001, doi:10.1029/2005SW000204.
26. H. Tsuchiya, Y. Muraki, K. Masuda et al., Detection efficiency of a new type of solar neutron detector calibrated by an accelerator neutron beam. Nucl. Instrum. Methods Phys. Res. Sect. A 463, 183–193 (2001)
27. Munakata, K., J. W. Bieber, S. Yasue, C. Kato, M. Koyama, S. Akahane, K. Fujimoto, Z. Fujii, J. E. Humble, and M. L. Duldig (2000), Precursors of geomagnetic storms observed by the muon detector network, J. Geophys.Res., 105(A12), 27,457–27,468, doi:10.1029/2000JA000064.
28. M. Rockenbach A. Dal Lago, W. D. Gonzalez, et.al.,eomagnetic storm's precursors observed from 2001 to 2007 with the Global Muon Detector Network (GMDN), J. Geophys.Res., 38, L16108, doi:10.1029/2011GL048556, 2011
29. H. Mavromichalaki, G. Souvatzoglou, C. Sarlanis et al., The new Athens center on data processing from the neutron monitor network in real time. Ann. Geophys. 23, 3103–3110 (2005)
30. H. Mavromichalaki, G. Souvatzoglou, C. Sarlanis, et al., Space weather prediction by cosmic rays. Adv.Space Res. 37(6), 1141–1147 (2006)
31. Zhang J.L., Tan Y.H., Wang H., et al., The YangbajingMuon–Neutron Telescope, NIMA, 623, 1030-1034, 2010, doi:10.1016/j.nima2010.08.091
32. D. Heck, J. Knapp, A Monte Carlo Code to Simulate Extensive Air Showers, ForschungszentrumKarlsryhe, FZKA Report 6019, 1998
33. Zazyan, M., Chilingarian, A. Calculations of the sensitivity of the particle detectors of ASEC and SEVAN networks to galactic and solar cosmic rays. Astropart. Phys. 32, 185–192, doi:10.1016/j.astropartphys.2009.08.001, 2009
34. M. Boezio, V. Bonvicini, P. Schiavon, A. Vacchi, et al., Astropart. Phys. 19 (2003) 583–604
35. http://www.geant4.org/geant4/
36. D. Ruffolo,J.W.Bieber, P.Evenson, and R. pile., Precursors to Forbush Decreases and Space Weather Prediction., Proceedings of the 26th International Cosmic Ray Conference. August 17-25, 1999. Salt Lake City, Utah, USA
37. A.V. Belov, L.I.Dorman, E.A. Eroshenko, N.Iucci, G. Villoresi, V.G. Yanke. Search forPredictors of Forbush Decreases., Proc. 24th Inter. Cosmic Ray Conf, 4, 888-891, 1995.

38. Dorman L. I. and Dorman I. V., Advances in Space Research, Volume 35, pp 476-483, 2005
39. Hatton C. J., Progress in Elementary Particles and Cosmic Ray Physics, 10, 1- 100, North Holland, 1971
40. Chilingarian, G. Hovsepyan, and A. Hovhannisyan, Particle bursts from thunderclouds: Natural particle accelerators above our heads, Physical review D 83, p. 062001, 2011
41. A. Chilingarian, T. Karapetyan; Calculation of the barometric coefficients at the start of the 24th solar activity cycle for particle detectors of Aragats Space Environmental Center, Advances in Space Research 47 (2011) 1140–1146
42. Kudela, K., Firoz, K.A., Langer, R., et al. On diurnal variation of cosmic rays: statistical study of neutron monitor data including LominskyŜtit, in: Proceedings of 21st ECRS-2008. Available from: <http://www.ecrs2008.saske.sk/dvd/s4.15.pdf>, 2008.
43. A. V. Gurevich, G. M. Milikh, and R. A. Roussel-Dupre, Phys. Lett. A 165, 463 (1992)
44. L. P. Babich, E. N. Donskoi, I. M. Kutsyk, and Kudryavtsev, Phys. Lett. A 245, 460 (1998).
45. J. R. Dwyer, Phys. Plasmas 14, 042901 (2007).
46. N. S. Khaerdinov, A. S. Lidvansky, and V. B. Atmos. Res. 76, 346 (2005)
47. B. B. Gvozdevsky, Yu. V. Balabin, E. V. Vashenyuk, L. I. Schur Neutron monitor multiplicity measurements during the 13.12.2006 GLE. in WEB site of conference SEE-2007
48. A. Chilingarian, L. Melkumyan, G. Hovsepyan, A. Reymers. The response function of the Aragats Solar Neutron Telescope, Nuclear Instruments and Methods in Physics Research. **A 574**, pp 255-263.
49. Gadalov A.N., Kaganovvv I.I., Silaev A.A. , Facilities and Techniques of Experiment N1, pp.39, 1973
50. Silaev A.A., Silant'ev O.A., Facilities and Techniques of Experiment N1, pp.100, 1981.
51. Stepanov V.I., Facilities and Techniques of Experiment N3, pp.115, 1969
52. Daryan A.V, Dolganov S.A., Khachatryan A.P., Preprint YerPhI 1485(2), 1997
53. http://www.atmel.com/
54. Pulse Power & Measurements Ltd.2008 http://www.ppmpower.co.uk/high_voltage_dc_dc_converters/
55. Freescale semiconductor. 2008, http://www.freescale.com/
56. Chilingaryan S., Chilingarian A., Danielyan V., Eppler W. The Aragats data acquisition system for highly distributed particle detecting networks. Journal of Physics: Conference Series 119 pp. 1-9, 2008
57. Space Weather, Environment and Societies Lilensten, Jean, Bornarel, Jean 2006

58. A. Chilingarian and N. Bostanjyan, Cosmic ray intensity increases detected by Aragats Space Environmental Center monitors during the 23rd solar activity cycle in correlation with geomagnetic storms, J. Geophys. Res., Vol. 114, No. A9, A09107
59. N.Gevorgyan for the ASEC team, (2005) Test Alert Service Against Very Large SEP Events, Advances in Space Research (ASR), Vol. 36, issue 12, pp 2351-2356
60. Balabin Yu.V., Gvozdevsky B.B., Schur L.I. et al. // Proc. 30th ICRC. Merida, Mexico. 2007. V. 1. P. 257.
61. Ромахин В. А.: Применение фотоэлектронного умножителя ФЭУ-49 в детекторах ионизирующего излучения (ФИАН), препринт № 28, 1980
62. Chilingarian A., Arakelyan K., et al.: Correlated measurements of secondary cosmic ray fluxes by the Aragats Space – Environmental Center monitors, Nucl. Instrum. Methods Phys. Res., Sect. A, 483-496, 2005.
63. Chilingarian A., Arakelyan K., et al.: Space Environmental Viewing and Analysis Network (SEVAN), Earth, Moon, and Planets; DOI:10.1007/s11038-008-9288-1, February, 2009
64. K. Arakelyan : Atmospheric Pressure Measurements at the Aragats Space Environmental Center, Proceedings of International Symposium FORGES, Nor-Amberd, Armenia, pp. 117-120, 2008.
65. Chilingarian A., Arakelyan K., et al.: New electronics for the Aragats Space-Environmental Center (ASEC) particle detectors, Proceedings of International Symposium FORGES, Nor-Amberd, Armenia, pp. 105-116, 2008.
66. Chilingarian A., Arakelyan K., et al.: Thunderstorm Correlated Enhancements of Cosmic Ray Fluxes Detected at Mt. Aragats, Proceedings of International Symposium FORGES, Nor-Amberd, Armenia, pp. 121-126, 2008.
67. Chilingarian A., Arakelyan K., et al: SEVAN CRO Particle Detector for Solar Physics and Space Weather research, Central European Astrophysical Bulletin, Vol. 34, p. 115-122
68. Chilingarian A., Arakelyan K., et al: Ground-based observations of thunderstorm-correlated fluxes of high-energy electrons, gamma rays, and neutrons, Phys. Rev. D 82, 043009 (2010)

69. Chilingarian A., Arakelyan K., et al: Space Weather Observatory at Aragats mountain in Armenia, Proceedings of the 29th International Cosmic Ray Conference. August 3-10, 2005, Pune, India, Volume 2, p.441
70. Chilingarian A., Arakelyan K., et al: Nor-Amberd multidirectional muon monitor: new detector for the world-wide network, Proceedings of the 29th International Cosmic Ray Conference. August 3-10, 2005, Pune, India, Volume 2, p.445
71. Chilingarian A., Arakelyan K., et al: Space Environmental Viewing and Analysis Network (SEVAN) – characteristics and first operation results, ISWI Newsletter - Vol. 4 No. 25
72. Chilingarian A., Arakelyan K., et al: New Particle Detector Network for Solar Physics and Space Weather research, PROCEEDINGS OF THE 31st ICRC, ŁOD´Z 2009
73. Chilingarian A., Arakelyan K., et al: Space Environmental Viewing and Analysis Network (SEVAN), Central European Astrophysical Bulletin, ISSN 1845-8319, pp. 259-272. 2007